Role of Heparan sulfate in Indian Hedgehog signaling and Glycosaminoglycan composition

Inaugural-Dissertation

zur

Erlangung des Doktorgrades

Dr. rer. nat.

der Fakultät für

Biologie

an der

Universität Duisburg-Essen

vorgelegt von

Velina Dimitrova Bachvarova

aus Kardzhali, Bulgarien

im August 2017

Die der vorliegenden Arbeit zugrunde liegenden Experimente wurden am Zentrum für Medizinische Biotechnologie in der Abteilung für Entwicklungsbiologie der Universität Duisburg-Essen und am Biomedizinischen Zentrum (BMC) in der Abteilung für Medizinische Biochemie und Mikrobiologie der Universität Uppsala durchgeführt.

1. Gutachter: Prof. Dr. Andrea Vortkamp
2. Gutachter: Prof. Dr. Daniel Hoffmann
3. Gutachter: Prof. Dr. Lena Kjellen

Vorsitzender des Prüfungsausschusses: Prof. Dr. Peter Bayer
Tag der mündlichen Prüfung: 16.01.18

DOI: 10.17185/duepublico/45208
URN: urn:nbn:de:hbz:465-20240326-083025-7

“Begin at the beginning," the King said, very gravely, "and go on till you come to the end: then stop.”

Lewis Carroll, Alice in Wonderland

Table of contents

List of abbreviations

°C	Temperature in degree Celsius
ADAM	A Disintegrin and Metalloprotease
Amp	Ampicillin
APS	Ammonium persulfate
ATP	Adenosine 5'- triphosphate
BDA1	Brachydactyly type a1
bm	Brachymorphic mouse
Bmp	Bone morphogenetic protein
Boc	Brother of Cdo
BSA	Bovine serum albumin
C4st	Chondroitin 4-*O*-sulfotransferases
C6st	Chondroitin 6-*O*-sulfotransferases
CA	Cyclopamine
Cdo	Cell adhesion molecule-related/Down-regulated by Oncogenes
ChPF	Chondroitin Polymerization Factor
Chsy	Chondroitin Synthase
cpm	Counts per minute
CS	Chondroitin sulfate
CS/DS5epi	CS/DS glucuronyl-C5-Epimerase
CSGalNAct	Chondroitin sulfate *N*-acetylgalactosaminyltransferase
CW	Cardin-Weintraub
DAPI	4', 6-diamidino-2-phenylindole
DEAE	Diethylaminoethyl
Dhh	Desert hedgehog
Disp	Dispatched
DMSO	Dimethyl sulfoxide
dNTP	Deoxynucleotide
DS	Dermatan sulfate
dtd	Diastrophic dysplasia mouse
ECM	Extracellular matrix
EDTA	Ethylenediaminetetraacetic acid
ER	Endoplasmic reticulum
ESCRT	Endosomal sorting complex required for transport

Ext	Exostosin
Extl3	Exostosin like glycosyltransferase 3
FDU	Fast Digest Unit
Fgf	Fibroblast growth factor
FPLC	Fast protein liquid chromatography
g	Relative centrifugal force normalized to the Earth gravity
Gal	Galactose
GalNAc	*N*-acetylgalactosamine
GalNAc4s-6st	GalNAc4-sulfate 6-*O*-sulfotransferase
Gas1	Growth arrest specific-1
GlcA	Glucuronic acid
Glce	Glucuronyl-C5-epimerase
GlcNAc	*N*-acetylglucosamine
Gli,	glioma-associated oncogene
GliA	glioma-associated oncogene activator form
GliFL	glioma-associated oncogene full length
GliR	glioma-associated oncogene repressor form
GPI	Glycosylphosphatidylinositol
HEPES	4-(2-Hydroxyethyl)piperazine-1-ethanesulfonic acid
Hh	Hedgehog
Hhat	Hedgehog acyltransferase
Hhip	Hedgehog Interfering Protein
HhNp	Hedgehog protein, processed N-terminal signaling domain
HS	Heparan sulfate
Hs2st	HS-2-*O*-sulfotransferase
Hs3st	HS-3-*O*-sulfotransferase
Hs6st	HS-6-*O*-sulfotransferase
HSPG	Heparan sulfate proteoglycan
IdoA	Iduronic acid
Ihh	Indian hedgehog
IhhNp	Indian hedgehog, processed N-terminal signaling domain
IN	Input
ITS	Insulin-Transferrin-Selenium
Kif7	Kinesin-2 family member 7
Km	Kanamycin
KS	Keratan sulfate

KSGal6st	KS-galactose-6*O*-sulfotransferase
L	Liter
LB	Luria Bertani
Lpp	Lipophorin
M	Molar
mg	Milligram
ml	Milliliter
mM	Millimolar
Mmp13	Matrix metalloproteinase 13
Ndst	*N*-deacetylase-*N*-sulfotransferase
NHS	*N*-hydroxysuccinimide
o/n	Overnight
PA	Purmorphamine
PAA	Polyacrylamide
PAPS	3′-phosphoadenosine 5′-phosphosulfate
PBS	Phosphate Buffered Saline
PCR	Polymerase chain reaction
PFA	Paraformaldehyde
PG	Proteoglycan
PNPP	*p*-Nitrophenyl Phosphate disodium salt hexahydrate
Ppr	Parathyroid hormone/Parathyroid hormone related protein receptor
Ptch	Patched
Pthrp	Parathyroid hormone related protein
PVDF	polyvinylidene difluoride
RPIP-HPLC	Reversed-phase ion-pairing high-performance liquid chromatography
Scube	Signaling sequence, cubilin domain, epidermal growth factor-like domain-containing protein
SDS	Sodium dodecyl sulfate
SDS-PAGE	Sodium dodecyl sulfate-polyacrylamide gel electrophoresis
Shh	Sonic hedgehog
ShhNp	Sonic hedgehog protein, processed N-terminal signaling domain
Smo	Smoothened
SS	Signaling peptide, signaling sequence
SSD	Sterol-sensing domain
Sufu	Suppressor of Fused

Sulf	HS-6-*O*-endosulfatase
TAE	Tris-acetate-EDTA
TBS	Tris-buffered saline
TCA	Trichloracetic acid
TE	Tris-EDTA
TEMED	Tetramethylethylenediamine
Tgf	Transforming growth factors
U	Unit
Ust	Uronyl-2-*O*-sulfotransferase
V_0	Void volume
V_t	Total column volume
Wnt	Wingless-type MMTV integration sites
Xyl	Xylose
µg	Microgram
µl	Microliter

Amino acids, three and one letter code

Alanine	Ala	A	Leucine	Leu	L
Arginine	Arg	R	Lysine	Lys	K
Asparagine	Asn	N	Methionine	Met	M
Aspartic acid	Asp	D	Phenylalanine	Phe	F
Cysteine	Cys	C	Proline	Pro	P
Glutamic acid	Glu	E	Serine	Ser	S
Glutamine	Gln	Q	Threonine	Thr	T
Glycine	Gly	G	Tryptophan	Trp	W
Histidine	His	H	Tyrosine	Tyr	Y
Isoleucine	Ile	I	Valine	Val	V

Index of figures

Index of tables

1 Introduction

The embryonic development is a complex process, during which a single-celled zygote transforms into a multicellular embryo that eventually will develop into an adult organism. This tremendous transformation requires a tight regulation of cell proliferation, differentiation and tissue patterning, which is achieved by the well-orchestrated action of a handful of signaling pathways. These include the Hedgehog (Hh), Wnt, Bone morphogenetic protein (Bmp) and other pathways, which are activated in response to secreted signaling molecules, acting as morphogens. The morphogens are expressed in precisely defined zones. Upon release, they form concentration gradients over several cell diameters and induce unique transcriptional responses in a dose-dependent manner, thereby coordinating organ growth and patterning. Over the last decades it has become evident that the actions of the extracellular signaling molecules are dependent on interactions with components of the extracellular matrix (ECM), particularly with heparan sulfate (HS) proteoglycans (PGs). These interactions are mediated by the negative charges of the highly sulfated HS chains and sequences of positively charged amino acids, often referred to as Cardin-Weintraub (CW) motifs (Cardin and Weintraub, 1989). Among the interacting partners of HSPGs are the members of the conserved family of Hh proteins, which regulate a large spectrum of events from early embryonic stages to adulthood (Kronenberg, 2003; Pak and Segal, 2016; Wuelling and Vortkamp, 2010). In the developing bone, Indian hedgehog (Ihh) is transported over large distances to regulate chondrocyte proliferation and differentiation. Although HSPGs have been shown to determine Ihh distribution and signaling in the tissue, the exact molecular mechanism by which this is achieved has not been uncovered so far (Koziel et al., 2004).

1.1 Endochondral ossification

Bones of the vertebrate skeleton develop by two mechanisms: intramembranous and endochondral ossification. These processes are initiated when mesenchymal cells condense to form the anlagen of the future bones, which produce Collagen type I-rich ECM (Mariani and Martin, 2003). During the process of intramembranous ossification, which is typical for the flat bones of the skull, parts of the clavicles and the craniofacial bones, mesenchymal cells directly differentiate into bone producing osteoblasts (Percival and Richtsmeier, 2013).

Most of the skeletal elements, however, develop by endochondral ossification–a multistep mechanism during which the cartilaginous templates are replaced by bone (Fig. 1. 1).

Initially, the cells in the core of a mesenchymal condensation differentiate into chondrocytes, which synthesize a Collagen type II- and Aggrecan-rich ECM. In parallel, the peripherally located cells elongate and differentiate into fibroblast-like perichondral cells, which express Collagen type I. The chondrocytes become increasingly organized into morphologically distinct subpopulations: at the distal ends of the anlagen they are small, round and proliferate at a low rate, while towards the center the cells become flattened, align into parallel, longitudinal columns and increase their proliferation rate. During this transition, the chondrocytes alter their morphology, differentiation status and gene expression profile, while still expressing high levels of Aggrecan and Collagen type II. The fast-proliferating, columnar chondrocytes eventually exit the cell cycle, mature, increase their cytoplasmic volume and differentiate into prehypertrophic-, Ihh-expressing chondrocytes (Fig. 1. 1 C, D) (Kronenberg, 2003). Once these cells have become hypertrophic, they produce a Collagen type X-rich matrix, which will allow mineralization (Jochmann et al., 2014; Wuelling and Vortkamp, 2011). Perichondral cells flanking the hypertrophic zone differentiate into osteoblasts, forming the periosteum and the bone collar. The hypertrophic chondrocytes express angiogenic factors to attract blood vessels, which invade the periosteum, and subsequently the terminal hypertrophic zone. The invasion is supported by a degradation of the ECM by the Matrix metalloproteinase 13 (Mmp13), which is expressed by terminal hypertrophic chondrocytes (Ortega et al., 2004). Subsequently, these cells undergo apoptosis, osteoclasts invade and degrade the Collagen type X-rich ECM allowing osteoblasts to form trabecular bone (Maes et al., 2010). The region of the developing bone, which is mineralized during embryonic development, is called primary ossification center. After birth, secondary ossification centers are formed at the ends of the bones (Fig. 1. 1 E). They remain separated from the primary ossification center by chondrocytes, which form the growth plate to allow postnatal bone growth.

The process of endochondral ossification is regulated by several signaling molecules, which act together to maintain the balance between chondrocyte proliferation and hypertrophic differentiation (reviewed in (Long and Ornitz, 2013; Wuelling and Vortkamp, 2010)).

These include HSPG-binding growth factors such as Bmps, Fgfs and Ihh. Malfunction in their actions can lead to mild-to-severe abnormalities in bone and skeletal development.

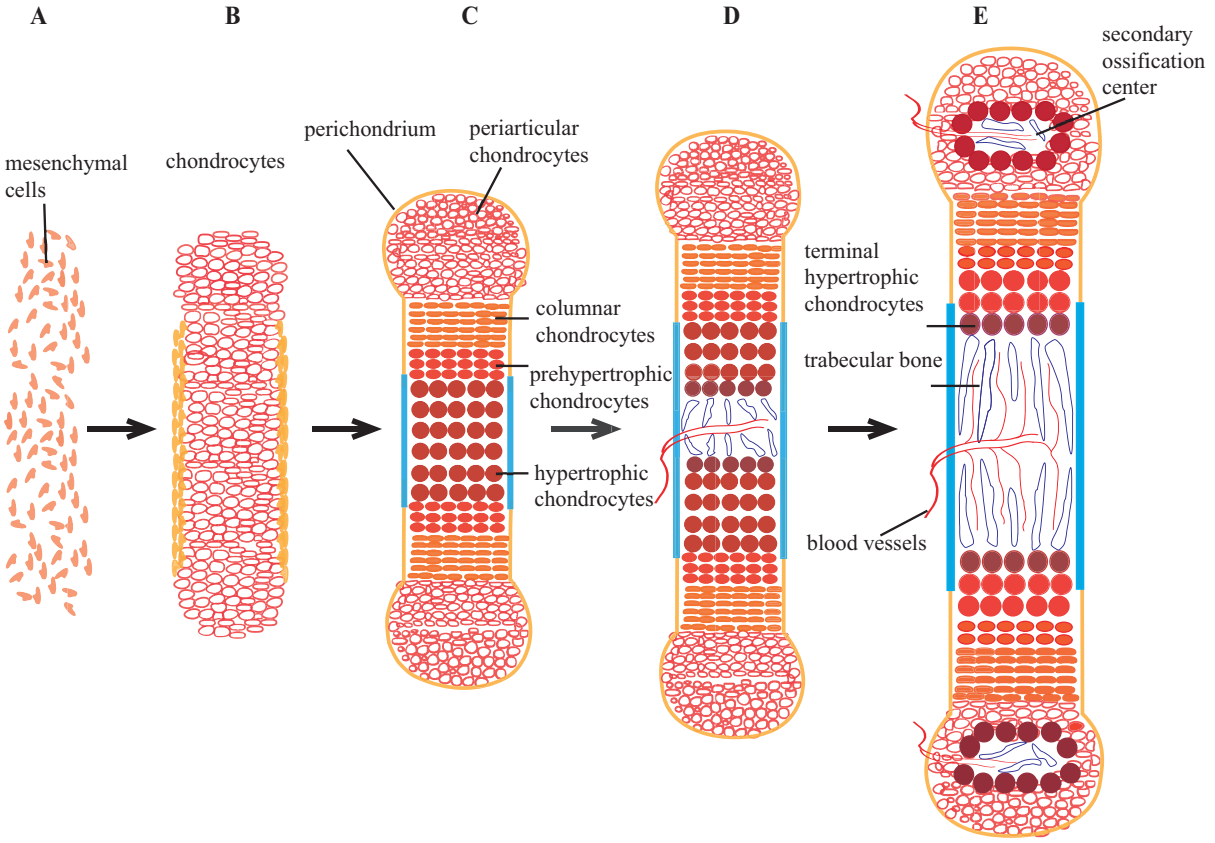

Fig. 1. 1 Schematic model of the endochondral ossification process.
Mesenchymal cells condense (A), and differentiate into chondrocytes, forming the template of the future bone (red), surrounded by perichondral cells (orange) (B). Periarticular chondrocytes (red circles) proliferate and differentiate into fast-proliferating, columnar chondrocytes (dark orange) (C). Columnar chondrocytes differentiate first to prehypertrophic (red) and then hypertrophic chondrocytes (dark red). Perichondral cells, surrounding the hypertrophic zone, differentiate into osteoblasts to form the bone collar (blue) (C, D). Blood vessels invade the periosteum and terminal hypertrophic zone, transporting osteogenic cells (D, E). Finally, the terminally hypertrophic chondrocytes undergo apoptosis allowing the osteoclasts and osteoblasts to replace the cartilage by bone. After birth, secondary ossification centers are formed at the distal ends of the bone (E). Modified after (Wuelling and Vortkamp, 2011).

1.1.1 Ihh as regulator of endochondral ossification

One of the key regulators of the endochondral ossification is Ihh, which belongs to the conserved family of Hedgehog proteins. In the developing bone Ihh is expressed by prehypertrophic chondrocytes and regulates the onset of hypertrophic differentiation, chondrocyte proliferation and osteoblast differentiation (Fig. 1. 2) (Lanske et al., 1996; St-Jacques et al., 1999; Vortkamp et al., 1996).

Ihh governs the onset of hypertrophic differentiation via a negative feedback mechanism involving the secreted growth factor Parathyroid hormone related protein (Pthrp) (Lanske et al., 1996; Vortkamp et al., 1996). In this mechanism, Ihh signals to the periarticular

chondrocytes to induce *Pthrp* expression (Koziel et al., 2004). In turn, Pthrp signals through its receptor, the Pth/Pthrp receptor (Ppr), expressed in proliferating and prehypertrophic chondrocytes. Signaling through Ppr inhibits the onset of hypertrophic differentiation and Ihh expression (Amizuka et al., 1994), thereby keeping chondrocytes in a proliferative state (Lanske et al., 1996; St-Jacques et al., 1999)(Fig. 1. 2).

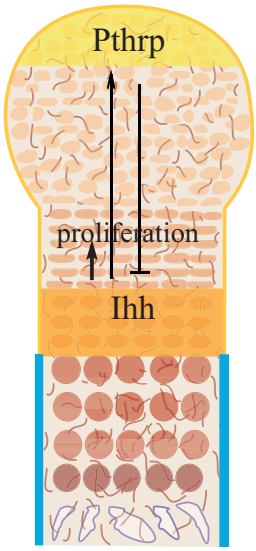

Fig. 1. 2 Ihh regulates endochondral bone formation.
Ihh is expressed by prehypertrophic chondrocytes (orange) and diffuses through the cartilage to induce the expression of *Pthrp* in periarticular chondrocytes (yellow). Pthrp signals back to prevent hypertrophic differentiation. Thus, the negative feedback loop keeps chondrocytes in a proliferative state and regulates the onset of hypertrophy. Ihh directly activates chondrocyte proliferation via its receptor Ptch, expressed by columnar chondrocytes. Modified after (Koziel et al., 2004).

Ihh regulates chondrocyte proliferation by a Pthrp-independent mechanism. *Ihh*$^{-/-}$ mice are characterized by an early onset of hypertrophic differentiation and severely reduced chondrocyte proliferation. Constitutive activation of Ppr rescues the differentiation defect in these mice but does not correct the low proliferation rate (Karp et al., 2000). This data were supported by an increased chondrocyte proliferation upon *Ihh* overexpression or constitutive activation of the Ihh receptor *Smoothened* (*Smo*) in chondrocytes and the decreased proliferation rate after deletion of *Smo* (Long et al., 2001; Minina et al., 2001).

The role of Ihh as a regulator of osteoblast differentiation is demonstrated by the absence of osteoblasts and bone collar found in Ihh deficient mice (St-Jacques et al., 1999; Vortkamp et al., 1996). In line with these data, Smo deficient perichondral cells fail to differentiate into osteoblasts (Long et al., 2004).

In summary, among the various signaling molecules regulating bone growth and development, Ihh seems to play a central role, regulating diverse processes by Pthrp-dependent and independent mechanisms.

1.2 The Hedgehog protein family

Mutations in the Hedgehog (*Hh*) gene were first described in a systematic screen in *Drosophila melanogaster* (Nusslein-Volhard and Wieschaus, 1980). The gene encodes a secreted protein, which directly regulates the patterning of the embryo. Soon after, the three mammalian homologs–Sonic hedgehog (Shh), Ihh and Desert hedgehog (Dhh), were described (Echelard et al., 1993; Riddle et al., 1993). These proteins share a high degree of identity but are expressed in different tissues, regulating a broad spectrum of developmental processes. These include ventral neural tube patterning and digit number, which are defined by Shh (Jessell, 2000; Riddle et al., 1993), while Dhh is known as a regulator of spermatogenesis and myelin sheath formation (Bitgood et al., 1996; Parmantier et al., 1999). Besides its role in bone development, Ihh stimulates primitive hematopoiesis and vasculogenesis during early embryogenesis (Becker et al., 1997; Dejana et al., 2017; Kelly and Hirschi, 2009), and is required for pancreatic development, primary gut patterning and cardiac morphogenesis (Bitgood and McMahon, 1995; Varjosalo and Taipale, 2008). In line with these, alterations in Hh signaling during embryogenesis lead to severe developmental defects such as failure in midline structure establishment, absence of distal limb elements, polydactyly and others, while in adult organisms Hh signaling has been linked to a large number of cancers (review in (Cohen, 2003; Vortkamp et al., 1991)).

1.2.1 Hedgehog signal transduction

The Hh signaling pathway is highly conserved in vertebrates and invertebrates. Hh proteins signal through a receptor complex consisting of the 12-pass transmembrane protein Ptch1 and the 7-pass transmembrane protein Smo (Motoyama et al., 1998). In absence of a ligand, Ptch1 inhibits Smo (Murone et al., 1999). As a result, the negative regulator Suppressor of Fused (Sufu) forms a complex with transcription factors of the Gli family. This interaction stabilizes the full-length form of Gli (GliFL) and sequesters it in the cytoplasm. Sufu, together with the Kinesin-2 family member Kif7, promotes phosphorylation of GliFL and its subsequent processing into a truncated repressor form (GliR). GliR translocates to the nucleus and inhibits Hh target genes (Fig. 1. 3 A) (Humke et al., 2010).

Upon binding of Hh to Ptch1 both are internalized and degraded. Ptch1 no longer inhibits Smo, which becomes phosphorylated and enters the primary cilium (Chen et al., 2011b; Pak and Segal, 2016; Shi et al., 2014). Kif7, Sufu and GliFL accumulate at the tip of the primary cilium, where Smo promotes dissociation of GliFL from the complex with Sufu. GliFL receives additional modifications resulting in the formation of Gli activator form, which shuttles to the nucleus to induce transcription of Hh target genes (Fig. 1. 3 B) (Goetz and Anderson, 2010).

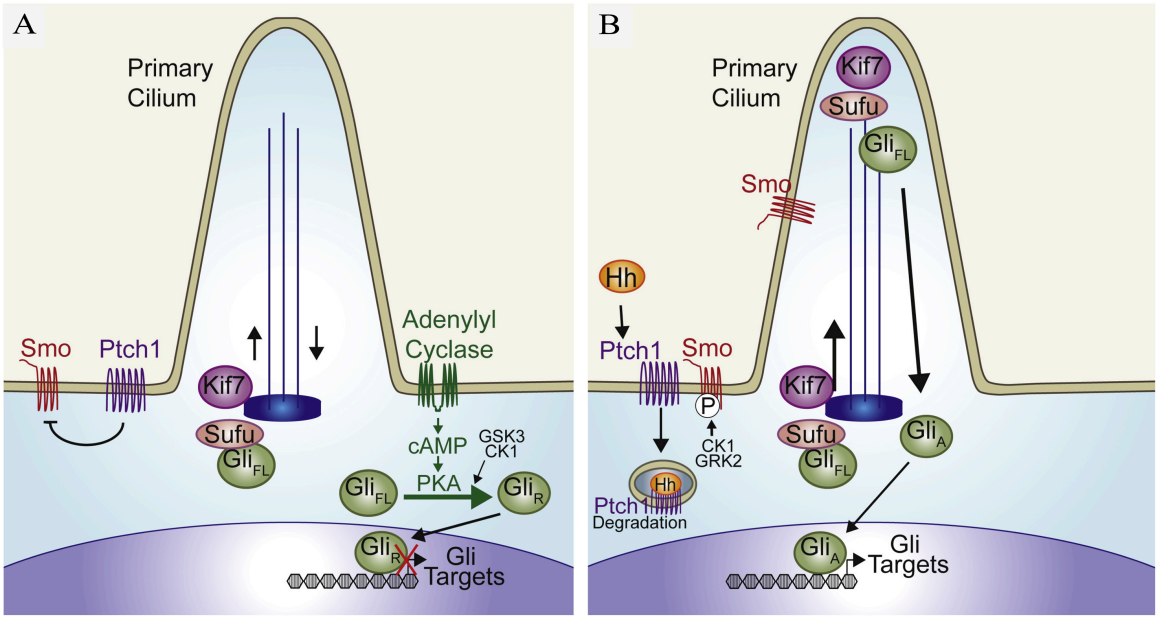

Fig. 1. 3 Hedgehog signal transduction.
In absence of Hh, Ptch1 inhibits Smo and its ciliary localization. Sufu forms a complex with GliFL and together with Kif7 promotes its phosphorylation and processing to GliR (A). Binding of Hh to Ptch1 releases the inhibition of Smo. Smo translocates to the primary cilium, where it stimulates the dissociation of GliFL from Sufu complexes. As a result, GliA is activated and translocates to the nucleus, where it induces Hh target genes (B) (Pak and Segal, 2016).

Besides Ptch1, further receptors can interact with Hh proteins and influence the activation of the pathway. These include the positive regulators Cell adhesion molecule-related/Down-regulated by Oncogenes (Cdo), Brother of Cdo (Boc) and Growth arrest specific-1 (Gas1), and the negative regulators Ptch1 and Hedgehog Interfering Protein (Hhip). The Hh activity is additionally modulated by interactions with HSPGs, which can either promote or inhibit Hh signaling making the pathway activation susceptible to alterations in ECM composition (reviewed in (Beachy et al., 2010)).

1.2.2 Hedgehog biochemistry

The Hedgehog protein is synthesized as a 45 kDa precursor, which undergoes several posttranslational modifications. The precursor contains a signaling peptide (SS) directing entry into the endoplasmic reticulum (ER), an N-terminal signaling domain ("Hedge" domain, HhN), and a C-terminal autoprocessing domain ("Hog" domain, HhC) (Fig. 1. 4). The HhC domain binds cholesterol via its sterol recognition region (SRR) and catalyzes an intein-related autoproteolytic reaction, in which a cholesterol moiety is added to the carboxy-terminus of the signaling domain (Porter et al., 1996; Porter et al., 1995). Subsequently, HhC is degraded by ER-associated degradation pathways (Chen et al., 2011a).

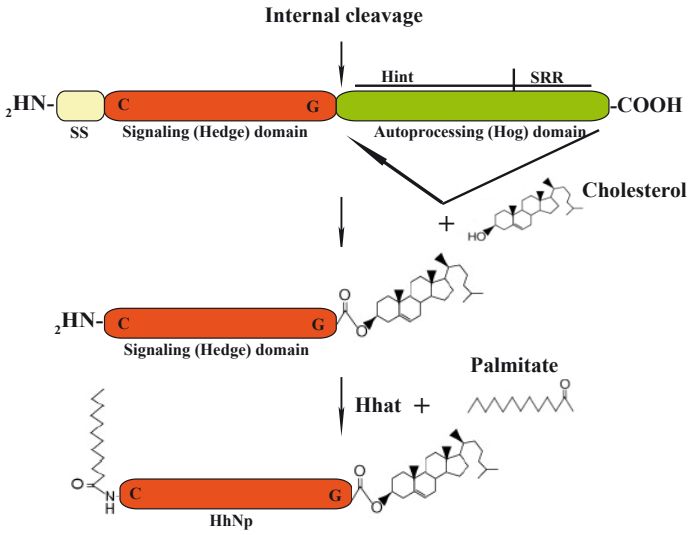

Fig. 1. 4 Hh processing reaction and lipid modifications.
The short signaling sequence (SS, yellow) directs Hh to the ER, where the protein undergoes autocatalytic cleavage catalyzed by the autoprocessing domain (HhC, green). This results in covalent coupling of cholesterol to the C-terminus of the signaling domain (HhN (red)). The second lipid modification is catalyzed by Hhat, which attaches a palmitic acid to the N-terminal cysteine of the signaling domain. Modified after (Varjosalo and Taipale, 2008). Abbr: HhNp–processed N-terminal domain, SS–signaling peptide, SRR–sterol recognition region, Hint–Hh-intein domain

The cholesterol-modified signaling domain enters the secretory pathway and undergoes a second lipid modification–a covalent attachment of palmitate (*N*-palmitoylation) to the amino-terminal cysteine residue. In mammals, the reaction is catalyzed by the transmembrane Hedgehog acyltransferase (Hhat) and requires cleavage of the signaling peptide to expose the N-terminal cysteine (Buglino and Resh, 2008, 2012; Dennis et al., 2012). The dual-lipidated N-terminal domain, called HhNp (p stands for processed) is transported and stays associated with the plasma membrane until released (Fig. 1. 4). Both lipid modifications have critical,

yet not fully understood roles in regulating the release, distribution and signaling of Hh proteins (Chen et al., 2004; Pepinsky et al., 1998).

1.2.3 Hedgehog release and transport through the tissue

Despite the initial tight association with the plasma membrane, Hh proteins exert their signaling activity over several cell diameters–in the developing limb bud, for example, Shh elicits a direct response at distance up to 300 μm from their source (Li et al., 2006; Wang et al., 2000). It is, however, not clear how the dual-lipidated protein is released and transported from the producing to the targeted cells. Several mechanisms have been proposed during the last decades (Fig. 1. 5).

1.2.3.1 Dispatched (Disp)-Scube2 regulated release

Disp is a transmembrane protein with high sequence similarity to Ptch1. It contains a sterol-sensing domain (SSD) shown to interact with the Hh cholesterol moiety, thereby regulating protein release (Burke et al., 1999). Recent findings demonstrated that Disp cooperates with the secreted protein Scube2 (Fig. 1. 5 B). Scube proteins also contain a cholesterol-interacting domain indicating a hand-over mechanism between Disp and Scube2 to release Hh proteins (Creanga et al., 2012; Tukachinsky et al., 2012).

1.2.3.2 HhN-oligomer formation

It has been established that Hh proteins accumulate into multimeric structures prior to their release (Fig. 1. 5 C) (Chen et al., 2004; Dierker et al., 2009a; Farshi et al., 2011; Vyas et al., 2008; Zeng et al., 2001). The exact mechanism of multimer assembly remains, however, unclear. Various studies of Shh have identified several amino acids to be crucial for the multimerization, including R33, L37, E71, R72, K74, R123, D152 and R155 (Shh, human nomenclature) (Chang et al., 2011; Farshi et al., 2011; Ohlig et al., 2011). Further reports have stated that sequestration of the C- and N-terminal lipids into the interior of micellous structures is a prerequisite for multimer assembly and release (Chen et al., 2004; Goetz et al., 2006; Zeng et al., 2001). In contrast, a recent study proposed a model of self-driven multimer formation, supported by the law of mass action. In this setup, the fatty acid and sterol do not play crucial role in the process, but likely augment the size of the complex by keeping the proteins tethered to the plasma membrane, thereby increasing their local concentration

(Koleva et al., 2015). Whether additional factors are involved in the process needs to be further investigated.

1.2.3.3 Lipoprotein-mediated Hh release

Experiments by Panakova and colleagues indicated that in *Drosophila* imaginal discs Hh associates with the lipoprotein Lipophorin (Lpp) to form complexes, which move with the hemolymph to promote Hh long-range signaling (Fig. 1. 5 D) (Panakova et al., 2005). Later studies, however, reported a release of two different Hh forms in the wing disc–a cholesterol-modified, Lpp-associated form and a cholesterol- and Lpp-free form. Notably, each of these forms was unable to activate Hh responsive genes, unless acting synergistically (Palm et al., 2013).

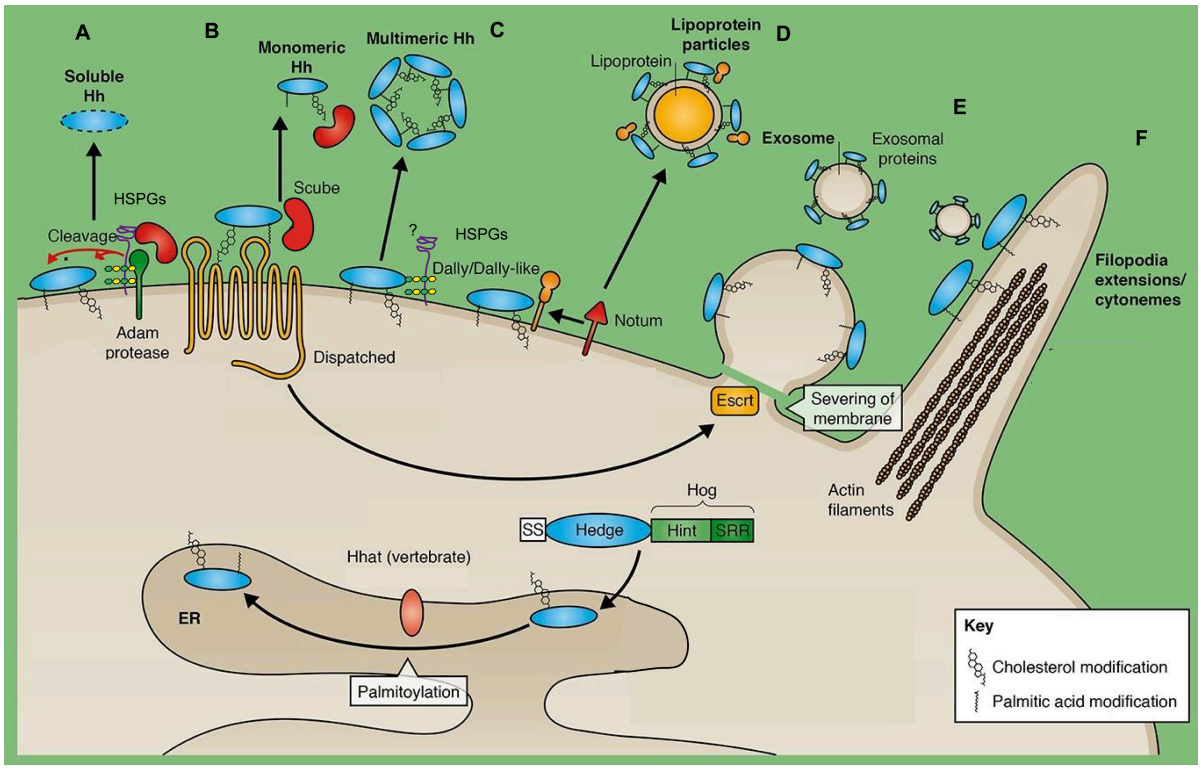

Fig. 1. 5 Models for Hh release and transport.
The cholesterol-binding protein Scube2 cooperates with HSPGs to induce sheddases-mediated Hh release (A) or acts with Disp in a hand-over mechanism of release (B). Hh organizes in multimers, which process is likely mediated by HSPGs prior to release (C). HSPGs recruit lipoprotein-Hh complexes, which are later solubilized by cleavage (D). Hh is released via ESCRT dependent exosomes either from the plasma membrane (E), or from cytonemes (F). Modified after (Lee et al., 2016). Abbr: SS–signaling peptide, ER–endoplasmic reticulum, Hhat–Hh acyltransferase, HSPGs–heparan sulfate proteoglycans, Hh–hedgehog, ESCRT–endosomal sorting complex required for transport.

1.2.3.4 Contribution of exosomes and cytonemes to Hh release and transport

A more recent model proposes that the dual-lipidated Hh molecules are released and transported in membrane vesicles called exosomes (Fig. 1. 5 E). Several studies in the *Drosophila* imaginal disc point to a dependence of Hh secretion and signaling on ESCRT (endosomal sorting complex required for transport) machinery (Gradilla et al., 2014; Matusek et al., 2014). Additionally, exosome-associated Shh has been detected in cultured human and primary chicken notochord cells (Vyas et al., 2014).

The exosome-dependent gradient formation of Hh might be supported by cytonemes–filopodia-like cellular extensions (Fig. 1. 5 F) (Gradilla et al., 2014), as Hh proteins and components of the Hh pathway have been detected on these cellular protrusions in *Drosophila* wing disc and in developing chicken limb bud by *in vivo* imaging (Bischoff et al., 2013; Sanders et al., 2013). Nevertheless, more extensive studies, besides *in vivo* imaging would be necessary to confirm a role of cytonemes in Hh transport to the receiving cells.

1.2.3.5 HSPG-mediated release and diffusion

Several lines of evidence suggest that HSPGs regulate Hh release and transport through the tissue and shape their concentration gradient. In *Drosophila*, loss of HS or HSPGs critically impairs Hh gradient formation and signaling (Bellaiche et al., 1998; The et al., 1999). In the developing bone, HS restricts the distribution of Ihh and low HS levels or an altered sulfation pattern increase the propagation of the signaling molecule (Dierker et al., 2016; Koziel et al., 2004). Although it is quite clear that HSPGs have a central function in Hh release and distribution, the molecular mechanism by which they regulate Hh biology has not been uncovered so far. Nonetheless, in all proposed mechanisms for Hh release and distribution HSPGs seem to play an indispensable role. Several lines of evidence have shown that the protein multimerization is mediated by an interaction of Hh with HSPGs (Dierker et al., 2009a; Rubin et al., 2002). In agreement with this, most of the residues involved in the multimerization are found in the HS-binding motifs of the protein (Farshi et al., 2011; Ohlig et al., 2011; Rubin et al., 2002). Moreover, analysis of Hh multimerization in *Drosophila* revealed a stepwise process, in which Hh monomers organize first in nanoscale clusters, which then interact with cell surface HSPGs to form larger complexes (Vyas et al., 2008).

HSPGs have been shown to regulate A disintegrin and metalloprotease (ADAM)-mediated shedding of Shh from its lipidated N- and C-termini, which results in solubilization of the protein (Dierker et al., 2009b; Ohlig et al., 2011; Ohlig et al., 2012; Ortmann et al., 2015).

Further development of this model implicated that Scube2 acts as an activator of sheddases, while HSPGs provide a "platform" for binding of Shh, sheddases and their activator Scube2, thereby underpinning the protein release (Fig. 1. 5 A) (Jakobs et al., 2014; Jakobs et al., 2016; Ortmann et al., 2015). Moreover, HSPGs have been described to recruit lipophorin particles carrying Hh in a model for lipoprotein-mediated Hh transport (Fig. 1. 5 D)(Eugster et al., 2007)

A recent study has proposed that HSPGs along with other ECM components stabilize and steer cytonemes carrying Hh and other signaling molecules through the tissue (Huang and Kornberg, 2016).

Taken together these findings indicate that ECM has a crucial role in regulating the distribution and signaling activity of Hh. Further aspects of this complex regulation are yet to be uncovered.

1.3 The extracellular matrix

The ECM is a complex and highly organized network of locally synthesized macromolecules, which provides not only a physical scaffold for the cells, but also regulates multiple cellular processes including cell growth, migration, differentiation, and tissue homeostasis (Clause and Barker, 2013; Frantz et al., 2010). The ECM composition is highly variable and has evolved to serve the unique physical and signaling requirements of each specific tissue at particular developmental stages.

The ECM has two major components–fibrous proteins and proteoglycans (PGs). Collagens are the major fibrous proteins in the ECM, providing elasticity, flexibility and tensile strength to the tissue. These functions are reinforced by non-collagenous proteins like Laminins, Fibronectins, Elastins and others (Theocharis et al., 2016).

The PGs provide hydration and compressive resistance to the tissue (Mouw et al., 2014). Based on their subcellular localization, PGs have been divided into four groups: intracellular PGs–represented only by serglycin, the cell surface PGs (membrane-spanning and glycosylphosphatidylinositol (GPI)-anchored PGs), pericellular PGs and such that are secreted into the extracellular space (Fig. 1. 6) (Bishop et al., 2007; Theocharis et al., 2016).

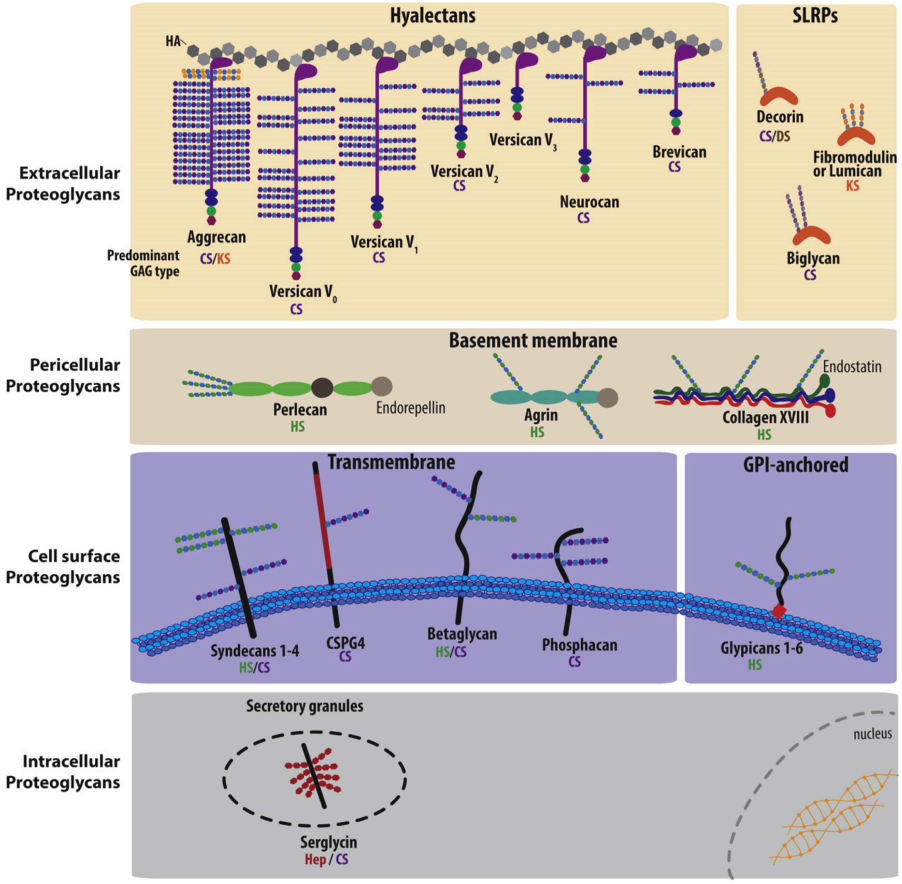

Fig. 1. 6 Schematic representation of the major PG classes.
Based on their subcellular localization PGs are divided into four groups: extracellular, predominantly Chondroitin sulfate (CS) carrying PGs, pericellular PGs carrying HS chains, cell surface-bound PGs, including the membrane spanning and the GPI-anchored PGs; and Serglycin–the only intracellular PG (Theocharis et al., 2016). Abbr: PG–proteoglycan, CS–chondroitin sulfate, KS–keratan sulfate, DS–dermatan sulfate, GPI–glycosylphosphatidylinositol.

1.3.1 PG composition

PGs are composed of a core protein carrying one or more highly acidic and hydrated glycosaminoglycan (GAG) chains. The chains consist of repeating disaccharide units, which contain *N*-acetylated hexosamines and $_{D/L}$-hexuronic acid, or $_{D}$-galactose (Gal) (Esko and Selleck, 2002; Jochmann et al., 2014). Based on their structural characteristics GAGs have been divided into two main groups. The first group consist of the galactosaminoglycans Chondroitin Sulfate (CS) and Dermatan Sulfate (DS), which are composed of *N*-acetylgalactosamine (GalNAc) and glucuronic acid (GlcA) (Fig. 1. 7 A, B). The second group comprises the glucosaminoglycans Heparan sulfate (HS) and Heparin–a highly sulfated version of HS, consisting of *N*-acetylglucosamine (GlcNAc) and GlcA, and Keratan sulfate (KS), which contains GlcNAc and Gal (Fig. 1. 7 C, D). Several enzymes, mainly

sulfotransferases, modify the GAG chains, which results in tissue- and age-specific modification patterns of the chains (Fig. 1. 7).

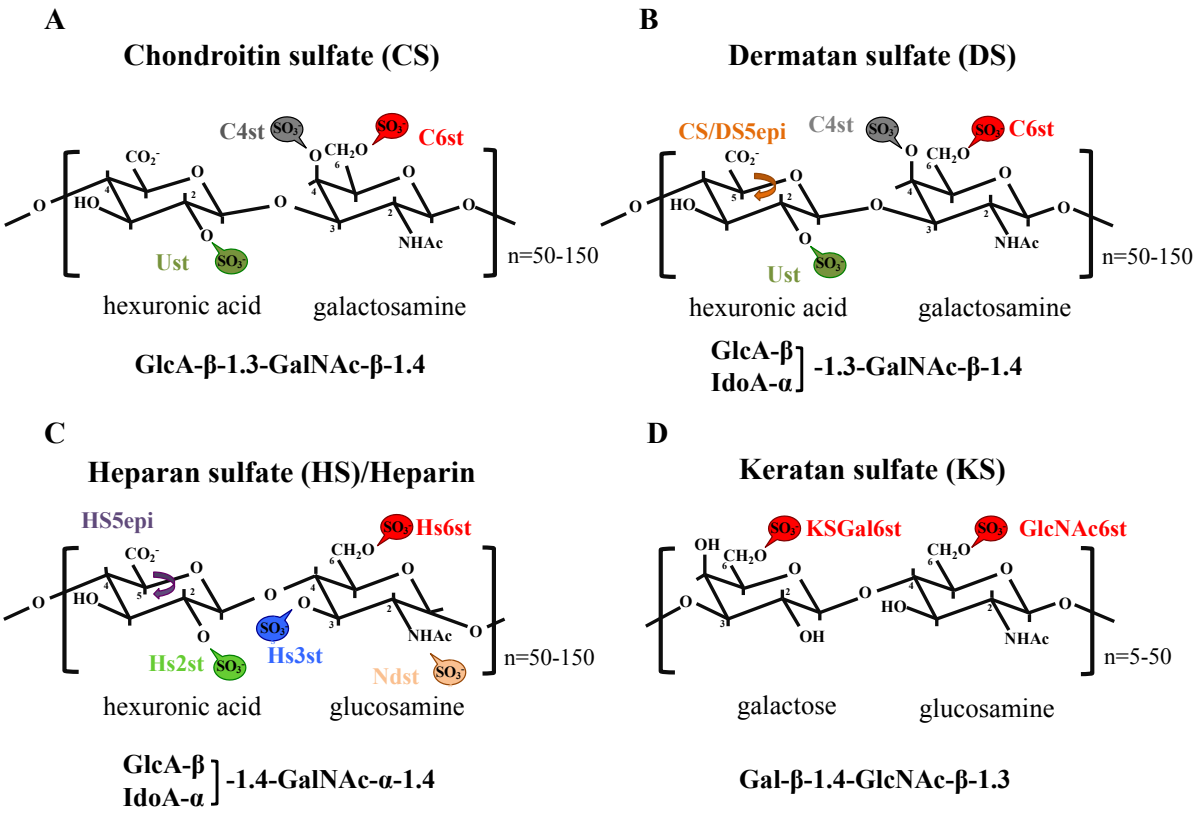

Fig. 1. 7 Chemical structures of the GAG disaccharide units.
Based on their disaccharide structure, GAGs are organized into two main groups. CS and DS belong to the galactosaminoglycans, while HS/Heparin, and KS are glucosaminoglycans. The modifications, specific for each GAG type are color indicated. Modified after (Bulow and Hobert, 2006). Abbr: Gal, Galactose; GlcNAc, *N*-acetylglucosamine; GalNAc, *N*-acetylgalactosamine; GlcA, glucuronic acid; IdoA, iduronic acid; Ndst, *N*-deacetylase-*N*-sulfotransferase; HS5epi, HS glucuronyl-C5-epimerase Hs2st, HS 2-*O*-sulfotransferase; Hs3st, HS 3-*O*-sulfotransferase; Hs6st, HS 6-*O*-sulfotransferase; C4st, CS 4-*O*-sulfotransferase; C6st, CS 6-*O*-sulfotransferase; Ust, CS/DS 2-*O*-sulfotransferase; CS/DS5epi, CS/DS glucuronyl-C5-epimerase; KSGal6st, KS-galactose 6-*O*-sulfotransferase.

PGs can carry one or more GAG chains, which are not necessarily of the same type (Bishop et al., 2007). CS carriers, like Versicans and the typical for the cartilage Aggrecan, are mostly extracellular PGs, while HS carrying PGs are located at the plasma membrane or in the pericellular space, like Glypicans and Perlecan, respectively. PGs and the fibrous ECM proteins form a three-dimensional structure, providing binding domains for plethora of extracellular proteins like growth factors, morphogens, chemokines and cytokines, thereby regulating cellular physiology and homeostasis (Sarrazin et al., 2011; Theocharis et al., 2016).

1.3.2 HS and CS biosynthesis

The assembly of HS and CS chains is initiated in the ER and completed in the Golgi apparatus using nucleotide sugars, imported from the cytoplasm. Despite the differences in the polysaccharide backbone, the syntheses of HS and CS share a common step. Both processes are initiated by the addition of a tetrasaccharide linker to a specific serine residue of the core protein (Fig. 1. 8). The linker is composed of a xylose, two Gal and GlcA residues, which are attached to the core protein in the Golgi apparatus. The addition of the first hexosamine commits the biosynthesis to either HS or CS. GlcNAc (α1–4) addition catalyzed by the enzyme Exostosin like glycosyltransferase 3 (Extl3) will initiate HS chains, while the addition of GalNAc (β1–4) catalyzed by the Chondroitin sulfate *N*-acetylgalactosaminyltransferases CSGalNAct1 and CSGalNAct2 will result in synthesis of CS (Esko and Selleck, 2002; Silbert and Sugumaran, 2002).

The polymerization of HS chains is catalyzed by a heteromeric complex of the glycosyltransferases Exostosin (Ext) 1 and Ext 2, which adds alternating units of GlcNAc and GlcA (Lind et al., 1998). Each enzyme posses combined β1–4 glucuronosyltransferase and α1–4 *N*-acetylglycosaminyltransferase activities, however, an Ext1-Ext2 complex has an augmented glycosyltransferase activity (Senay et al., 2000). In parallel to their synthesis, the HS chains are modified by several sulfotransferases and an epimerase (Bishop et al., 2007; Esko and Selleck, 2002; Sarrazin et al., 2011). The first modification is an *N*-deacetylation and *N*-sulfation of GlcNAc residues, which is catalyzed by the enzymes *N*-deacetylase-*N*-sulfotransferases (Ndst) 1-4. This process is incomplete along the chain, leading to the formation of highly sulfated domains (NS) separated by unmodified *N*-acetylated (NA) stretches. The enzyme $_{D}$-glucuronyl-C5-epimerase (Glce) catalyzes the conversion of many, but not all GlcA residues to $_{L}$-iduronic acid (IdoA), most of which are sulfated at 2-*O*-position by a 2-*O*-sulfotransferase (Hs2st). Additionally, sulfations can occur at 3-*O*- and 6-*O*-position of GlcNAc/GlcNS residues, catalyzed by the sulfotransferases Hs3st (1–6), and Hs6st (1–3), respectively (Esko and Lindahl, 2001; Kreuger and Kjellen, 2012).

The complexity of the HS structure is further increased by the activity of the secreted 6-*O*-endosulfatases Sulf1 and Sulf2, which remove sulfate groups from 6-*O*-position of GlcNAc/GlcNS residues, once the chain has been transported to the cell surface (Ai et al., 2006).

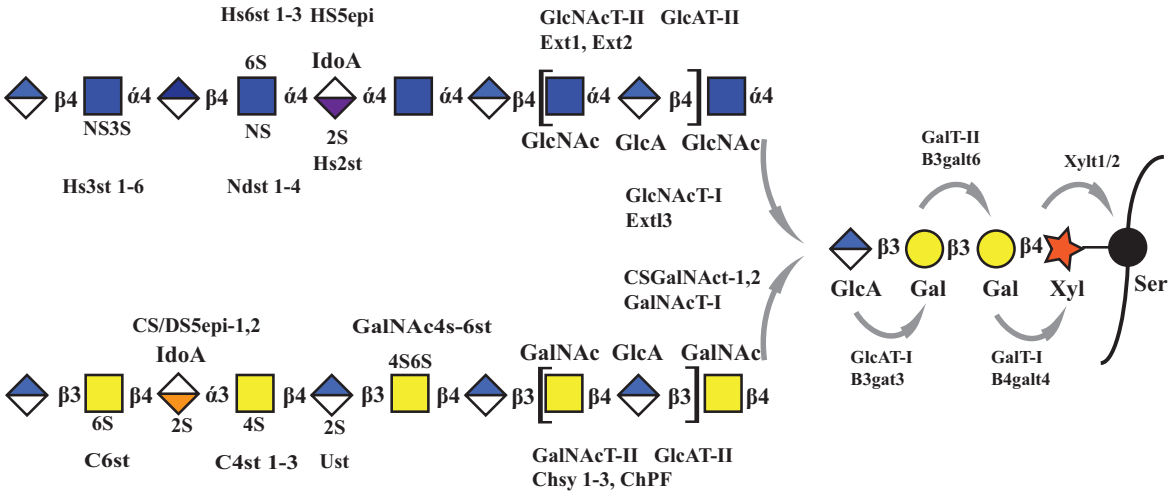

Fig. 1. 8 CS and HS chains share a common tetrasaccharide primer.
HS and CS syntheses are initiated by the addition of a tetrasaccharide primer to a serine (Ser) residue of the core protein. The fifth nucleotide sugar commits the synthesis to either CS or HS chains. The synthesis and modification of these GAGs are catalyzed by distinct sets of enzymes. The chain modifications and corresponding enzymes are indicated. Modified after (Bulow and Hobert, 2006). Abbr Xyl, Xylose; NA, *N*-acetylated; NS, *N*-sulfated; GalNAcT, galactosaminyltransferase; XylT, xylosyltransferase; GalT, galactosyltransferase; GlcAT, glucuronyltransferase; GlcNAcT, glucosaminyltransferase.

Different set of enzymes orchestrates the assembly and modification of the CS backbone. The CS chain consists of alternating GalNAc and GlcA units, which are added to the growing chain by Chondroitin sulfate synthases–Chsy 1-3 and a Chondroitin polymerization factor (Chpf). Each of these enzymes posses combined β1–3 glucuronosyltransferase and β1–4 *N*-acetylgalactosaminyltransferase activities, but cannot polymerize the chain by themselves. The chain polymerization is achieved by the cooperative activity of at least two of the four enzymes (Kitagawa et al., 2003; Kitagawa et al., 2001; Mikami and Kitagawa, 2013). Multiple sulfotransferases create a unique modification pattern by adding sulfate groups at various positions. The activity of Chondroitin 4-*O*-sulfotransferases (C4st) 1-3 and Chondroitin 6-*O*-sulfotransferase (C6st) results in the CS unit A (GlcA-GalNAc(4S)) and C (GlcA-GalNAc(6S)), respectively. Additional sulfation of each of these units leads to D and E unit formation. The uronyl 2-*O*-sulfotransferase Ust catalyzes 2-*O*-sulfation of the GlcA residue in unit C, resulting in the disulfated unit D (GlcA(2S)-GalNAc(6S)), while an activity of the GalNAc4-sulfate-6-*O*-sulfotransferase (GalNAc4S-6ST) adds a sulfate group at 6-*O*-

position of the unit A, modifying it to an E unit (GlcA-GalNAc(4,6S)) (Mikami and Kitagawa, 2013). Two D-glucuronyl C5-epimerases transform the molecule into the stereoisomer DS, which is modified by the same set of enzymes.

The expression of the HS and CS synthesizing and modifying enzymes is tightly regulated to generate tissue-specific levels and sulfation patterns of the GAGs, which is critical for the activity of numerous signaling molecules, including Ihh (Cortes et al., 2009; Dierker et al., 2016; Grobe et al., 2005; Koziel et al., 2004; Li et al., 2003).

1.3.3 HS as a regulator of Ihh signaling during bone development

During the last decades, various mouse strains carrying inactivating alleles of HS synthesizing and modifying enzymes have been developed. Besides the developmental abnormalities affecting other organs, these mutants exhibit a large variety of skeletal defects, many of which might be linked to an aberrant Ihh signaling (reviewed in (Jochmann et al., 2014)). The low HS level in the *Ext1*$^{gt/gt}$ mouse, which carries a hypomorphic allele of *Ext1* (Mitchell et al., 2001) results in skeletal defects including short stature, shortened fore- and hindlimbs and joint fusions (Koziel et al., 2004). Molecular analyses revealed that the reduced HS level in these mice leads to an augmented propagation of Ihh. Consequently, chondrocyte proliferation and *Pthrp* expression are increased, indicating an increased Ihh signaling. Importantly, Ihh propagation in the cartilage seems to be specifically regulated by HS, since CS failed to rescue the mouse phenotype in an explant culture experiment (Koziel et al., 2004). Inactivation of *Ext1* in limb mesenchyme or in joint-specific progenitors and perichondral cells leads to a disturbed endochondral ossification, which has been linked to alterations in Bmp signaling (Huegel et al., 2013; Matsumoto et al., 2010; Mundy et al., 2011). Nevertheless, a conditional ablation in *Gdf5-Cre;Ext1*$^{f/f}$ mutants leads to aberrant Ihh and Wnt signaling as well (Mundy et al., 2011).

The role of HS sulfation pattern for chondrocyte differentiation has been less well examined *in vivo*. The impaired mandibular and temporomandibular joint formations in *Ndst1*$^{-/-}$ mutants have been linked to an increased Ihh diffusion (Yasuda et al., 2010). Additionally, these mice are characterized by midline defects, impaired craniofacial and skeletal development, which have been related to a low binding affinity of Shh and Fgf to the mutant HS (Grobe et al., 2005; Pallerla et al., 2007). Moreover, a reduced Ihh binding to HS resulting in increased protein distribution and Ihh signaling has been demonstrated for the *Glce* deficient mice (Dierker et al., 2016), while *Sulf1*$^{gt/gt}$*;Sulf2*$^{gt/gt}$ compound mutants, which carry hypomorphic

alleles for the either enzyme, showed an accelerated hypertrophic differentiation, which agrees with reduced Ihh signaling (Ratzka et al., 2008; Ratzka et al., 2010). In summary, these data demonstrated that Ihh signaling requires specific HS levels and sulfation pattern.

1.4 Heparan sulfate–Hedgehog protein interaction

HS interacts and modulates the activity of numerous secreted proteins, including the members of the Hh family. Numerous studies have been performed to identify the HS-binding protein domains and have shown that these interactions are mediated by motifs of positively charged amino acids, called CW motifs (Cardin and Weintraub, 1989). These domains share the characteristic signatures XBBXBX or XBBBXXBBX, where B stands for a positively charged residue and X–for any residue. Among the first identified proteins containing a CW motif were the Fgfs, for which XBXGXXBBG has been described as a consensus binding sequence (Luo et al., 1998). A CW sequence has been identified in Shh (Farshi et al., 2011; Rubin et al., 2002), which is located in the N-terminus of the protein. The motif has the consensus sequence BBBXXBB and is highly conserved in all Hh family members. Despite the high conservation, the motif differs between the three mammalian Hh paralogs by the number of proline, arginine and lysine residues. Such differences are likely to affect the motif conformation raising the question, whether the CW composition defines essential differences in the mode of HS interaction of each paralog (Billings and Pacifici, 2015).

Other studies on the subject described an additional, discontinuous CW motif located in the globular domain of Shh (Whalen et al., 2013). This motif is composed of the amino acids K88, E124, R154 and R156 and K178 (Shh, human nomenclature). Both sequences were confirmed to mediate binding of Shh to HS (Chang et al., 2011; Farshi et al., 2011; Whalen et al., 2013).

In contrast to Shh, little is known of how Ihh interacts with HS and how this regulates the protein propagation and signaling. Taking into account the critical role of HS and ECM composition in Ihh signaling (Cortes et al., 2009; Koziel et al., 2004), it is important to get deeper insight into the exact molecular mechanisms that regulate the interaction.

2 Aim of the study

Ihh is a member of the conserved family of Hh proteins, governing large spectrum of developmental events during embryogenesis and tissue homeostasis in adults. One of the key functions of Ihh is regulation of chondrocyte proliferation and differentiation during the multistep process of endochondral ossifications. During this process, Ihh cooperates with several interacting partners to assure proper coordination of bone development. The extracellular HSPGs have been identified among the binding partners of Hh proteins, including Ihh. These interactions are mediated by positively charged amino acid sequences of the protein and the negative charge of the highly sulfated HS chains. For the closely related Shh, two conserved HS-binding motifs, regulating HS interaction and protein multimerization have been recently described (Farshi et al., 2011; Rubin et al., 2002; Whalen et al., 2013), which are present in Ihh as well. Despite the numerous studies, which have shown that the HS regulates Hh activity, the mechanisms by which this is achieved are poorly understood.

The aim of the current work is a detailed analysis of the molecular mechanisms mediating Ihh-HS interaction and protein multimerization, and the role of HS in regulating Ihh signaling, bone development and ECM integrity.

To answer these questions, the relevant for the HS-Ihh interaction amino acid residues will be identified and their role in Ihh binding will be evaluated by mutation analysis and heparin/HS affinity chromatography. Size-exclusion chromatography will be employed to study the role of the identified motifs in protein multimerization.

Several studies have shown that Ihh signaling is altered upon changes in HS sulfation pattern. Therefore, the HS motifs, which are crucial for the binding of Hh proteins, will be analyzed by affinity chromatography using HS of mice, which lack specific HS modifications. Whether the multimerization process is dependent on the HS sulfation pattern will be investigated in primary chondrocytes, lacking HS synthesizing or modifying enzymes.

Despite the high identity between Shh and Ihh, their N-terminal HS-binding domains differ, suggesting that the paralogs may vary in their affinity to HS. The importance of these differences for the interaction with HS and protein multimerization will be studied by exchanging the binding motif of the proteins.

Importantly, the effect of alterations in HS levels and modification pattern on the ECM structure, and their role in the embryonic development will be investigated by combining

histological, immunofluorescence and structural analyses of the GAG composition in mice with deficiency in the HS structure.

The data obtained in this study will enrich the knowledge about Ihh biochemistry, and the role of HS in Ihh biology and ECM homeostasis.

3 Materials and Methods

3.1 Materials

All reaction buffers were prepared in MilliQ™ purified water. The pH was adjusted using NaOH or HCl. Reaction tubes, laboratory glassware and pipette tips were steam sterilized prior use. Bacterial media and buffers were subjected to steam sterilization or sterile filtration. Disposable cell culture consumables were purchased as gamma sterilized products from Corning (Amsterdam).

All chemicals used in this work were purchased from AppliChem (Darmstadt), Merck (Darmstadt), Roth (Karlsuhe) and Sigma-Aldrich (Munich) if not indicated otherwise.

3.1.1 Chemicals

Chemical	Manufacturer
4-(2-Hydroxyethyl)piperazine-1-ethanesulfonic acid (HEPES)	Roth (Karlsruhe)
4', 6-diamidino-2-phenylindole (DAPI)	Sigma-Aldrich (Munich)
Ace Glow™-Solution Chemiluminiscence Substrate	Peqlab (Erlangen)
Acetic acid	VWR Chemicals (Darmstadt)
Acetone	Bernd Kraft (Dusiburg)
Acrylamide 4K solution (30%), 37.5:1	Serva (Heidelberg)
Adenosine 5'-triphosphate (ATP)	Thermo Scientific (Dreieich)
Agar-Agar	Roth (Karlsruhe)
Agarose	Serva (Heidelberg)
Albumin Factor V	AppliChem (Darmstadt)
Ammonium Persulfate (APS)	AppliChem (Darmstadt)
Ammonium sulfamate ($NH_4SO_3NH_2$)	Sigma-Aldrich (Munich)
Ampicillin	Calbiochem (Bad Soden)
Bacto-Yeast Extract	BD Difco (Heidelberg)
Barium nitrite monohydrate ($Ba(NO_2)_2.H_2O$)	Sigma-Aldrich (Munich)
Blue Dextran 2000	GE Healthcare Life Sciences (Freiburg)
Bromphenol blue sodium salt	Roth (Karlsruhe)
Carbazole	Sigma-Aldrich (Munich)
Coomassie brilliant blue R250	Roth (Karlsruhe)
Deoxynucleotide (dNTP) Solution Set	Thermo Scientific (Dreieich)

Dextran sulfate	Sigma-Aldrich (Munich)
Diethanolamine	Roth (Karlsruhe)
Dimethyl sulfoxide (DMSO)	Acros Organics (Geel)
DPX-Mounting Medium	Fluka (Deisenhofen)
Ethanol	VWR (Darmstadt)
Ethanolamine	Roth (Karlsruhe)
Ethidium bromide	Calbiochem (Bad Soden)
Ethylenediamine-tetraacetic acid (EDTA)	AppliChem (Darmstadt)
Glycerol	AppliChem (Darmstadt)
Glycin	AppliChem (Darmstadt)
Heparin-agarose beads, type I	Sigma-Aldrich (Munich)
Hydrogen peroxide (30%)	Bernd Kraft (Dusiburg)
Isopropanol	VWR (Darmstadt)
Kanamycin	Calbiochem (Bad Soden)
Magnesium sulfate ($MgSO_4$)	AppliChem (Darmstadt)
Magnesiumchloride ($MgCl_2$)	Merck-Millipore (Darmstadt)
Methanol	Fischer Scientific (Schwerte)
Methyl green	Sigma-Aldrich (Munich)
Monopotassium phosphate (KH_2PO_4)	AppliChem (Darmstadt)
Monosodium phosphate (NaH_2PO_4)	Roth (Karlsruhe)
Mowiol mounting medium	Sigma-Aldrich (Munich)
$Na_2{}^{35}SO_4$ (NEX 041H)	Perkin-Elmer (Waltham, USA)
Optiphase HiSafe Scintillation cocktail	PerkinElmer (Waltham, USA)
OrangeG	Sigma-Aldrich (Munich)
p-Nitrophenyl Phosphate disodium salt hexahydrate (PNPP)	Roth (Karlsruhe)
Packard ^{3}H Water	Perkin-Elmer (Waltham, USA)
Paraffin-paraplast	Sherwood Medical Co, (USA)
Paraformaldehyde (PFA)	Merck (Darmstadt)
Pierce ECl Western Blot Substrate	Thermo Scientific (Dreieich)
Potassium acetate (CH_3CO_2K)	AppliChem (Darmstadt)
Potassium chloride (KCl)	AppliChem (Darmstadt)
SafraninO	Roth (Karlsruhe)
Skimmed milk powder	AppliChem (Darmstadt)
Sodium acetate ($C_2H_3NaO_2$)	Merck (Darmstadt)
Sodium carbonate (Na_2CO_3)	AppliChem (Darmstadt)

Sodium chloride (NaCl)	Roth (Karlsruhe)
Sodium dodecyl sulfate (SDS), p.a.	Sigma-Aldrich (Munich)
Sodium hydrogen carbonate ($NaHCO_3$)	Roth (Karlsruhe)
Sodium nitrite ($NaNO_2$)	Sigma-Aldrich (Munich)
Sodium tetraborate ($Na_2B_4O_7 \cdot 10H_2O$)	Roth (Karlsruhe)
Sulfuric acid (H_2SO_4)	VWR (Darmstadt)
Tetramethylethylendiamin (TEMED)	AppliChem (Darmstadt)
Trichloracetic acid (TCA)	AppliChem (Darmstadt)
Tris-base	AppliChem (Darmstadt)
Tris-HCl	AppliChem (Darmstadt)
Triton X-100	AppliChem (Darmstadt)
Tryptone	BD Difco (Detroit)
Tween-20	AppliChem (Darmstadt)
Water, HPLC grade	Sigma-Aldrich (Munich)
Weigert solutions A and B	Roth (Karlsruhe)
Xylene	Roth (Karlsruhe)
β-Mercaptoethanol 98%	AppliChem (Darmstadt)

3.1.2 Enzymes

Enzyme	Concentration	Manufacturer
Benzonase	29 U/ µl	Merck Millipore (Darmstadt)
Chondroitinase ABC	2 U/µl	Sigma-Aldrich (Munich)
Collagenase NB4	0.3 U/ml	Serva (Heidelberg)
DNaseI, RNase free	10 U/µl	Roche (Mannheim)
Dream Taq Polymerase	5 U/µl	Thermo Scientific (Dreieich)
FastAP Thermosensitive Alkaline Phosphatase	1 FDU/µl	Thermo Scientific (Dreieich)
FastDigest Restriction enzymes	1 FDU/µl	Thermo Scientific (Dreieich)
Heparitinases (heparin lyses) I, II, III	0.1 U/ µl	IBEX Pharmaceuticals (Montreal)
Hyaloronidase	100 U/ml	Sigma-Aldrich (Munich)
KOD Hot Start DNA Polymerase	2 U/µl	Calbiochem (Bad Soden)
Neutral protease	1 U/ml	Serva (Heidelberg)
Pronase	10 mg/ml	Sigma-Aldrich (Munich)

Proteinase K	10 mg/ml	Roche (Mannheim)
RNase	10 mg/ml	Roche (Mannheim)
T4-DNA-Ligase	5 U/µl	Thermo Scientific (Dreieich)
Trypsin-EDTA	0.5%	Life technologies (Darmstadt)

3.1.3 Kits

Kit	Manufacturer
DirectPCR-Tail	PeqLab (Erlangen)
Gel Filtration Calibration Kit HMW	GE Healthcare Life Sciences (Freiburg)
Gel Filtration Calibration Kit LMW	GE Healthcare Life Sciences (Freiburg)
jetPrime DNA Transfection Reagent	Polyplus-Transfection (Illkirch Cedex)
KOD Hot Start DNA Polymerase Kit	Calbiochem (Bad Soden)
My-Budget Double Pure Kit	Bio-Budget (Krefeld)
NucleoSpin Extract II	Macherey-Nagel (Düren)
Pierce™ DAB Substrate Kit	Thermo Fischer Scientific (Dreieich)
QIAGEN Plasmid Midi Kit	Qiagen (Hilden)
QuikChange® II XL Site- Directed Mutagenesis Kit	Agilent Technologies (Böblingen)
TOPO-TA Cloning Kit	Life Technologies (Darmstadt)

3.1.4 Molecular markers

Name	Distributor
1kb DNA ladder	Fermentas (Dreieich)
100 bp DNA ladder	Fermentas (Dreieich)
PageRuler™ Prestained Protein Ladder	Thermo Fischer Scientific (Dreieich)

3.1.5 Chromatographic media and columns

Product	Method	Manufacturer
Diethylaminoethyl (DEAE)™ – Sephacel®	Ion-Exchange Chromatography	Sigma-Aldrich (Munich)
HiTrap™ Heparin HP	Affinity Chromatography	GE Healthcare Life Sciences (Freiburg)

HiTrap™ NHS-activated HP	Affinity Chromatography	GE Healthcare Life Sciences (Freiburg)
NAP-10 columns	Ion-Exchange Chromatography	GE Healthcare Life Sciences (Freiburg)
PD-10 columns	Ion-Exchange Chromatography	GE Healthcare Life Sciences (Freiburg)
Phenomenex Luna 5u C18(2) 100A	Reversed-phase HPLC column	Shimadzu (Kyoto)
Superdex 200 10/300 GL	Size-Exclusion Chromatography	GE Healthcare Life Sciences (Freiburg)
Superose 6 10/300 GL	Size-Exclusion Chromatography	GE Healthcare Life Sciences (Freiburg)
Vivaspin® Turbo 15, 5000 MWCO, PES	Ultracentrifugation, Ion-Exchange	Sartorius (Göttingen)

3.1.6 Antibodies

The antibodies applied in western blot analysis were diluted in 5% skimmed milk (MP) or 1% BSA in TBS-T. When used in immunofluorescence analysis, antibodies were diluted in 1% BSA, 10% goat serum (g.s.), or 10% horse serum (h.s.) in PBS (Table 3. 1, Table 3. 2).

Table 3. 1 Primary antibodies

Antibody	Species, dilution	Manufacturer
αChondroitin Sulfate (1B5, 2B6, 3B3)	mouse, IHC; 1:5-1:10 in g./h.s.	Bruce Caterson (Cardiff)
αHeparan Sulfate (F58-10E4)	mouse, IHC; 1:100 in 10% g.s.	Amsbio (Abingdon)
αShh	goat, WB; 1:2000 in 5% MP/TBS-T	R and D Systems (Wiesbaden)

Table 3. 2 Secondary antibodies and conjugates

Antibody	Species, dilution	Manufacturer
Biotinylated α-mouse IgG	Horse, IF; 1:200 in h.s.	Vector Laboratories (Burlingame)
Biotinylated α-mouse IgM	Goat, IF; 1:200 in g.s.	Vector Laboratories (Burlingame)
Streptavidin-Alexa Fluor® 488	1:500, IF in h.s.	Life Technologies (Darmstadt)

Streptavidin-HRP	1:100, IF in g.s.	Perkin-Elmer (Waltham)
α-goat HRP	Rabbit, WB; 1:10000 in 5% MP in TBS-T	Abcam (Cambridge)

3.1.7 Vectors

The following vectors were used in cloning experiments.

Vector	Application	Manufacturer
pCR®II-TOPO	Cloning	Life Technologies (Darmstadt)
pcDNA™3.1/myc-His (A)	Cloning/High level constitutive mammalian expression vector	Life Technologies (Darmstadt)

List of expression vectors used in the work.

Plasmid	Vector, restriction sites	Description
IhhNp	pcDNA™3.1/myc-His (A); *Hind*III, *Apa*I	cDNA for wild-type murine Ihh
$IhhNp^{K130S}$	pcDNA™3.1/myc-His (A); *Hind*III, *Apa*I	cDNA for murine Ihh, mutations at K^{130}
$IhhNp^{K221S}$	pcDNA™3.1/myc-His (A); *Hind*III, *Apa*I	cDNA for murine Ihh, mutations at K^{221}
$IhhNp^{K81A}$	pcDNA™3.1/myc-His (A); *Hind*III, *Apa*I	cDNA for murine Ihh, mutations at K^{81}
$IhhNp^{R75A/R76A/R77A/R80A/K81A}$	pcDNA™3.1/myc-His (A); *Hind*III, *Apa*I	cDNA for murine Ihh, mutations at R^{75}, R^{76}, R^{77}, R^{80}, K^{81}, R^{75} and K^{81}
$IhhNp^{R75A/R77A}$	pcDNA™3.1/myc-His (A); *Hind*III, *Apa*I	cDNA for murine Ihh, mutations at R^{75}, R^{77}
$IhhNp^{R75K/P78H/R80K}$	pcDNA™3.1/myc-His (A); *Hind*III, *Apa*I	cDNA for murine Ihh, mutations at R^{75}, P^{78}, R^{80}
$IhhNp^{R76A/R80A}$	pcDNA™3.1/myc-His (A); *Hind*III, *Apa*I	cDNA for murine Ihh, mutations at R^{76}, R^{80}

IhhNp$^{V71G/V72F/S74\Delta/R75K/P78H/R80K}$	pcDNA™3.1/myc-His (A); *Hind*III, *Apa*I	cDNA for murine Ihh, mutations at V^{71},V^{72}, S^{74}, R^{75}, P^{78} and R^{80}
IhhNp$^{\Delta CW}$	pcDNA™3.1/myc-His (A); *Hind*III, *Apa*I	cDNA for murine Ihh, deletion of CW1 motif
ShhNp	pcDNA™3.1/myc-His (C); *Hind*III, *Xho*I; provided by Prof. Dr. Kay Grobe, University of Münster	cDNA for wild-type murine Shh
ShhNp $^{K33R/H36P/K38R}$	pcDNA™3.1/myc-His (C); *Hind*III, *Xho*I	cDNA for murine Shh, mutations at K^{33}, H^{36} and K^{38}

3.1.8 Oligonucleotides

All oligonucleotides were purchased from Ambion (Thermofisher Scientific) and applied in site-directed mutagenesis (Table 3. 3) of murine Ihh and Shh and genotyping (Table 3. 4).

Table 3. 3 Site-directed mutagenesis primers

Name	Sequence (5'-3')
IhhNp NotI s IhhNp NotI as	TCGCGCTGCCCATGGCGCGGCCGCATGGAGTCCCCAAGAG CTCTTGGGGACTCCATGCGGCCGCGCCATGGGCAGCGCGA
IhhNp^{K130S} s IhhNp^{K130S} as	CTACAATCCCGACATCATCTTCAGCGACGAGGAGAACACGGGTG C GCACCCGTGTTCTCCTCGTCGCTGAAGATGATGTCGGGATTGTAG
IhhNp^{K221S} s IhhNp^{K221S} as	GACTGGGTGTATTACGAGTCCAGCGCCCACGTGCATTGCTCTGTC GACAGAGCAATGCACGTGGGCGCTGGACTCGTAATACACCCAGT C
IhhNp^{K81A} s IhhNp^{K81A}as	CCGCCGGAGGCCGCCTCGCGCCCTCGTGCCTCTTGCCTACAAG CTTGTAGGCAAGAGGCACGAGGGCGCGAGGCGGCCTCCGGCGG
IhhNp^{R166S} s IhhNp^{R166S} as	CAGTGGCCTGGTGTGAAACTGAGCGTGACCGAAGGCTGGGATGA A TTCATCCCAGCCTTCGGTCACGCTCAGTTTCACACCAGGCCACTG
IhhNp$^{R196S/R198S}$ s IhhNp$^{R196S/R198S}$ as	GTGGATATCACCACCTCAGACAGCGACAGCAATAAGTATGGACT GCTGGCG CGCCAGCAGTCCATACTTATTGCTGTCGCTGTCTGAGGTGGTGAT ATCCAC
IhhNp$^{R75A/R76A/R77A/R80A/K81A}$ s IhhNp$^{R75A/R76A/R77A/R80A/K81A}$ as	GCCGGGTGGTGGGCAGCGCCCGGGCGCCGCCTCGCGCGCTCGTG CCTCTTGCCTAC GTAGGCAAGAGGCACGAGCGCGCGAGGCGGCGCCCGGGCGCTGC CCACCACCCGGC

IhhNp$^{R75A/R77A}$ s IhhNp$^{R75A/R77A}$ as	GGCCGGGTGGTGGGCAGCGCCCGGGCGCCGCCTCGCAAGCTCGTG CACGAGCTTGCGAGGCGGCGCCCGGGCGCTGCCCACCACCCGGCC
IhhNp$^{R75K/P78H/R80K}$ s IhhNp$^{R75K/P78H/R80K}$ s	GTGGGCAGCAAGCGGAGGCACCCTAAGAAGCTCGTGCCTCTT AAGAGGCACGAGCTTCTTAGGGTGCCTCCGCTTGCTGCCCAC
IhhNp$^{R76A/R80A}$ s IhhNp$^{R76A/R80A}$ as	GGGTGGTGGGCAGCCGCGCGAGGCCGCCTGCCAAGCTCGTGCCTCTTGC GCAAGAGGCACGAGCTTGGCAGGCGGCCTCGCGCGGCTGCCCACCACCC
IhhNp$^{V71G/V72F/S74\Delta/R75K/P78H/R80K}$ s IhhNp$^{V71G/V72F/S74\Delta/R75K/P78H/R80K}$ as	CGGGGCTGCGGGCCGGGCCGGGGCTTCGGCAAGCGGAGGCACCCTAAGAAGCTCG CGAGCTTCTTAGGGTGCCTCCGCTTGCCGAAGCCCCGGCCCGGCCCGCAGCCCCG
IhhNp$^{\Delta CW}$ s IhhNp$^{\Delta CW}$ as	GCCGGGCCGGGTGGTGGGCAGCCTCGTGCCTCTTGCCTACAAGCAGT ACTGCTTGTAGGCAAGAGGCACGAGGCTGCCCACCACCCGGCCCGGC
ShhNp $^{K33R/H36P/K38R}$ s ShhNp $^{K33R/H36P/K38R}$ as	GTGGGCCCGGCAGGGGGTTTGGACGCAGGCGGCCGCCCCGCAAG CTGACCCCTTTAGCCTACAAGCAGTT AACTGCTTGTAGGCTAAAGGGGTCAGCTTGCGGGGCGGCCGCCTG CGTCCAAACCCCCTGCCGGGCCCAC

Table 3. 4 Primers for mouse genotyping

Strain	Primer	Sequence (5'-3')
Ext1$^{Gt/Gt}$	Ext1 Fw Ext1 Rv 5'pgto	CACATCAGGTGCCTCACAAC CTCCCAGCACTTTTCCTGAC TACATAGTTGGCAGTGTTTGGG
Glce	JP46 JP54 LoxP1	ACTCCATGCTGCTCTGAC AGTGTTCAAAGGATAAACTACAA CGAGATCAGCAGCCTCTGTTCCA
Hs2st	2Ost P1 LAR1	GTGCGGCCGTGGGGTCC TGCCCTAGGCTCAGGCATG
Ndst1	NDST1-16R NDST1-10R NDST1 17F	CATCCTCTGAGGTGACCGC CCAGGGCGTCAGGGCCTCCTG CCCAGATGGCGAGACTGAGG
Sulf1	S1 F1 S1 R1 AK30R neo	GAGGGAACAGCGCTATCYAAATG GAGATACACAGCAAAGGTCCG CGGCTGCATACGCTTGATCCG
Sulf2	S2 Fw S2 Rev AK31R neo	GAATCCCATCCTCACGACAC AGCTCCACATCCTGGTCATC CCTGCGTGCAATCCATCTTG

3.1.9 Consumables

The consumables, utilized in cell and bacterial culture experiments, were steam sterilized prior use or purchased as sterile disposable products.

Consumable	Manufacturer
15/50 ml reaction tubes	Corning (Amsterdam)
Cell culture flasks	Corning (Amsterdam)
Cell scrapers	Corning (Amsterdam)
Combitips advanced®	Eppendorf (Hamburg)
Cover glass	Roth (Karlsruhe)
Disposable pipettes (5, 10 and 25 ml)	Corning (Amsterdam)
Falcon cell strainer, 40 µm	BD Bioscience Falcon (Heidelberg)
Filter pipette tips (10, 100, 1000 µl)	StarLab (Hamburg)
HPLC tubes	VWR Chemicals (Darmstadt)
Immobilon-P, PVDF Transfer Membrane	Merck Millipore (Darmstadt)
Micro centrifuge tubes (1.5, 2, 5 ml)	Roth (Karlsruhe), Eppendorf (Hamburg)
Micro centrifuge tubes, 1.5 ml, RNase free	Corning (Amsterdam)
Microtome blades	Microm (Walldorf)
Multiwell Culture plates	Corning (Amsterdam)
Nalgene® "Mr. Frosty" Freezing container rack	Thermo Scientific (Dreieich)
Plastic Culture Dishes	Corning (Amsterdam)
Poly-Prep® empty chromatography column	Bio-Rad (Munich)
Superfrost™ Plus Microscope Slides	Thermo Scientific (Dreieich)
Whatman paper	Macherey-Nagel (Düren)
Whatman syringe filters	GE Healthcare (Freiburg)

3.1.10 Technical equipment

Equipment	Manufacturer
ÄktaFPLC	GE Healthcare Life Sciences (Freiburg)
ÄktaPrime Plus	GE Healthcare Life Sciences (Freiburg)
Analytical scale	Mettler Toledo AL54 (Giessen)
Automatic tissue processor	Mikrom (Walldorf)
Bacteria incubator	Memmert (Schwabach)
Bench centrifuge	Eppendorf (Hamburg)

Biophotometer Genesys 6	Thermo Fischer Scientific (Bonn)
CO_2 Incubators	Labotect (Göttingen)
Dry freezer Alpha 1-4 LD plus	Christ (Osterode am Harz)
Embedding station	Leica (Wetzlar)
Freezers (-20, -80, -152°C)	Liebherr, Bosch, Thermo, Sanyo
Fusion FX7 Gel Doc	PeqLab (Erlangen)
Gel electrophoresis chamber (horizontal)	PeqLab (Erlangen)
Gel electrophoresis chamber (vertical)	PeqLab (Erlangen), bsb11 (Nottuln)
Gel imager	INTAS (Göttingen)
Hotplate for paraffin sections	MEDAX (Neumuenster)
HPLC system	Merck (Sweden)
Laboratory scale	Mettler Toledo PL 3002 (Gießen)
Laminar Flow Cabinet	BDK (Sonnenbühl-Genkingen)
Laminar Flow Cabinet (HERAsafe, MSC-Advantage)	Thermo Fischer Scientific (Bonn)
Micropipettes	Eppendorf (Hamburg)
Microplate Reader (GeniosPro)	Tecan (Männedorf)
Microscope Axioplan2, Axiovert 200M	Zeiss (Göttingen)
Microscope Camera Spot 23.0	Diagnostic Instruments (Sterling Heights)
Microtome Microme HM 325	Microm (Walldorf)
Microwave oven	Sharp (Hamburg)
MilliQ Water System	Millipore (Schwalbach)
Multipette Xtream®	Eppendorf (Hamburg)
NanoDrop spectrophotometer	PeqLab (Erlangen)
PCR thermal cycler	Eppendorf (Hamburg), Biometra (Göttingen)
pH-Meter	Mettler Toledo (Giessen)
Pipette Controller (Pipetboy)	Thermo Scientific (Dreieich)
Power supply Consort EV231	PeqLab (Erlangen), Biometra (Göttingen)
Radrotator drive STR4	Bibby Scientific (Staffordshire)
Rocking Platform Shaker Duomax 1030	Heidolph (Schwabach)
Shaking incubator	HT Infors (Einsbach)
Stereomicroscope	Leica (Wetzler)
Stirring hotplate	IKA (Staufen)
Thermo block with shaker	Eppendorf (Hamburg)
Trans-Blot® SD Semi-Dry Transfer Cell	Bio-Rad (Munich)
Tri-Carb Liquid Scintillation Counters	Perkin-Elmer (Waltham)

Vacuum pump	KNF Lab, (Freiburg)
Vortex shaker	Scientific Industries (Bohemia)
Water bath	GFL (Burgwedel)
Water bath for tissue sections	MEDAX (Neumuenster)

3.1.11 Softwares

Software	Version	Manufacturer
Adobe package CS4 Extended	11.0	Adobe
ApE, A plasmid Editor	2.0.51	M. Wayne Davis
D-7000 HPLC System Manager (HSM)	4.1	Hitachi-hightechnologies
Fusion capt	15.09	Vilber Lourmat
GraphPad Prism 5	5.04	GraphPad Software
ImajeJ	1.48v	National Institute of Health, USA
INTAS	3.22	GDS
Jalview	2.10.1	University of Dundee and BBSRC
MetaMorph	6.3r6	Molecular devices
Microsoft® Office for Mac	14.0.0	Microsoft
ND-1000	3.2.1	Coleman Technologies
PyMol	1.7.4.5	Schrodinger, LLC
Spot Advanced	4.5.7	Diagnostic instruments
T-coffee	8.99	Notredame's Lab (CRG)
Unicorn	5.1	GE Healthcare

3.1.12 Buffers and Solutions

Buffer/Solution	Composition
Affinity Chromatography Elution Buffer	2 M NaCl 10 mM NaH_2PO_4, pH7 0.1% (v/v) Triton X-100
Affinity Chromatography Loading Buffer	10 mM NaH_2PO_4, pH7 0.1% (v/v) Triton X-100

Alkaline Phosphatase reaction buffer	23.2% (v/v) Diethanolamine 500 µM $MgCl_2$ 0.5 mg (w/v) BSA 12 mM PNP (*p*-nitrophenolphosphate)
Bjerrum Buffer	48 mM Tris 29 mM Glycin 20% (v/v) Methanol
Chondroitinase digestion solution	50 mM Tris, pH 8 30- 60 mM Sodium acetate 0.02% Bovine serum albumin
Collagenase digestion solution	0.3 U/ml Collagenase NB4 5% (v/v) FCS 0.05% (v/v) Trypsin
DEAE Elution buffer	50 mM Acetate buffer, pH 4.0 2 M NaCl 0.1% Triton X-100
DEAE Washing buffer 1	50 mM Tris-HCl, pH 7.5 200 mM NaCl 0.1% Triton X-100
DEAE Washing buffer 2	50 mM Acetate buffer, pH 4.0 200 mM NaCl 0.1% Triton X-100
GAG Binding Buffer	20 mM Sodium acetate, pH 6 100 mM NaCl
GAG Elution Buffer	20 mM Sodium acetate, pH 6 1.5 M NaCl
Heparinase buffer, 2X	10 mM HEPES pH 7.0 2 mM $CaCl_2$
Lysis buffer (primary chondrocytes)	50 mM Tris-HCl, pH 7.5 150 mM NaCl 1% Triton X-100
Methyl Green staining solution	0.5 g Methyl green 0.1 M Sodium acetate, pH 4.2

NHS-Activated column Coupling Buffer	0.2 M $NaHCO_3$ 0.5 M NaCl pH 8.3
NHS-Activated column Buffer A	0.5 M Ethanolamine 0.5 M NaCl pH 8.3
NHS-Activated column Buffer B	0.1 M Sodium acetate 0.5 M NaCl pH 4
Nitrous acid treatment 1.5 pH reagent	0.5 M $Ba(NO_2)_2.H_2O$ in H_2O 0.5 M H_2SO_4
Nitrous acid treatment 3.9 pH reagent	6.8 M $NaNO_2$ in MilliQ H_2O
Orange G-Sample Buffer	300 ml/l Glycerol 2 g/l Orange G
P1 (Miniprep)	50 mM Tris-HCl, pH 8 10 mM EDTA 100 µg/ml DNase-free RNase
P2 (Miniprep)	200 mM NaOH 1% (w/v) SDS
P3 (Miniprep)	3 M Potassium acetate, pH 5.5
Paraformaldehyde (PFA)	4% (w/v) in PBS
PBT	X% Triton X-100 (v/v) in PBS
Phosphate Buffered Saline (PBS), 10x	1.37 M NaCl 26.8 M KCl 100 mM Na_2HPO_4 17 mM KH_2PO_4 pH 7.4
Pronase Buffer	100 mM Sodium acetate 320 mM NaCl pH 5.5

Protease Buffer	50 mM Tris-HCl pH 8.0 1 mM $CaCl_2$ 1% Triton X-100
SafraninO solution	0.1% (w/v) SafraninO
Scott's Buffer	83 mM $MgSO_4$ 24 mM $NaHCO_3$
SDS Resolving gel Buffer, 4x	1.5 M Tris, pH 8.8 0.4% (w/v) SDS
SDS Running Buffer, 10x	1M Tris 3.84 M Glycin 1% (w/v) SDS
SDS Sample Buffer, 4x	200 mM Tris-HCl, pH 8.8 8% (w/v) SDS 40% (v/v) Glycerol 0.5% (v/v) β-Mercaptoethanol 0.4% (w/v) Bromophenol blue
SDS Stacking gel Buffer, 4x	0.5 M Tris, pH 6.8 0.4% (w/v) SDS
SDS-PAGE Resolving gel	X% (v/v) Acrylamide 25% SDS-Resolving gel Buffer 0.1% (w/v) APS 1:1000 TEMED
SDS-PAGE Stacking gel	4% (v/v) Acrylamide 25% Stacking gel Buffer 0.1% (w/v) APS 1:1000 TEMED
Superose 6 Separation buffer	50 mM Tris-HCl, pH 7.4 1 M NaCl 0.1% Triton X-100
TBS-T	1% Tween-20 (v/v) in TBS
TE-Buffer	10 mM Tris, pH 8.0 1 mM EDTA

Tris-Acetate-EDTA (TAE)	40 mM Tris 1 mM EDTA 20mM Acetic acid pH 8
Tris-buffered saline (TBS), 20x	3 M NaCl 200 mM Tris pH 7.5
Weigert solution	1:1 mixture of Weigert solutions A and B

3.1.13 Bacterial strains and culture media

Escherichia Coli (*E.coli*) strains DH5α, Top10 und Mach1 were cultured in steam sterilized liquid or agar Luria Bertani (LB) medium. The culture media were supplemented with 100 µg/ml Ampicillin or 50 µg/ml Kanamycin, when selection of transformants was intended.

Strain	Genotype	Reference
DH5α	F^- ϕ80d*lac*ZΔM15 Δ(*lac*ZYA-*arg*F)U169 *deo*R, *rec*A1 *end*A1 *hsd*R17(r_K^- m_K^+) *pho*A *sup*E44 *thi*-1 *gyr*A96 *rel*A1 λ^-	Life Technologies (Darmstadt)
Top10	F^- *mcr*A Δ(*mrr-hsd*RMS-*mcr*BC) ϕ80*lac*ZΔM15 Δ*lac*X74 *rec*A1 *ara*D139 Δ(*ara-leu*)7697 *gal*U *gal*K *rps*L(Str^R) endA1 nupG	Life Technologies (Darmstadt)
Mach1	F^- ϕ80*lac*ZΔM15 Δ*lac*X74 *hsd*R(r_K^-, m_K^+)Δ*rec*A1398 *end*A1 *ton*A	Life Technologies (Darmstadt)

Medium	Composition
LB-liquid Medium	1% (w/v) Tryptone 0.5% (w/v) Yeast-Extract 1% (w/v) NaCl pH 7.0
LB-Agar	1.5% (w/v) Agar in LB medium

3.1.14 Eukaryotic cells

Established cell lines and primary chondrocytes were maintained in appropriate medium, supplemented with Fetal Bovine Serum (FBS/FCS) and antibiotics. Differentiation was

induced by treatment with Insulin-Transferrin-Selenium supplement, added fresh to the medium.

The cell culture media, PBS, Penicillin/Streptomycin (P/S) used in this work were purchased from Life Technologies (Darmstadt). FBS was purchased from PAN-Biotech (Aidenbach)

Cell line	Description	Reference
HEK-293Ebna	Human embryonic kidneys	(Graham et al., 1975)
C3H10T1/2	Murine embryonic fibroblasts	(Reznikoff et al., 1973)

Medium	Composition
HEK-293Ebna complete medium	DMEM-GlutaMAX™-I 10% FCS 1% P/S
Freezing medium	DMEM-GlutaMAX™-I 20% FCS 10% DMSO 1% P/S
C3H10T1/2 complete medium	DMEM-GlutaMAX™-I 10% FCS 1% P/S
C3H10T1/2 differentiation medium	DMEM/F12 2.5% FCS 1% P/S X% tested protein
Primary chondrocytes complete medium	DMEM/F12 10% FCS 1% P/S
Primary chondrocytes differentiation medium	DMEM/F12 2.5% FCS/ 1x Serum Replacement 1% ITS 1% P/S

The following agonists, antagonists and supplements were used in cell culture experiments:

- Purmorphamine–Abcam (Cambridge)
- Cyclopamine–Calbiochem (Bad Soden)
- Insulin-Transferrin-Selenium (ITS) supplement– Life Technologies (Darmstadt)
- Serum replacement 1 (50X)–Sigma-Aldrich (Munich)
- Protease Inhibitor Cocktail–Calbiochem (Bad Soden)

3.1.15 Mouse lines

Mouse lines	Genotype	Reference
NMRI	Wild type	Harlan-Winkelmann (Borchen)
Ext1$^{Gt/Gt}$	Ext1 Gt(pGT1.8TM)64Wcs	(Mitchell et al., 2001)
Glce$^{-/-}$	Glce tm1Jpli	(Li et al., 2003)
Hs2st$^{-/-}$	Hs2st1$^{tm1.1Je}$	(Bullock et al., 1998)
Ndst1$^{-/-}$	Ndst1^{tm1Grob}	(Grobe et al., 2005)
Sulf1$^{gt/gt}$*;Sulf2*$^{gt/gt}$	Sulf1 Gt(XM190)Byg/Sulf2 7Gt(PST111)Byg	(Ratzka et al., 2008)

3.2 Methods

3.2.1 Molecular biology

3.2.1.1 PCR Methods

Polymerase chain reaction (PCR) is a rapid and versatile method used for amplification of predefined DNA sequence. The method is usually designed to permit selective amplification of specific DNA fragment within a heterogeneous population of DNA sequences. To permit such selectivity oligonucleotide primers specific to the targeted sequence are designed. Dependent on the aim of the experiment the conditions and the applied polymerase can vary. For standard PCR the composition of the reaction mix and composition were the following:

Plasmid/ Genomic DNA	10 ng-100 ng
10X Dream Taq Buffer	2.5 µl
DMSO	1.25 µl
dNTPs (100mM)	0.2 µl
forward primer	0.4 µM
reverse primer	0.4 µM
Dream Taq (5U/µl)	1U
ddH_2O	to 25 µl

PCR amplification conditions:

Step	Temperature	Time	Number of cycles
Initial denaturation	95°C	5’	1
Denaturation	95°C	30’’	35
Annealing	52-64°C	20’’	
Extension	72°C	1’	
Final extension	72°C	5’	1
End	4°C	∞	

The optimal annealing temperature for each primer pair was first determined via gradient-PCR. When the DNA amplicons were intended for cloning a high-fidelity polymerase (KOD Hot Start DNA Polymerase (Calbiochem)) was used. High-fidelity PCR utilizes a DNA polymerase with a low error rate and results in a high degree of accuracy in the replication of

the DNA of interest. The PCR mix was prepared according to the guidance of the manufacturer. Due to the 3' to 5' exonuclease activity, KOD polymerase synthesizes PCR products with no 3'-dA, which results in amplicons with blunt ends. Prior to TOPO-TA cloning the 3'-dA overhangs were additionally synthesized by supplementing the PCR product with 1U of Dream Taq polymerase followed by an incubation at 72°C for 10 min. The resulting PCR products were analyzed by agarose-gel electrophoresis.

3.2.1.2 Agarose-gel electrophoresis

Agarose-gel electrophoresis is commonly used method for visualization of nucleic acids. It can be used for analytic purposes and excision and purification of targeted DNA fragment prior cloning. The agarose-gel was prepared in Tris-acetate-EDTA (TAE) buffer and in concentration ranging between 0.8-2% agarose, depending on the expected size of the DNA fragments. The gels were run in TAE buffer for 1hr at 120V and stained with 0.5 µg/ml ethidium bromide supplemented to the liquid agarose. Ethidium bromide intercalates between the base pairs in the double helix and emits light with wavelength 605 nm (orange light) as result of excitation with ultraviolet light (300 nm and 520 nm).
When loaded on agarose-gel nucleic acid samples were supplemented with OrangeG loading buffer and 100 bp / 1kb DNA ladder (Fermentas) was used to determine the size of the DNA fragments.

3.2.1.3 Purification of DNA fragments

DNA fragments, obtained by PCR amplification or plasmid restriction, were separated via agarose-gel electrophoresis and excised using sterile scalpel. The purification was performed using NucleoSpin ExtractII (Macherey-Nagel) following instructions of the manufacturer.

3.2.1.4 Enzymatic restriction of plasmid DNA

Enzymatic digestion of plasmids aimed to confirm the insert and vector backbone size. All restriction enzymes used in this work belong to the FastDigest line of restriction enzymes by Thermo Scientific.

3.2.1.4.1 Diagnostic restriction of plasmids

Plasmid digest was performed in 10 µl total reaction volume. The reaction mix contained 1 µl of FastDigest Buffer (10X), 0.5 U of each restriction enzyme, 0.5 µg plasmid and X µl of MilliQ H_2O to reach 10 µl final volume. The reaction was homogenized, centrifuged and incubated for 20 min at 37°C. The enzymes were inactivated at temperature recommended by

the manufacturer and analyzed by agarose-gels electrophoresis.

3.2.1.4.2 Enzymatic digestion of plasmids and DNA fragments for cloning

When restriction products were used in a cloning reaction, the volume of the digestion reaction was increased to 30 µl with scaled amount of each component and purified as described (see section 3.2.1.3).

3.2.1.5 Ligation of DNA fragments

Ligation is a mechanism, which allows joining of two nucleic acids through the catalytic action of an enzyme. In this reaction, the ends of DNA fragments are joined together by the formation of phosphodiester bonds between the 3'-hydroxyl group of one DNA terminus with the 5'-phosphoryl group of the other DNA terminus. The activity of the ligase, the enzyme catalyzing this reaction, requires a co-factor, ATP or NAD^+.

In this work, ligation reactions were catalyzed by the T4-DNA-Ligase (Thermo Scientific) following instructions of the manufacturer. The reactions were performed overnight (o/n) at 25°C.

3.2.1.6 Quantitation of nucleic acids

The accurate nucleic acid concentration was assessed by measuring the absorbance of a sample (optical density-OD) at wavelength of 260 nm (λmax for DNA and RNA), 280nm and 230 nm using NanoDrop spectrophotometer (Peqlab). The quantification is based on a spectrum measurement at a defined pathway of 1 mm. The reading at 260 nm allows calculation of the concentration of nucleic acids in the sample. An OD of 1 corresponds to 50 µg/ml of dsDNA, 40 µg/ml RNA and 33 µg/ml ssDNA. The ratio between the readings at 260nm/280 nm (OD_{260}:OD_{280}) and 260 nm/230 nm (OD_{260}:OD_{230}) was used to estimate the purity of the nucleic acids. Pure preparations of DNA and RNA have OD_{260}:OD_{280} of 1.8 and 2, respectively, while OD_{260}:OD_{230} should be greater than 1.5.

3.2.1.7 DNA sequencing

Sanger sequencing was performed by GATC (Cologne). The sequences were analyzed using ApE software and compared to sequences in NCBI BLAST (http://www.ncbi.nlm.nih.gov).

3.2.1.8 Cloning of expression plasmids

3.2.1.8.1 Cloning of full length *Ihh* (mus musculus)

Full length *Ihh* (nucleotides 1-2464, NCBI), containing the 5' and 3' Ihh UTRs cloned in pCMV-SPORT6 was purchased from GE Healthcare Dharmacon (MGC Mouse Ihh cDNA, Accession: BC046984 Clone ID: 6477118). Due to insufficient overexpression levels the coding sequence (called IhhNp, 324-1673 nucleotides, accession number NM_010544.2) was subcloned in expression vector pcDNA™3.1/myc-His(A) (Invitrogen). An additional *Not*I restriction site was introduced into the 5'UTR of the Ihh sequence directly upstream from the initiation codon using site-directed mutagenesis (section 3.2.1.9) and primer pair IhhNp NotI (Table 3. 3). The pCMV-SPORT6 containing the *Ihh* sequences and the pcDNA™3.1/myc-His(A) were digested using *Not*I and *Apa*I enzymes. The Ihh pCMV-SPORT6 digestion products were separated on an agarose-gel followed by purification of the Ihh fragments (section 3.2.1.3). The gel-purified fragments were ligated in pcDNA™3.1/myc-His(A) using T4-DNA ligase following manufacturer instruction. 5 µl of the reaction mix was used for transformation of chemically competent cells. Transformed cells were plated onto LB agar plates supplemented with ampicillin as a selection marker. Plasmid DNA was purified from several colonies. A diagnostic plasmid restriction using *Not*I and *Apa*I was performed to confirm fragment insertion (section 3.2.1.4.1). Clones with expected size of the insert and backbone were sent for sequencing to confirm a correct insertion of the Ihh coding sequence.

3.2.1.9 Generation of mutants via site-directed mutagenesis

Site-directed mutagenesis is an *in vitro* method used to introduce a desired mutation into dsDNA plasmid. One can make use of the method when interested in the relationship between protein structure and function, protein engineering or willing to perform vector modification. The QuickChange II XL Site-Directed Mutagenesis Kit (Agilent Technologies) was used to generate *Ihh* mutants. Successful mutagenesis reaction requires the design of sense and antisense primers with the desired mutation. Extension of the primers by the *PfuUltra* high-fidelity polymerase results in synthesis of mutant plasmid with nicks. DNA, purified from the majority *E.coli* strains, is Dam methylated, which make it susceptible to *Dpn*I enzymatic digest. The digest was performed after the synthesis of the mutant chains was completed (5 U enzyme, 37°C for 1 hr). The endonuclease targets the parental DNA template, while the PCR amplified DNA strands remain unaffected by this treatment. Following *Dpn*I digest the reaction mix was used for transformation of XL-10 Gold Ultracompetent cells for nick repair,

plated onto LB agar plates supplemented with antibiotic and incubated o/n at 37°C. The mutagenesis reaction conditions were the following:

Mutagenesis reaction mix composition:

10x Reaction buffer	2.5 µl
dNTPs mix	0.5 µl
Sense primer	63 ng
Antisense primer	63 ng
Quick Solution	1.5 µl
PfuUltra polymerase	1.25 U
DNA template	50 ng
ddH_20	to 25 µl

Cycling parameters for site-directed mutagenesis:

Step	**Temperature**	**Time**	**Number of cycles**
Initial denaturation	95°C	1’	1
Denaturation	95°C	50’’	18
Annealing	60°C	50’’	
Extension	68°C	7’ (1’/ kb plasmid length)	
Final extension	68°C	7’	1
End	4°C	∞	

3.2.1.10 Transformation of chemically competent cells

XL-10 Gold Ultracompetent cells were used for bacterial transformation with plasmids following site-directed mutagenesis. 30 µl cells were supplemented with 1 µl DMSO and incubated on ice for 10 min. 3 µl of *Dpn*I digested PCR product was added to the cells and gently mixed for a minute. The mixture was incubated on ice for 30 min and then heat shocked at 42°C for 30”. After additional incubation for 2 min on ice, 200 µl LB medium was added to the reaction. The cells were incubated for 20 min at 37°C with shaking and then plated onto LB-agar plates, supplemented with ampicillin or penicillin. After o/n incubation at 37°C, 5-10 colonies were transferred onto fresh LB-agar plates and in 5 ml liquid medium. The cultures were grown o/n followed by plasmid purification via alkaline lysis.

DH5α/Mach1/Top10 cells were used for bacterial transformation with established plasmids, products of ligation or cloning reaction. 100 µl competent cells were thawed on ice. 100 ng

plasmid DNA or 2-4 µl ligation mixture was added to the competent cells, gently mixed for about a minute and then incubated for 30 min on ice. After this, a heat-shock at 42°C for 30" was performed, followed by an incubation on ice for 2 min. The transformation mix was supplemented with 200-400 µl LB medium. The cells were incubated for 30-60 min at 37°C dependent on the antibiotic resistance of the plasmid and then plated onto LB-agar plates, supplemented with either ampicillin or penicillin.

3.2.1.11 Plasmid purification

Plasmids were purified via alkaline lysis (Birnboim and Doly, 1979). Qiagen Plasmid Midi Kit was utilized for purification of a highly pure plasmid DNA, sufficient for transfection in eukaryotic cells.

When intended for cloning, enzymatic digestion or sequencing, the plasmids were purified using the following plasmid mini preparation protocol. Following transformation, the *E.coli* cells were plated onto LB-agar plate, supplemented with an appropriate selective mark. After an o/n incubation at 37°C, single colonies were picked and inoculated into 3 ml liquid LB medium. Transformants were harvested after an o/n incubation via centrifugation at 13000 g for 5 min. The supernatant was discarded and the resulting bacterial pellets-resuspended in 200 µl Buffer P1. Cells were lysed in 200 µl Buffer P2. Finally, neutralization and precipitation of genomic DNA and proteins was attained by the addition of 200 µl Buffer P3. The precipitates were sedimented via centrifugation at 13 000 g for 5 min at 4°C. The supernatant, containing plasmid DNA, was transferred to a fresh 1.5 ml and precipitated by the addition of 0.7 volumes 100% isopropanol followed by an incubation for 2 hrs at -20°C. Following centrifuged at 13000 g for 30 min at 4°C, the supernatant was discarded and DNA pellets were air-dried and resuspended in 50 µl TE-Buffer. The amount and purity of the obtained plasmids were assessed using NanoDrop spectrophotometer and verified by diagnostic restriction and sequencing.

3.2.2 Protein purification and analysis

3.2.2.1 Trichloroacetic acid (TCA) precipitation of proteins

TCA precipitation is a commonly used method for concentration of diluted protein solutions and simultaneous removal of contaminants. Equal volumes of protein solution and 20% ice-cold TCA were mixed and incubated on ice for 1 hr or o/n at -20°C. The samples were centrifuged (14000 g, 20 min, 4°C) and the supernatant discarded. The protein pellets were washed with 400 µl ice-cold acetone and incubated for 10 min at -20°C followed by a

centrifugation (14000 g, 20 min, 4°C). The supernatants were discarded, pellets–air-dried and stored at 4°C for further analyses (Fic et al., 2010).

3.2.2.2 Sodium dodecyl sulfate polyacrylamide gel electrophoresis (SDS-PAGE)

SDS-PAGE is a commonly used method for separation of protein mixtures according to their electrophoretic mobility. In this method, discontinuous polyacrylamide (PAA) gels are used as a support medium in combination with a protein-denaturing agent–sodium dodecyl sulfate (SDS). As an anionic detergent, SDS disturbs the tertiary structure of the proteins, which brings the folded proteins into a linear molecule. Additionally, SDS coats the protein with a uniform negative charge, which masks the native charge of the protein. The PAA matrix can be prepared in various concentrations, resulting in different pore size of the matrix and, respectively–in variety of separation conditions. The presence of a reducing agent like dithiotreithol (DTT) or β-mercaptoethanol, which breaks disulfide bonds, ensures that the 3D structure of the protein is fully disturbed (Laemmli, 1970).

PAA gel consists of two phases–a stacking gel with pH 6.8 and a resolving gel with pH 8.8. For the preparation of 10 ml of 15% resolving SDS-PAA gels 0.1% (v/v) TEMED and 0.1% (w/v) APS were added to 2.5 ml dd H2O, 2.5 ml SDS resolving gel buffer, 5 ml of 30% Acrylamide/Bis solution 37.5:1. The solution was poured between PAA gel glass plates, covered with 100% isopropanol and allowed to polymerize. Once the gel had polymerized, the isopropanol was removed and a 4% stacking gel mix was poured onto it, and allowed to polymerize after positioning of the well-forming comb.

Cell lysates and protein mixtures were resolved in 15% SDS-PAGE. Samples were diluted in SDS-PAGE sample buffer, boiled for 15 min and applied to the gel. The separation was performed at 80 V in the stacking gel and 120 V in the resolving gel.

3.2.2.3 Western blot (Immuno blot)

Western blot is a widely used technique for identification of individual protein in complex protein mixtures. In this method, proteins are first separated by electrophoresis and then transferred by electric current onto a carrier membrane (polyvinylidene difluoride (PVDF) or Nitrocellulose) where they are accessible to protein specific antibodies for immunodetection.

Bjerrum buffer was selected as a protein transfer buffer. The PVDF membrane was pre-activated in methanol whatmann paper and the SDS-PAA gels were equilibrated in Bjerrum buffer and assembled in a western blot transfer sandwich. Protein transfer was achieved by semi-dry blotting (Bio-Rad) for 1hr at 5 mA/cm^2.

After protein transfer, the membranes were blocked in 5% skim milk in TBS-T for one hr in order to avoid unspecific antibody binding. The membranes were incubated with primary antibody (goat α-ShhN) diluted 1:2000 in 5% skim milk /TBS-T, o/n at 4°C. An unspecifically bound antibodies were removed by washing in TBS-T buffer. A horseradish peroxidase (HRP)-labeled secondary antibody (α-goat HRP) was applied onto the membrane and incubated for one hr followed by membrane washing in TBS-T and developing using a "Pierce enhanced chemiluminescence substrate" (ECL) (Thermo scientific, Dreieich) or „AceGlowTM-Solution" (Peqlab) for detection of HRP activity. The resulting chemiluminescence signal was detected using a Phospho-/Chemiluminescence Imager Fusion-SL 4.2MP and quantified using ImageJ software.

3.2.2.4 Fast protein liquid chromatography (FPLC)

FPLC is a type of liquid chromatography, commonly used to analyze or purify molecules in complex mixtures as they travel along a mobile phase (buffer) through a porous matrix (stationary phase). The flow rate of the mobile phase is controlled and usually kept constant, while the characteristics of the mobile and stationary phase can vary, generating a wide range of separation conditions.

3.2.2.4.1 Size-exclusion chromatography

Size-exclusion chromatography is a technique, which allows separation of molecules, such as proteins, peptides, polysaccharides and nuclear acids, by size as they travel through porous matrix in form of spherical particles. Large molecules or multimers cannot enter the pores of the matrix. Consequently, they are eluted first and leave the column with the Void volume (V_0) as they travel with the same speed as the flow of the buffer. Smaller molecules enter the pores of the matrix and are delayed in the column, eluting according to their size. Small molecules, such as salts, have full access to the pores of the matrix, but do not separate from each other and are eluted just before one total column volume of buffer (V_t) has passed through the column.

Superdex 200 10/300 GL containing spherical composite of cross-linked agarose and dextran as a matrix was selected for separation of Hh multimers by size-exclusion chromatography. The medium was equilibrated with PBS at 4°C. 500 µl of medium derived from HEK-293Ebna cells expressing wild-type or mutant Ihh protein was filtered through a 0.22 µm filter and applied onto the column. Another 500 µl were subjected to heparin-agarose beads (Sigma-Aldrich) pull-down in order to control the amount of overexpressed protein in the input. The separation was performed at a flow rate of 0.5 ml/min. Eluted proteins were

separated in 24 fractions with a volume of one ml, subjected to TCA precipitation (3.2.2.1) and stored for further analyses.

Superose 6 10/300 GL (matrix: cross-linked agarose) was employed for preparative separation of ^{35}S labeled proteoglycans and, subsequently, for determination of the length of the attached GAG chains. The separation medium was equilibrated with two column volumes of Superose 6 separation buffer. For preparative separation of PGs, the column was loaded with two ml DEAE-purified and filtered PGs solution. The separation was performed at a flow rate of 0.25 ml/min in 50 fractions. 20 ul of each fraction were supplemented with HiSafe scintillation cocktail and analyzed in scintillation counter to identify the PG peak.

Analytical separations were performed on samples containing 10 000 cpms (counts per minute) of ^{35}S labeled total GAGs, CS, or HS. Separation was performed in Superose 6 separation buffer at flow rate 0.25 ml/min and in 50 fractions (0.5 ml/fraction). The resulting fractions were analyzed in scintillation counter after supplementing with HiSafe scintillation cocktail.

3.2.2.4.2 Affinity chromatography

Affinity chromatography is a technique allowing separation of molecules using bio-recognition. The method is based on reversible interactions between the molecule of interest and a specific ligand, coupled to a chromatography matrix. Advantage of this method is its high selectivity. The method is performed in four steps: equilibration of the chromatography matrix; loading of the sample in conditions, favoring interactions with the ligand; washing off the unbound material and elution. During the elution step the conditions are changed to reverse the binding to the ligand. This is achieved by change of the pH, the ionic strength of the buffer or others.

The heparin/HS affinity chromatography column (one ml) was equilibrated with three column volumes of Affinity chromatography loading buffer. Two ml conditioned medium derived from HEK-293Ebna cells, expressing wild-type or mutant Ihh protein, was passed through 0.22 um filter and applied onto the equilibrated column. The unspecifically bound material was washed off with five column volumes of Affinity chromatography loading buffer. The specifically bound protein was eluted with a linear NaCl gradient ranging from 0 to 2 mol/L NaCl concentration in loading buffer (pH7). The linear gradient was verified by continuous conductivity measurement. The obtained fractions were subjected to TCA precipitation, resolved on 15% SDS-PAA gel and immunoblotted, followed by immunodetection.

3.2.2.5 Desalting with PD-10 /NAP-10 columns

PD-10/NAP-10 columns (GE Healthcare) are prepacked columns containing Sephadex G-25 resin, which can be used for separation of substances based on their molecular weight, desalting, buffer exchange and sample clean up, were employed for desalting of samples.
The storage buffer of a PD-10 column was removed and the column was equilibrated with 25 ml of 10% ethanol or MilliQ H_2O. After equilibration, the column was loaded with 2.5 ml of the sample followed by elution with 3.5 ml of 10% ethanol/MilliQ H_2O. The eluate was subjected to freeze-drying.
NAP-10 (GE Healthcare) columns were used for desalting of samples of smaller volumes. Columns were first equilibrated with six column volumes of 10% ethanol/MilliQ H_2O. The maximum sample volume applied was 0.9 ml, which was eluted with 1.4 ml 10% ethanol/MilliQ H_2O.

3.2.2.6 Hh bioactivity assay

The biological activity of wild-type and mutant Ihh and Shh proteins was assessed by their ability to induce osteoblast differentiation of the mesenchyme cell line C3H10T1/2. The C3H10T1/2 cells display fibroblastic morphology when cultured under undifferentiating condition, but are able to differentiate into osteoblasts, chondrocytes or adipocytes upon induction (Zhao et al., 2009). This precursor cells express the Hh receptor Ptch1 and an exposure to Hh protein activates the pathway, leading to osteoblast differentiation and the associated alkaline phosphatase expression, which can be used as a read-out of Hh protein signaling activity (Nakamura et al., 1997).
The analyzed proteins were expressed for 48 hours in HEK-293Ebna cells. The conditioned medium, enriched on Hh protein, was harvested and sterile-filtered. 500 µl sample was subjected to a heparin pull-down, followed by immunoblot using Hh specific antibody. The relative secreted Hh amount was quantified in order to assure that similar amount of the mutant and wild-type proteins was applied in the analysis. The quantification was performed using ImageJ Software. Protein levels were normalized to the wild-type protein, which was set to 100%.
C3H10T1/2 cells ($5x10^4$/well) were seeded in 12 well plates and grown for 24 hrs in complete medium. After reaching 100% confluence, the medium was exchange with differentiation medium, supplemented with a predefined amount of the tested protein. The assays were performed in triplicates. C3H10T1/2 cells treated with Cyclopamine (2 µM), a Smo antagonist, in parallel to the tested protein were used as negative controls. As a positive

control cells were treated with the Hh agonist Purmorphamine (2 μM). Following 5 days of differentiation, cells were washed in PBS and lysed in 150 μl of PBS, 1% Triton X-100. The cell lysates were mixed with 150 μl alkaline phosphatase reaction buffer and incubated for 30 min at room temperature (RT). The alkaline phosphatase activity was measured on a microplate absorbance reader at 405 nm.

3.2.3 Glycosaminoglycan (GAG) purification and analyses

3.2.3.1 Purification of GAGs for affinity column preparation

Total embryonic heparan sulfate was purified from the following mouse strains: *NMRI*, *Ndst1*$^{-/-}$, *Hs2st*$^{-/-}$ and wild-type littermates.

3.2.3.1.1 Tissue digest

Mouse embryos were harvested via C-section at embryonic day E16.5 and subjected to snap freezing in liquid N_2. Small pieces of the embryonic tail were harvested for preparation of genomic DNA, followed by genotyping. Four embryos of each genotype and their wild-type littermates were selected for HS purification. The embryos were manually homogenized and digested o/n at 40°C in Pronase buffer supplemented with 1mg/ml Pronase and 1mg/ml Proteinase K. Following a complete tissue digest, the enzymes were heat inactivated at 85°C for 20 min. The digestion product was centrifuged for 30 min at 13 000 x g, the supernatants were filtered through 0.45 μM filter and diluted in sterile water in ration 1:3. to bring the NaCl concentration bellow 150 mM. GAGs were purified by ion-exchange chromatography using the cross-linked cellulose–DEAE Sephacel™ (Sigma-Aldrich) as a medium.

3.2.3.1.2 DEAE Sephacel™ purification

2.5 ml DEAE Sephacel™ was packed in a Poly-Prep® empty chromatography column. The medium was equilibrated with 30 ml GAG-Binding buffer. The digested embryonic tissue was applied to the column and allowed to pass through by gravity. The loaded column was washed with 50 ml GAG-Binding buffer, followed by an elution of the GAGs with 12.5 ml GAG-Elution buffer. The resulting eluate was desalted using PD-10 columns, freeze-dried and reconstituted in HPLC grade water. The amount of the purified GAGs was determined by carbazole assay (Bitter and Muir, 1962). The CS in the complex GAG mixture was digested and the remaining HS was purified by a second round of DEAE Sephacel™ purification prior to the generation of the affinity columns.

3.2.3.2 Generation of HS affinity chromatography columns

Prepacked *N*-hydroxysuccinimide (NHS)-activated Sepharose™ (GE Helathcare) was selected as a matrix for HS coupling. HiTrap NHS-activated HP is composed of an NHS ester attached by epichlore-hydrine to Sepharose High Performance via a spacer arm. This type of esterification leads to formation of activated esters, which can react with ligands containing–NH_2 groups, resulting in very stable amide linkage. The usually performed reaction of *β*-elimination after a GAG purification was excluded for samples intended for affinity column preparation in order to preserve the GAG core protein as a source of amino groups.
HS (100 μg) purified from mouse embryos at E16.5 was dissolved in 1 ml of NHS-coupling buffer. The prepacked HiTrap NHS column was activated by washing with 6 ml of ice-cold HCl (1mM). The diluted HS was injected through the column, the column was sealed and incubated o/n at 4°C. The incubation was followed by washing with Buffer A and B in the following order: 6 ml Buffer A, 6 ml Buffer B, 6 ml Buffer A. After an incubated for 2 hr at 4°C, buffers A and B were used to wash off the unspecifically bound material in the following order: 6 ml Buffer B, 6 ml Buffer A, 6 ml Buffer B. Finally, the column was equilibrated to pH7 with sodium phosphate buffer. For long-term storage, the column was washed with water and stored at 4°C in 20% ethanol. All solutions used in this procedure were passed through 0.2 μM filter prior use.

3.2.3.3 Purification of radioactively labeled GAGs for chain length analysis

Radioactive labeling of GAGs in primary chondrocytes, PG purification and the following GAG chain length analysis were performed at Lena Kjellen research group, BMC, University of Uppsala.

3.2.3.3.1 Radioactive labeling of primary chondrocytes

Primary chondrocytes were obtained from fore and hind limbs of E13.5 *Ext1*$^{gt/gt}$, *Hs2st*$^{-/-}$ and control mouse embryos. The cells were cultured for 24 hrs or differentiated for 5 days prior labeling with 100 uCi/ml $Na_2{}^{35}SO_4$ (NEX 041H Perkin-Elmer). Following a 16 hours incubation, the cells and conditioned medium were harvested. The cells were washed in PBS and lysed in 2 ml lysis buffer supplemented with proteinase inhibitor for 1 hour on a rocking table. After centrifugation (5 min, 13000 x g, 4°C), the supernatant was collected and the GAGs were purified using DEAE™ (Sigma-Aldrich) ion-exchange medium.

3.2.3.3.2 Purification of radioactively labeled GAG

0.3 ml DEAE^{TM}-Sephacel medium was packed in Poly-Prep® empty chromatography column and equilibrated with six column volumes of DEAE wash buffer 1. Samples were loaded onto the column followed by washing with 10 column volumes of DEAE wash buffer 1, and the same amount of DEAE wash buffer 2. Elution was performed with 6 x 0.3 ml of DEAE Elution buffer, resulting in six elution fractions, which were kept separately. Three µl of each elution fraction was counted in *β*-counter to determine the content of labeled material. The fractions with highest radioactivity were pooled and subjected to size-exclusion chromatography on a Superose 6 10/300 column to separate intact PG (eluting as high molecular weight molecules) from cell debris and lysosomes. The fractions containing PGs were pooled. Samples counting ≈50 000 cpms were subjected to alkali treatment with 10M NaOH o/n at 4°C with continuous homogenization to release the GAG chains from the core proteins. The amount of NaOH, optimal for the reaction, was calculated by the following formula: (Volume of the sample x 0.5)/9.5=V of NaOH in ml. Samples were neutralized with equal amount of 10 M HCl and desalted using PD-10 desalting columns and MilliQ H_2O as a buffer. GAGs were concentrated by freeze-drying and dissolved in 100 µl MilliQ H_2O. After quantification, an aliquot counting ≈10 000 cmps was directly separated on a Superose 6 column or subjected to HS/CS digestion prior separation (Dagalv et al., 2015).

3.2.3.4 CS/HS digestion in complex GAG mixtures

3.2.3.4.1 CS digest by chondroitinase ABC

Chondroitinase ABC catalyzes the eliminative degradation of polysaccharides containing (1-4)-*β*-$_D$-hexosaminyl and (1-3)-*β*-$_D$-glucuronosyl or (1-3)-*α*-$_L$-iduronosyl linkages to disaccharides containing 4-deoxy-*β*-$_D$-gluc-4-enuronosyl groups. It acts on chondroitin 4-*O*-sulfate, chondroitin 6-*O*-sulfate, and DS. CS in physiologically relevant GAG mixtures was subjected to chondroitinase ABC digest when coupling of HS to a chromatography matrix or HS chain length analysis was intended.

When aiming HS purification to generate a chromatography, ligand the sample was treated with 0.08 U chondroitinase ABS from *Proteus vulgaris* (Sigma-Aldrich) in Chondroitinase digestion solution. The digestion was performed at 37°C for 4 hrs followed by an inactivation of the enzyme at 85°C for 15 min. To remove the digested CS chains the samples were subjected to DEAE Sephacel purification and desalting using PD-10 columns. The CS-free and desalted samples were freeze-dried and reconstituted in 100 µl HPLC grade water. The amount of the purified HS was determined by carbazole assay (Bitter and Muir, 1962).

In order to analyze the chain length of HS produced by primary chondrocytes, a desalted ^{35}S labeled GAG sample, counting ≈10000 cpms was mixed with 20 µl of 5x Chondroitinase Buffer, 1 mU chondroitinase ABC and diluted to 100 µl final volum with MilliQ water. The sample was homogenized, centrifuged and incubated o/n at 37°C. The enzyme was inactivated by 10 min incubation at 95°C.

3.2.3.4.2 HS cleavage by deamination with nitrous acid

Chemical depolymerization of heparin and HS was attained by deamination using nitrous acid treatment at pH 1.5, pH 3.9 or combination of both. This method is based on the susceptibility of *N*-sulfated and *N*-unsubstituted glucosamine residues to a deamination at pH 1.5 or pH 3.9, respectively. *N*-acetylated glucosamine residues are resistant to either reaction conditions. Susceptible glucosamine residues are converted into 2,5-anhydromannose units, along with cleavage of the corresponding glucosaminidic linkages. Deamination of both *N*-sulfated and *N*-unsubstituted glucosamine residues in the same polysaccharide sample is achieved by combined pH 1.5-pH 3.9 treatment (Riesenfeld et al., 1982). ^{35}S labeled GAGs (10 000 cpms) were freeze-dried and incubated with 200 µl pH 1.5 nitrous acid reagent, vortexed and incubated at RT for 10 min. The reaction mix was supplemented with 250 µl of 6.8 M $NaNO_2$ (final concentration 3.9 M), mixed well and incubated for 10 min at RT. The reaction was neutralized by the addition of appropriate amount of Na_2CO_3. Samples were filtered through 0.22 µm filter and subjected to analysis.

3.2.3.5 Disaccharide analysis by reversed-phase ion-pairing (RPIP)-high performance liquid chromatography (HPLC)

HPLC is a chromatographic method, which involves the use of high pressure to drive analyzed components along with a mobile phase through a chromatographic column based on their polarity. In normal-phase chromatography the stationary phase is made of hydrophilic/polar matrix, while the mobile phase is non-polar. This organization will lead to longer retention time in the column of polar components, which are able to interact with the polar matrix, while non-polar molecules will pass more quickly through the column. In the case of Reversed-phase HPLC the stationary phase is a non-polar matrix, typically a silica modified by attachment of long hydrocarbon chains, while the mobile phase is generally polar, leading to earlier elution of polar molecule. In RPIP-HPLC a volatile lipophilic ion-pairing reagent is typically introduced into the mobile phase to aid formation of ion-pairs with the targeted analyte aiming longer retention time on the hydrophobic stationary phase (Yang et al., 2011). This characteristic makes RPIP-HPLC a popular method for disaccharide

analysis of the polar GAGs. Structural analysis of the polydisperse and heterogeneous GAGs involves partial or complete depolymerization of the GAGs to produce constituent disaccharides. The commonly performed exhaustive enzymatic depolymerization using bacterial lyases converts the polymers into disaccharides with 4,5-unsaturated uronic acid residues at the nonreducing end, which are then separated and analyzed (Volpi et al., 2014).

3.2.3.5.1 Sample lysis and purification

The disaccharide analysis was performed by Dr. Tabea Dierker at BMC, University of Uppsala. Samples were dissolved in Protease Buffer (1ml / 30 mg dry weight sample), boiled for 10 min, and centrifuged. In the next step, the tissue mixture was homogenized by passing through series of needles with descending diameters. The homogenized solution was supplemented with Pronase (0.8 mg/ml final concentration) and incubated for 24 hrs at 55°C with constant rotation in hybridization oven. After a tissue digest for 24 hrs, the Pronase was inactivated by a 10 min incubation step at 95 °C followed by centrifugation at 14000 g for 10 min. A small aliquot (4µl) was stored for determination of DNA amount. Samples were supplemented with $MgCl_2$ (final concentration 2 mM) and 38 U Benzonase per ml lysate, incubated o/n at 37°C followed by heat inactivation of the enzymes. The salt concentration of the lysates was adjusted to 250 mM, followed by purification by ion-exchange chromatography using the cross-linked cellulose–DEAE Sephacel^{TM} (Sigma-Aldrich) as a medium. The purified GAGs were desalted using NAP-10 desalting columns (GE Healthcare).

Following lyophilization the purified GAGs were subjected to chondroitinase ABC digest as described. 20% of each CS digested sample was separated, brought to 100 µl final volume with HPLC H_2O and subjected to disaccharide analysis using RPIP-HPLC.

The remaining sample volume was brought to salt concentration below 100 mM NaCl and purified by DEAE ion-exchange chromatography (200 µl bed volume). In the next step the samples were desalted and lyophilized. The reconstituted in 100 µl HPLC H_2O GAGs were mixed with 100 µl 2x HS digestion buffer. Half of each sample was subjected to heparinase digest by adding 0.4 mU of each–Heparinase I, II and II enzymes and incubated o/n at 37 °C. Treated and untreated samples along with disaccharide standards were separated by RPIP-HPLC in the same sample series to minimize changes in buffer conditions between the runs. Data were analyzed using D-7000 HSM software.

3.2.3.6 Quantification of GAGs by Carbazole assay

The carbazole assay is a commonly used colorimetric method for quantification of total uronic acids in a sample. The method is based on the specific color reaction of hydrolyzed sugar in presence of carbazole. The assay is performed in two steps: samples are first incubated in H_2SO_4 at high temperature, which leads to hydrolysis of the polysaccharides and dehydrates the sugars. In the next step samples are incubated with carbazole to generate a chromophore.

The GAG concentration was evaluated using a standard curve generated using heparin solutions of predefined concentrations. To estimate the GAG content in the samples of interest 5 and 10 µl of the purified GAGs were diluted in HPLC grade water to reach 200 µl final volume. The heparin solutions for the standard curve and the analyzed samples were homogenized and supplemented with 20 µl of 4 M ammonium sulfamate and 1 ml of 25 µM Sodium tetraborate in H_2SO_4. The reaction mix was homogenized and incubated at 100°C for 10 min. Samples were allowed to chill to RT, followed by an addition of 40 µl of 0.125% (w/v) carbazole in absolute ethanol. The homogenized samples were incubated at 100°C for 15 min. After reaching RT the absorbance of the samples was determined at 530 nm with spectrophotometer.

3.2.4 Cell culture experiments

All cell culture experiments were performed in safety level 1 (S1) laboratory under laminar flow cabinet using sterile equipment and solutions. Experiments were performed using cell lines as well as primary chondrocytes. Cells were cultured in culture flasks or multiwell plates with appropriate surface area at 37°C, 5% CO_2 and 90% humidity. Cell count was determined using a Neubauer chamber.

3.2.4.1 Freezing and thawing of cells

Upon reaching 85% confluence the cells were rinsed with PBS and dissociated from the flask by applying 2 ml of 0.5% Trypsin-EDTA. The detached cells were resuspended in 8 ml medium by gentle pipetting. The cell count of the suspension was determent. After centrifugation at 1000 g for 5 min the cell pellet was resuspended in a cell culture medium to a concentration of $1x10^6$/ml. 500 µl cell suspension was aliquoted into cryogenic vials followed by a drop wise addition of 500 µl freezing medium. The vials were transferred into a cell freezing container, which provides 1°C/ minute cooling rate, and placed directly at -80°C. After 24 hrs the frozen cells were transferred into -150°C freezer for long-term storage. Cell

lines were stored at -150 °C in 2 ml cryogenic vials in a concentration of 5 x 10^5 cells. Thawing of cells was performed via snap defrosting by a short incubation in water bath at 40°C. 1 ml cell culture medium was added to the cell suspension and homogenized. Cells were centrifuged for 5 min at 200 g. The supernatant was discarded, the cell pellet was gently resuspended in 500 µl fresh medium, and transferred to a cell culture flask containing an appropriated amount of complete medium.

3.2.4.2 Maintaining and passaging of cell lines

HEK-293Ebna and C3H10T1/2 were maintained in DMEM-GlutaMAX™-I supplemented with 10% FCS and 1% Pen/Strep. Cells were passaged upon reaching ≈80% confluence. For this purpose, the medium was removed and the residual serum was rinsed with PBS. The cells were incubated with 2-3 ml 0.5% trypsin at 37°C for 2-3 minutes and resuspended in fresh medium. The cell suspension was centrifuged at 1000 g for 5 min. The cell pellet was resuspended in appropriate volume of medium to obtain predetermined cell count and seeded in cell culture flask or multiwell plate.

3.2.4.3 Transfection of cell lines

DNA or RNA can be delivered to the nuclei of eukaryotic cells using liposome-mediated transfection. In this method, the DNA plasmid is enclosed into a liposome and transported via endocytosis to the cytoplasm where the nucleic acids are released. During the cell division, the plasmid enters the nucleus by being trapped into the reassembling nuclear envelope.
All transfections in this work were transient and performed in HEK-293Ebna cells. The cells were plated in concentration $7x10^5$ /well in 6 well plates or $1.4 x10^6$ /25 cm^2 cell culture flask and cultured in DMEM GlutaMAX-I medium for 24 hours prior transfection. The transfections were performed at maximum 80% confluence of the cell monolayer. 2 µg plasmid DNA was diluted in 200 µl transfection buffer, homogenized and centrifuged. 4µl JetPrime reagent was added, mixed, centrifuged and incubated for 10 min at RT, and finally added drop-wise to the cells. The analyzed proteins were expressed for maximum 48 hours with two medium replacements–4-5 hours post transfection and 16-19 hours before analysis.

3.2.4.4 Culturing and differentiation of primary chondrocytes

Primary chondrocyte cultures were prepared in order to analyze the multimer size of endogenous Ihh and GAG chain length using size-exclusion chromatography.
Fore- and hindlimbs of stage E13.5 mouse embryos were harvested, washed 3 times in sterile PBS and subjected to dispase digestion (1 U/ml) for 15 min at 37°C. The limbs were rinsed 3

times with sterile PBS to remove the digested skin, and subjected to further enzymatic digestion in collagenase solution for 30 min at 37°C. The digested tissue was homogenized by pipetting, passed through cell strainer (40 µm), washed with 20 ml medium and transferred to a 175 cm^2 cell culture flask. Upon reaching 100% confluence the complete medium was replaced with differentiation medium to induce differentiation. The medium was replaced every other day and finally 16 hours before analysis. Cells and cell supernatants were analyzed after 10 days of differentiation. For GAG chain length analysis primary chondrocytes were cultured in complete chondrocyte medium in 25 cm^2 flask. Cells were cultured for 24 hrs to reach 90% confluence and then incubated in medium supplemented with 100 µCi/ml of $Na_2{}^{35}SO_4$ (NEX 041H Perkin-Elmer). For analysis of GAGs synthesized by differentiated chondrocytes culture medium was exchanged with differentiation medium followed by 5 days of differentiation and finally ^{35}S metabolical labeling for 16 hrs prior to analysis.

3.2.5 Transgenic mice

Mice were kept and bred according to the institutional guidelines of the University Duisburg-Essen and the University Hospital Essen, specifically approved by the animal welfare officer of the University Duisburg-Essen. Mouse husbandry was approved by the city of Essen.

3.2.5.1 Quick preparation of genomic DNA for mouse genotyping

Small piece of mouse tail was incubated in 100 µl DirectPCR tail (PeqLab Biotcehnology GmbH) supplemented with Proteinase K (0.2 mg/ml) at 55°C o/n. After enzyme inactivation at 85°C for 45 min 2µl of the lysate was used to performed genotyping PCR.

3.2.5.2 Genotyping of mice by PCR

Genotyping of mice was performed using the following PCR protocol and primers listed in Table 3. 4.

Protocol for genotyping of *Hs2st* mice:

PCR Mix

ddH_2O	18.7 µl
10 x PCR Buffer	2.5 µl
DMSO	1.25 µl
2OstP1 (100 µM)	0.1 µl
LAR1 (100 µM)	0.1 µl
dNTPs (100 mM)	0.2 µl
Taq-Polymerase 5U/ µl	0.2 µl
Template	2 µl

PCR program

Temperature	Time	Number of cycles
94°C	5’	1
94°C	25”	28
60°C	40”	
72°C	60”	
4°C	∞	

The presence of a knock out allele is indicated by PCR product with size 360 bp, while a 870 bp band indicates a wild-type allele.

Protocol for genotyping of *Ndst1* mice:

PCR Mix

ddH_2O	18.6 µl
10 x PCR Buffer	2.5 µl
DMSO	1.25 µl
NDST1-16R (100 µM)	0.1 µl
NDST1-10R (100 µM)	0.1 µl
NDST1 17F (100 µM)	0.1 µl
dNTPs (100 mM)	0.2 µl
Taq-Polymerase 5 U/ µl	0.2 µl
Template	2 µl

PCR Program

Temperature	Time	Number of cycles
94°C	5’	1
94°C	25”	28
60°C	40”	
72°C	60”	
4°C	∞	

The resulting PCR products were separated on 2% agarose gel. A 500 bp PCR product indicates a knock out allele, while the 250 bp fragments indicates a wild-type allele.

Protocol for genotyping of *Glce* mice:

PCR Mix

ddH_2O	19.65 µl
10 x PCR Buffer	2.5 µl
DMSO	1.25 µl
Primer JP54 (100 µM)	0.1 µl
Primer JP46/LoxP1 (100 µM)	0.1 µl
dNTPs (100 mM)	0.2 µl
Taq-Polymerase 5U/ µl	0.2 µl
Template	2 µl

PCR Program

Temperature	Time	Number of cycles
95°C	2’	1
95°C	15”	33
54°C	60”	
72°C	60”	
4°C	∞	

The combination of the primers JP54-JP46 results in a 729 bp PCR product, indicating a wild-type allele, while a PCR product obtained with the primer pair JP54-LoxP1 results in a 350 bp band indicating a knock out allele.

Protocol for genotyping of *Ext1*$^{gt/gt}$ mice:

PCR Mix

ddH_2O	20 µl
10 x PCR Buffer	2.5 µl
DMSO	1.25 µl
Primer*Ext*1Fw (100 µM)	0.1 µl
Primer*Ext*1Rv (100 µM)	0.1 µl
Primer 5’pgto (100 µM)	0.2 µl
dNTPs (100 mM)	0.2 µl
Taq-Polymerase 5 U/ µl	0.2 µl
Template	2 µl

PCR Program

Temperature	Time	Number of cycles
95°C	5’	1
95°C	45”	32
54°C	45”	
72°C	60”	
72°C	7’	
4°C	∞	

The resulting 800 bp fragment indicates a transgenic allele, while the 600 bp fragments–a wild-type allele.

Protocol for genotyping of *Sulf1;Sulf2* compound mutants

Sulf1 PCR conditions

PCR Mix

ddH_2O	19 µl
10 x PCR Buffer	2.5 µl
DMSO	1.25 µl
F1 (100 µM)	0.1 µl
R1 (100 µM)	0.1 µl
AK30R (100 µM)	0.2 µl
dNTPs (100 mM)	0.2 µl
Taq-Polymerase 5U/ µl	0.2 µl
Template	2 µl

PCR Program

Temperature	Time	Number of cycles
94°C	2’	1
94°C	15”	30
56°C	15”	
72°C	45”	
72°C	2’	1
4°C	∞	

The resulting PCR fragments are of size of 900 bp indicating a knock out allele, and 300 bp indicating a wild-type allele.

Sulf2 PCR conditions

PCR mix

ddH_2O	20 µl
10 x PCR Buffer	2.5 µl
DMSO	1.25 µl
S2 Fw (100 µM)	0.1 µl
S2 Rev (100 µM)	0.1 µl
AK31R neo (100 µM)	0.2 µl
dNTPs (100 mM)	0.2 µl
Taq-Polymerase 5U/ µl	0.2 µl
Template	2 µl

PCR Program

Temperature	Time	Number of cycles
94°C	2’	1
94°C	15”	30
54°C	15”	
72°C	45”	
72°C	2’	1
4°C	∞	

The presence of knock out allele is indicated by PCR product of size 400 bp. The wild-type allele produces a fragment corresponding to 250 bp.

3.2.5.3 Harvesting and processing of murine tissues

Murine embryos were harvested via C-section at noon of the desired embryonic day. For timed pregnancies, noon of the day when a vaginal plug was observed was considered to be embryonic day 0.5. Limbs were harvested, washed in PBS and fixed in 4% PFA. Tissues of

different stage were dehydrated in ethanol solutions with stepwise increasing concentration (Table 3. 5) followed by incubation in xylene. The processed limbs were subsequently embedded into paraffin and sectioned on microtome at 6 μm to obtain 5-6 parallel sections. Sections were incubated in water bath, then transferred onto Superfrost microscope slides, followed by an incubation at 60°C on a hot plate. Sections were stored at 4°C for further analysis.

Table 3. 5 Protocol for tissue dehydration in ethanol

Stage / Solution	E 14.5	E 16.5	E 18.5
70% Ethanol	10 min	30 min	90 min
80% Ethanol	10 min	30 min	90 min
95% Ethanol	10 min	30 min	90 min
100% Ethanol	3 x 10 min	3 x 1 min	2 x 90 min; 1 x 60 min
Xylene	3 x 20 min	3 x 30 min	3 x 30 min
Paraffin	2 x 60 min	2 x 60 min	2 x 60 min

When intending purification of GAGs for column preparation whole embryos were subjected to snap freezing in liquid nitrogen. For analysis of skeletal GAG composition, skeletons were manually cleaned from skin, muscles and inner organs and frozen in liquid nitrogen.

3.2.6 Histology and immunofluorescence analysis

3.2.6.1 Safranin-Weigert staining

SafraninO is a cationic dye, which is often used to detect PGs and GAGs. Due to the high content of these molecules, the stained cartilage can be observed in intense red color. Additional staining with Weigert solution and Fast Green results in nuclei, stained in black on a green background.

Sections were deparaffinized in xylene for 15 min, rehydrated by short incubations in ethanol solutions with stepwise descending concentrations, and subsequently incubated in the following solution: Weigert Solution (2-3 min), Scotts Buffer (2 min) and Fast green (2 min). Following these steps, slides were rinsed in 1% glacial acid and tap water and incubated for 5 min in 0.1% SafraninO. Finally, slides were rinsed in tap water, dehydrated by short

incubation in alcohol solution with stepwise increasing concentrations, incubated in xylene and embedded in DPX mounting medium.

3.2.6.2 Glycosaminoglycan immunochistochemistry

Numerous antibodies are available for immunodetection of GAGs. Each of these antibodies recognizes a specific sulfation domain, which can be native or result of enzymatic digestion.

3.2.6.2.1 Detection of *N*-sulfated HS with 10E4 antibody

The 10E4 antibody recognizes mixed (GlcA-GlcNS)/(GlcA-GlcNAc) region therefore can be used for determination of the overall distribution of HS in the tissue (David et al., 1992).
Sections were deparaffinized in xylene for 15 min, rehydrated by short incubations in ethanol solutions with stepwise descending concentrations and finally rinsed in PBS. The following hyaluronidase I digest (40 min with 100 U/ml enzyme) was performed at 37°C in a humidified chamber. After the digest, samples were washed with PBS. The endogenous peroxydase was inactivated with 3% H_2O_2 / PBS for 30 min at RT. The slides were rinsed in PBS and unspecific binding was blocked by an incubation in 10% goat serum/PBS for 40 min. The primary antibody 10E4 was diluted in blocking buffer (1:100 in 10% goat serum), applied onto the tissue and allowed to bind o/n at 4°C. During all incubations with antibodies or enzymes the slides were covered with plastic coverslips and kept in humidified chamber. After the o/n incubation, the slides were washed with PBS to remove unbound antibody and then incubated for 40 min with goat biotinylated secondary antibody against mouse IgM (1:200 in blocking solution). After washing with PBS (3X, 5 min) a Strepatvidin-HRP was applied (1:100 in 10% goat serum) for 40 min at RT. Slides were washed 3 times for 5 min. in 1xPBS and then incubated with DAB for 5 min. Sections were then counterstained with methyl green or directly mounted with DPX.

3.2.6.3 Detection of CS neoepitopes

The CS neoepitopes generated by chondroitinase ABC digestion were detected with monoclonal antibodies 1B5 (*O*-sulphated unsaturated disaccharide ‘stubs’ (C-0-S)/ΔUA-GalNAc), 2B6 (4-*O*-sulphated unsaturated disaccharides (C-4-S)/ΔUA-GalNAc4S) and 3B3 (6-*O*-sulphated unsaturated disaccharides (C-6-S)/ΔUA-GalNAc6S) (Hayes et al., 2008).
Paraffin section were deparaffinized, rehydrated and washed 3 times for 5 min in chondroitinase digestion solution. CS was digested with 0.4 U/ml chondroitinase ABC from *Proteus vulgaris* (Sigma-Aldrich) at 37°C for 1 hr in humidified chamber. After digestion the slides were washed in PBS followed by incubation in blocking solution (10% goat serum for

IgM primary antibodies or 10% horse serum for IgG primary antibodies) for 1 hour. The CS antibodies were applied in an appropriate dilution (1B5 1:10, 2B6 1:5 and 3B3 1:5) onto the slides and allowed to bind o/n at 4°C. Following the o/n incubation the slides were rinsed with PBS and incubated for 40 min at RT with either goat biotinylated secondary antibody against mouse IgM or horse biotinylated secondary antibody against mouse IgG (1:200 in blocking solution). After washing with PBS, Streptavidin-Alexa 488 (1:500 in blocking solution) was applied onto the slides and allowed to bind for 40 min at RT. The slides were washed, permeabilized with 0.05% Triton X-100 in PBS and incubated with DAPI for 10 min to stain the cell nuclei. After additional washing, the slides were mounted with MOWIOL.

3.2.7 Quantification and statistical analysis

3.2.7.1 Multiple sequence alignment

Multiple sequence alignment of Hh protein sequences was constructed using and Jalview software and T-coffee algorithm.

3.2.7.2 Quantification of immunoblots

Immunoblots were quantified using a tool for gel analyses, part of the ImageJ software package. Total pixels in each lane were quantified and normalized to total recovered protein, detected on the blot.

3.2.7.3 Size-exclusion chromatography for GAG chain length analysis

The cpm values in each fraction were normalized to the value of total cpm obtained in the separation. The results were plotted against the exact elution volume corresponding to each measurement point. The relative GAG amount in the polymer peak and the disaccharide peak (dp2) were quantified as a sum of the cpms normalized to the total cpms recovered in a separation run.

3.2.7.4 Determination of relative size of protein multimers and GAG chains

Equilibration of Superdex 200 10/300 was performed using Gel Filtration Calibration Kit HMW and LMW, following instructions of the manufacturer. Kav values were determined by the formula $Kav = (Ve - Vo)/(Vc - Vo)$, where Ve is elution volume of the samples, V_0–void volume and Vc–one total column volume. V_0 was determined using dextran blue.

To determine the GAG chain length Kav values were calculated according to the formula $Kav = (Ve - Vo)/(Vt - Vo)$, where Ve is elution volume of the samples, V_0–void volume

and Vt–total column volume. The obtained *K*av values were compared to those of known disaccharide standards, allowing calculation of the apparent molecular size of the GAGs (Dagalv et al., 2015; Deligny et al., 2016). V_0 and V_t were determined using dextran blue and ^3H_2O, respectively.

3.2.7.5 Quantification of fluorescence pictures using ImageJ software

To quantify relative DAPI and GFP fluorescence signal the same region of columnar, proliferating chondrocytes was selected using ROI Manager option in the DAPI and then in the GFP channel. The area, integrated density and mean gray value were quantified. Based on these values, the corrected total cell fluorescence was calculated using the formula: CTCF = Integrated Density – (Area of selected cell x mean fluorescence of background readings). Background readings were calculated as average of at least 3 regions without a fluorescence signal (McCloy et al., 2014). CTCF was calculated for the fluorescence signal in each channel. CTCF of the desired probe was normalized to the CTCF of the nuclear DAPI staining.

3.2.7.6 Statistical analyses

Statistical analyses were performed using unpaired, two-tailed Student's *t*-test and two-way ANOVA with Bonferroni post-test. Significance was assumed if $p < 0.05$

4 Results

4.1 Analyses of Ihh interaction with HS and multimerization

4.1.1 Identification and modeling of HS-binding sites in the mouse Ihh protein

The interactions of the extracellular GAGs with secreted proteins are mediated by the high negative charge of the GAG chains and motifs of positively charged residues within the proteins. To identify such binding sites within the Ihh protein, the amino acid sequences of the Hh family members in human, mouse, chicken and the fruit fly were aligned. The comparison revealed 27% overall identity in the protein sequences and 56% in the N-terminal signaling domain. Two highly conserved motifs of basic amino acids were identified as potential HS-binding domains of Ihh (Fig. 4. 1 A, B). These motifs are present in all analyzed Hh family members and have previously been characterized as HS-binding motifs in Shh (Chang et al., 2011; Farshi et al., 2011; Rubin et al., 2002; Whalen et al., 2013). One of the motifs, hereinafter referred to as CW1, is located in the extended N-terminal tail of the protein (Fig. 4. 1 A, A'). It represents a classical Cardin-Weintraub motif and is composed of five basic amino acids with the characteristic signature BBBXXBB, where B stands for positively charged and X for any amino acid. Differently to the CW1 motif of the closely related mouse Shh protein, which contains three lysine (K) and two arginine (R) residues (K-R-R-H-P-K-K), the Ihh sequence (R-R-R-P-P-R-K) comprises four R and one K residues. Additionally, while the Shh CW1 motif includes only one proline (P), an amino acid common in tight polypeptide turns, the Ihh motif contains two. These two P residues define a more pronounced and complex "kink" in the highly flexible Hh N-terminus, characterized by a random coil-like conformation, compared to other family members (Billings and Pacifici, 2015).

The second binding motif, hereinafter referred to as CW2, is discontinuous and consists of five basic amino acids, located in the globular domain of the protein (Fig. 4. 1 C) (Chang et al., 2011; Whalen et al., 2013). It comprises the residues K130, R166, R196, R198 and K221, which are highly conserved across different species. Crystal structure analysis (by Dr. Rocio Rebollido-Rios) (Fig. 4. 1 C, B') revealed that in the folded protein these amino acids position in close proximity, forming a potential HS-binding site on the surface of the globular domain. The two HS-binding motifs are located on the same side of the Ihh molecule, albeit with some distance. Such location might enable a simultaneous interaction with HS, either in a monomeric or in a multimeric organization.

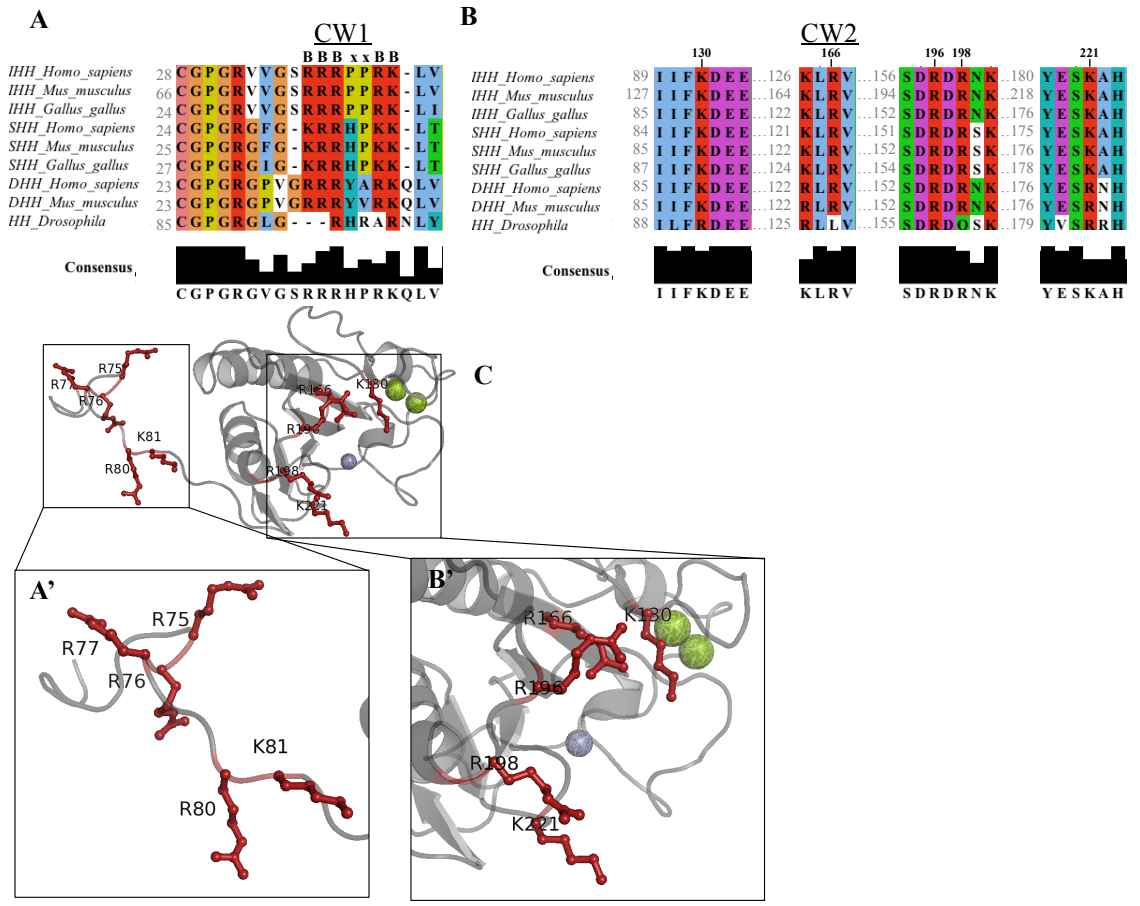

Fig. 4. 1 The HS-binding motifs, CW1 and CW2, are highly conserved among the Hedgehog family members.
Multiple sequence alignment of the vertebrate N-terminal Shh, Ihh and Dhh and the *Drosophila* Hh domains reveals the presence of two conserved HS-binding motifs: the previously described N-terminal motif, CW1 (A, A') and a motif in the globular domain, CW2 (B, B'). Basic amino acids are indicated in red. Metal ions are shown as slate (zinc) and green (calcium) spheres. The orientation of CW1 and CW2 binding sites are revealed in a modeled murine IhhNp crystal structure (template: pdb:3n10) (C).

4.1.2 Ihh CW motifs vary in their affinity to differently sulfated HS

To evaluate the role of the Ihh CW motifs in an interaction with HS, the positively charged amino acids were stepwise mutated either to the nonpolar alanine (A) residue in the CW1 motif or to the polar amino acid serine (S) in the CW2 sequence (Fig. 4. 2 A, B). Due to the high flexibility of the Ihh N-terminal "tail" containing the CW1 domain, it is unlikely that an alteration of the charged R and K residues to an A will greatly affect the conformation of the region. In contrast, preserving the polarity of the CW2 motif, which overlaps with the binding domain of the Ihh receptor Ptch1, is crucial in terms of maintaining the site topology and protein activity (Maun et al., 2010).

4.1.2.1 In Ihh, the CW2 rather than the CW1 motif regulates the interaction with highly sulfated HS

To characterize the importance of the Ihh CW motifs for the interaction with HS, wild-type IhhNp and the CW mutants were overexpressed in HEK-293Ebna cells, and the binding properties of the proteins released into the conditioned medium were examined by affinity chromatography. The elution step in all affinity chromatography experiments was performed using a buffer with an increasing ionic strength, applied as a linear gradient (0-2 mol/L NaCl). The resulting protein fractions were analyzed on western blot using an α-ShhN antibody (recognizing also the signaling domain of Ihh) and quantified using ImageJ software. The protein amount in each fraction was normalized to the total recovered protein.

The protein affinity was initially evaluated using commercially available heparin affinity column (Fig. 4. 2 C, D, E). In heparin affinity chromatography, wild-type IhhNp eluted between 0.5-0.9 mol/L NaCl, producing two peaks at 0.6 and ≈0.8 mol/L NaCl, respectively. The observed protein affinity was slightly higher than the previously reported data for ShhN (non cholesterylated Shh form) (Chang et al., 2011). Alterations in the CW1 motif moderately decreased the affinity to heparin for the majority of the mutant proteins. While compound mutation at positions R76 and R80 ($IhhNp^{R76A/R80A}$) had limited effect on the IhhNp-heparin interactions, a substitution of R75 and R77 with A residues in $IhhNp^{R75A/R77A}$, or K81 in $IhhNp^{K81A}$ resulted in decreased affinities to the ligand, demarcated by an elution at lower salt concentration (between 0.4-0.7 mol/L NaCl, elution peak at 0.5 mol/L NaCl). Mutating all five CW1 residues to alanine ($IhhNp^{R75A/R76A/R77A/R80A/K81A}$) or a deleting the complete sequence ($IhhNp^{\Delta CW}$) did not further decrease the protein affinity to heparin (Fig. 4. 2 C).

Interestingly, analysis of the Ihh CW2 mutants revealed a more pronounced effect of the motif on the interaction with heparin. Mutation of the residue K130 (Ihh^{K130S}) or K221 ($IhhNp^{K221S}$) decreased the protein affinity to the same degree as the complete substitution with A ($IhhNp^{R75A/R76A/R77A/R80A/K81A}$) or deletion ($IhhNp^{\Delta CW}$) of the CW1 motif (Fig. 4. 2 C, D). A similar effect was observed for the $IhhNp^{R166S/K221S}$ mutant. More severe perturbation of the heparin binding was observed if three or more positively charged residues within the motif were mutated, leading to an elution of the mutants $IhhNp^{K130S/R166S/R196S}$, $IhhNp^{K130S/R166S/R196S/R198S}$ and $IhhNp^{K130S/R166S/R196S/R198S/K221S}$ at 0.4 mol/L NaCl (Fig. 4. 2 E). In contrast to all other CW2 mutant proteins, $IhhNp^{K130S/R166S}$ interacted with higher affinity with heparin compared to the wild-type IhhNp.

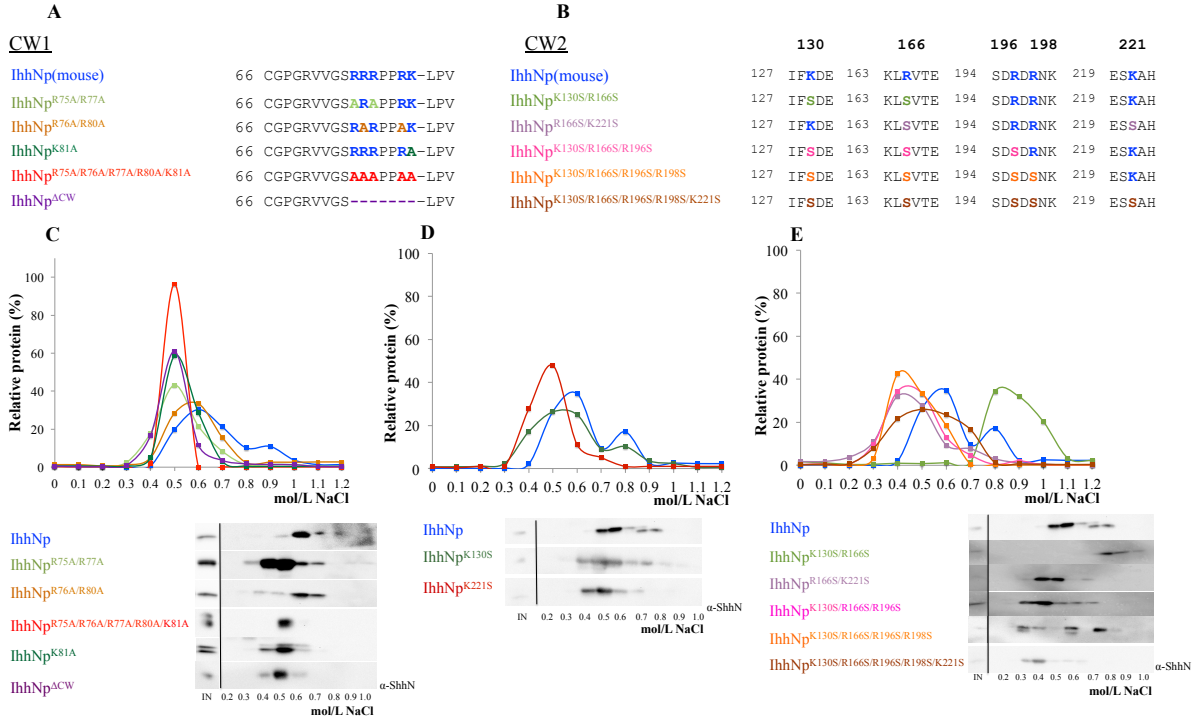

Fig. 4. 2 In Ihh, the CW2 rather than the CW1 motif regulates the interaction with the highly sulfated heparin.

Wild-type IhhNp was used as a template to generate the CW mutants depicted in A (CW1 mutants) and B (CW2 mutants). The wild-type and mutant proteins were expressed in HEK-293Ebna cells. The affinity of the conditioned medium-derived proteins to heparin was evaluated using affinity chromatography. Wild-type IhhNp eluted between 0.5-0.9 mol/L NaCl (C, D). CW1 mutants showed a moderately decreased affinity to heparin, eluting between 0.4-0.7 mol/L NaCl (C), while mutations in CW2 motif resulted in elution between 0.3-0.7 mol/L NaCl, indicating a stronger perturbation in heparin binding (D, E). The experiments were performed in duplicates. Protein levels were quantified using ImageJ software and are given as (%) relative to the total recovered protein. Chromatograms represent mean values of two independent experiments. Western blots show one representative experiment. IN=20% of the input.

4.1.2.2 The IhhNp CW1 motif defines the IhhNp interaction with HS

In biological systems, heparin is exclusively produced by mast cells (Carlsson and Kjellen, 2012), whereas other tissues synthesize the less sulfated HS (Bishop et al., 2007; Esko and Lindahl, 2001; Sarrazin et al., 2011). To elucidate the importance of CW1 and CW2 motifs for the IhhNp interaction with HS, embryonic HS was purified from E16.5 *NMRI* mice and coupled to a HiTrap NHS-activated HP column. The HS column was employed in affinity chromatography experiments, performed and analyzed as described for the heparin affinity chromatography experiment (section 4.1.2.1).

The wild-type IhhNp bound with lower affinity to embryonic HS compared to heparin and eluted between 0.3-0.6 mol/L NaCl with an elution peak at 0.4 mol/L NaCl. Importantly, all IhhNp CW1 mutants exhibited a reduced affinity to HS as shown by the onset of elution at salt concentrations at and below 0.2 mol/L NaCl (Fig. 4. 3 A, B). The most pronounced reduction in HS affinity was observed for the CW1 deletion mutant ($Ihh^{\Delta CW}$) demarcated by a shift in the elution profile by 0.2 mol/L NaCl compared to the wild-type protein (Fig. 4. 3 B).

In contrast to the strong influence of the CW2 motif on the interaction with heparin, the motif does not seem to be the main contact region for the lower sulfated HS (Fig. 4. 3 C, D). A slightly decreased affinity to HS was detected for $IhhNp^{R166S/K221S}$ and $IhhNp^{K130S/R166S/R198S}$ protein, as shown by the shift in the elution profile by 0.1 mol/L lower salt concentration. Introducing an additional mutation at position R198 ($IhhNp^{K130S/R166S/R196S/R198S}$) and K221 ($IhhNp^{K130S/R166S/R196S/R198S/K221S}$) resulted in a severely reduced recovery of the proteins, although each was expressed at similar levels as the other analyzed mutants. Nevertheless, the elution profile of the recovered $IhhNp^{K130S/R166S/R196S/R198S}$ protein showed binding to HS with an affinity similar to that of wild-type IhhNp (Fig. 4. 3 D).

Taken together, these data demonstrate that the interaction of Ihh with HS is mediated by both CW domains of positively charged amino acids. Moreover, each motif seems to have distinct preference of binding to low and highly sulfated HS (heparin/HS) underlining a specificity of the interaction.

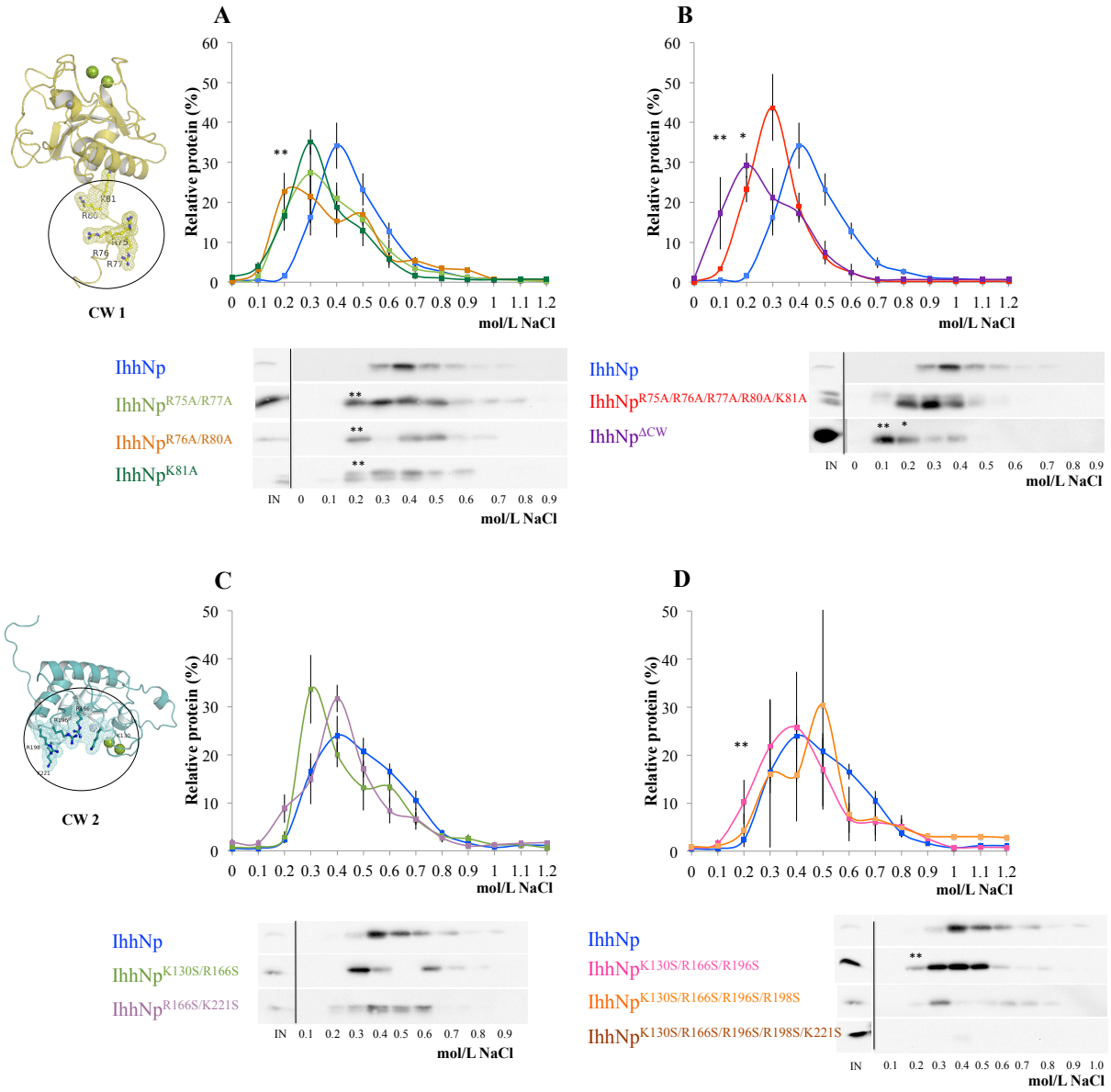

Fig. 4. 3 The binding of IhhNp to HS is mainly determined by the CW1 sequence.
Recombinant full-length wild-type and CW-mutant IhhNp proteins were expressed in HEK-293Ebna cells. The affinity of the conditioned medium-derived proteins to HS, purified from E16.5 embryos was analyzed by affinity chromatography. Wild-type IhhNp eluted between 0.3–0.7 mol/L NaCl (blue). Mutations in the CW1 motif significantly reduced the protein affinity, demarcated by a shift in the elution peaks (A, B). The effect of CW2 motif on the interaction with HS was less prominent (C, D) and a decreased affinity was only observed for the mutant IhhNp$^{K130S/R166S/R196S}$ (purple) (D). Mutating the complete CW2 sequence caused a severe decrease of the recovered protein (brown, western blot, D). IN contains 20% of protein amount applied on the column. Protein levels, quantified using ImageJ software, are expressed as (%) relative to the total recovered protein. Chromatograms represent mean values ± s.e.m. The levels of the mutant proteins at each data point were compared to these of the wild-type protein. Unpaired, two-tailed Student's *t*-test was performed to calculate significance. *p* -values <0.05 were considered significant. * p <0.05, ** p <0.01. n≥4. For the mutants IhhNp$^{R75A/R76A/R77A/R80AK81A}$, IhhNp$^{R166S/K221S}$, IhhNp$^{K130S/R166S}$ and IhhNp$^{K130S/R166S/R196S/R198S}$ n=2. Western blot analysis shows one representative experiment.

4.1.3 The HS-binding motifs mediate the protein multimerization

A key characteristic of Hh proteins is their ability to form large multimers (Chen et al., 2004; Goetz et al., 2006), which have been detected on the cell surface of the producing cells and upon release in the extracellular space. HS have been implicated as mediators of the multimerization process (Dierker et al., 2009a; Vyas et al., 2008).

To investigate the role of the HS-binding motifs in the multimerization of IhhNp, the CW1 and CW2 mutants were expressed in HEK-293Ebna cells and analyzed by size-exclusion chromatography using a Superdex 200 column. The recovered proteins were immunoblotted and quantified using ImageJ software.

Wild-type IhhNp formed mainly large multimers of more than 660 kDa (Fig. 4. 4), which were observed in all experiments, while only in two out of eleven experiments a monomeric (19 kDa) protein was detected. In contrast, all CW1 mutants formed a variety of smaller clusters beside the large multimers (Fig. 4. 4 A, B), indicating that the CW1 domain is important for the organization of Ihh into multimers. Interestingly, a single amino acid substitution at position K81 (IhhNp^{K81A}) by alanine resulted in the formation of mainly ≈300 and ≈600 kDa multimers, while the multimers of the compound mutants IhhNp$^{R75A/R77A}$ and IhhNp$^{R76A/R80A}$ ranged between >660 kDa to 100 kDa (Fig. 4. 4 A). Surprisingly, the complete deletion of the CW1 sequence (IhhNp$^{\Delta CW}$) restored the formation of predominantly large multimers (Fig. 4. 4 B).

The capacity of IhhNp to form large multimers was affected in a different manner by mutations in the CW2 motif. Alteration of two amino acids in the motif (IhhNp$^{K130S/R166S}$ and IhhNp$^{R166S/K221S}$) did not affect the protein multimerization (Fig. 4. 4 C), whereas alterations of three or more residues reduced the formation of multimers >660 kDa (mutants IhhNp$^{K130S/R166S/R196S}$, IhhNp$^{K130S/R166S/R196S/R198S}$, IhhNp$^{K130S/R166S/R196S/R198S/K221S}$) (Fig. 4. 4 D). Interestingly, these mutants exhibited a lower affinity to embryonic HS as well (Fig. 4. 3 D). Nevertheless, except for the IhhNp$^{K130S/R166S/R196S/R198S}$, no decrease in multimer size below 350 kDa was observed.

These data show that the HS-binding domains, and likely an interaction with HS, are crucial for the formation of Ihh multimers.

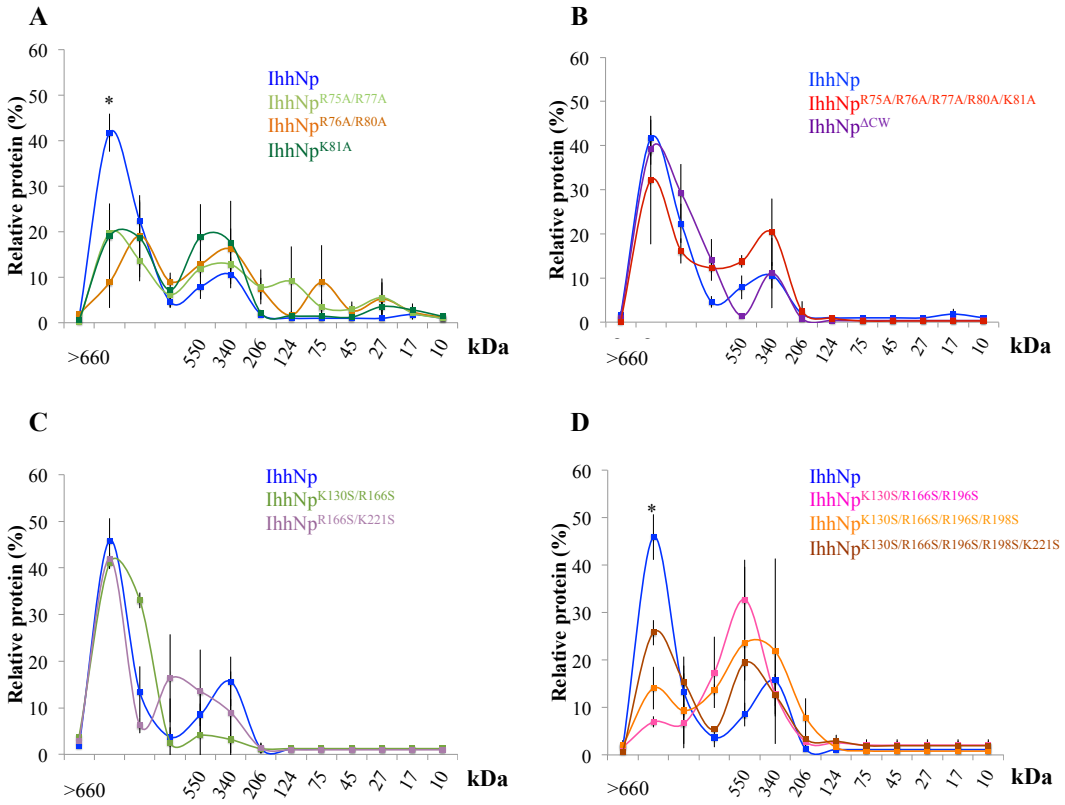

Fig. 4. 4 CW1 and CW2 motif integrity is required for Ihh multimerization *in vitro*. Recombinant IhhNp CW1 (A) and CW2 (B) mutant and wild-type proteins were expressed in HEK-293Ebna cells and analyzed by size-exclusion chromatography, followed by immunoblotting. The wild-type IhhNp multimers had a size of >660 kDa. Substitution of amino acids in the CW1 domain resulted in multimer size ranging between 660-100 kDa (A). Mutations in the CW2 motif had distinct influence on protein multimerization. Mutants with three or more amino acid exchanges formed multimers mostly of ≈550 kDa size (B). The sizes of molecular weight standards are indicated. Chromatograms represent mean values ± s.e.m. The levels of mutant and wild-type proteins of each molecular size were compared. Statistical analyses were carried out using two-tailed, unpaired Student's *t*-test, * $p < 0.05$. In (A) * indicates significant difference in the amount of large multimers for $IhhNp^{R75A/R77A}$, $IhhNp^{R76A/R80A}$, $IhhNp^{K81A}$ and in (D) for $IhhNp^{K130S/R166S/R196S}$ compared to IhhNp. n ≥ 3. For $IhhNp^{R166S/K221S}$, $IhhNp^{K130S/R166S}$, $IhhNp^{R75A/R76A/R77A/R80A/K81A}$, n=2.

4.1.4 Homolog-specific variations in the CW1 sequence define distinct HS-binding affinities and multimer sizes

Despite the 88% identity of the N-terminal signaling domains of Shh and Ihh they share only four identical amino acids in the CW1 motif. As outlined above, the Shh CW1 motif is composed of K-R-R-H-P-K-K, while the Ihh sequence (**R**-R-R-**P**-P-**R**-K) is predominated by R and contains only one K residue. Additionally, the Ihh CW1 motif includes two proline residues instead of the H-P combination found in Shh (Fig. 4. 5 A). Further differences are observed in the sequence upstream of the CW1 motif, which in Ihh comprises the residues V-V-G-S, while in Shh it consists of G-F-G-, lacking the residue at the last position. It is conceivable that such relatively high concentration of amino acid variation in a conserved

binding motif determines differences in HS interaction and multimerization between the paralogs. To test this possibility, the affinity to HS and the multimer size of ShhNp and IhhNp expressed in HEK-293Ebna cells were compared by affinity and size-exclusion chromatography.

4.1.4.1 Variations in CW1 sequence of Shh and Ihh determines difference in their affinity to HS

Wild-type ShhNp and IhhNp were bound with rather similar strength to HS and eluted between 0.3-0.6 mol/L NaCl. However, in comparison to IhhNp, larger amounts of ShhNp were eluted with lower salt concentration (0.3 mol/L NaCl) indicating slightly weaker binding to HS (Fig. 4. 5 B). To confirm that this difference is due to the variation in the Hh N-terminal HS-binding sequence, the following mutants were generated and analyzed: IhhNp bearing the Shh CW1 (sCW1) motif (IhhNp$^{R75K/P78H/R80K}$), a IhhNp containing the extended Shh N-terminal CW1 sequence (IhhNp$^{\underline{V71G/V72F/S74\Delta}/R75K/P78H/R80K}$), and a ShhNp mutant carrying the Ihh CW1 (iCW1) sequence (ShhNp$^{K33R/H36P/K38R}$) (Fig. 4. 5 A). An exchange of IhhNp CW1 with the sCW1 sequence (IhhNp$^{R75K/P78H/R80K}$) resulted in a HS affinity similar to Shh, demarcated by the elevated protein elution at 0.3 mol/L NaCl, (Fig. 4. 5 B (green)). The IhhNp mutant with the extended sCW1 motif (IhhNp$^{\underline{V71G/V72F/S74\Delta}/R75K/P78H/R80K}$) was characterized by a decreased protein elution at higher salt concentration (0.5-0.6 mol/L NaCl), exhibiting an even more similar elution profile to ShhNp. According to this result, the amino acid sequence located upstream of the iCW1 motif seems to contribute to the Ihh/HS interaction. Unexpectedly, ShhNp$^{K33R/H36P/K38R}$ carrying the iCW motif did not reproduce the IhhNp elution profile, but was characterized by weaker and stronger binding affinity compared to both wild-type proteins (Fig. 4. 5 C). This further supports the hypothesis that the environment of the CW1 motif contributes to the HS binding.

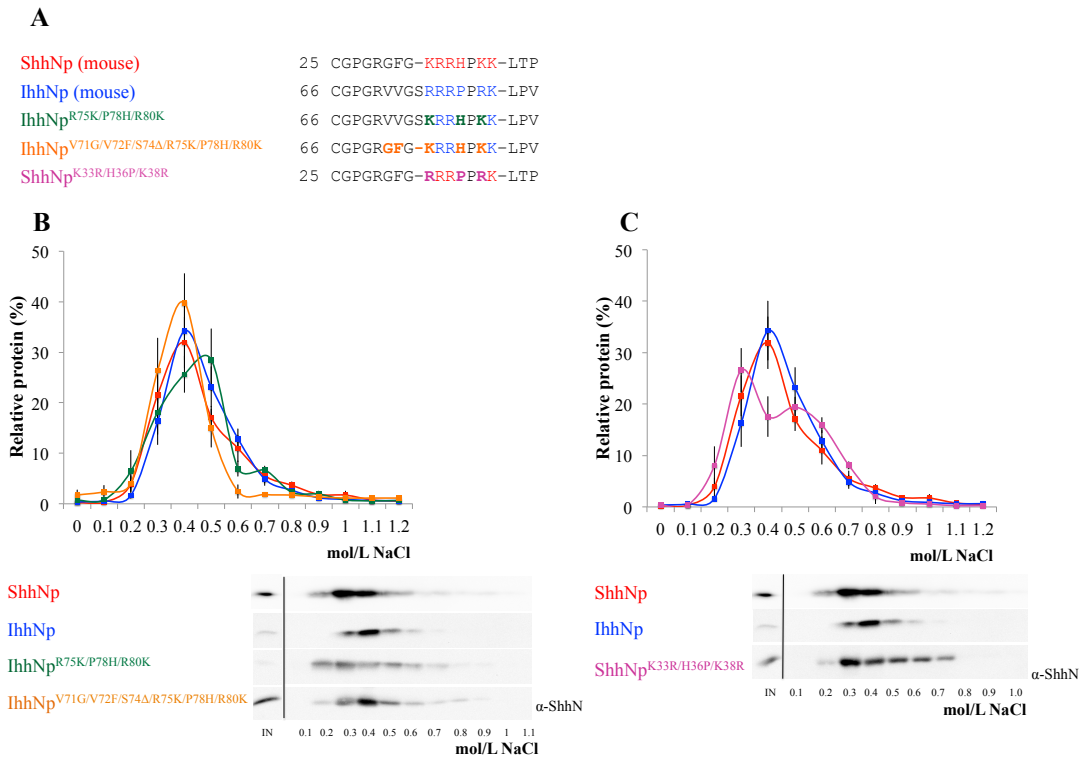

Fig. 4. 5 The R-rich CW1 sequence of Ihh determines a higher affinity to HS compared to Shh.
Shh and Ihh differ in their CW1 sequences (A). HS affinity chromatography of IhhNp and ShhNp expressed in HEK-293Ebna cells showed a mild difference in their HS affinity, with Shh binding weaker (B, C). IhhNp protein mutants containing a partial or complete sCW1, as well as Shh with an iCW1 motif were generated (A). An increase of CW1 motif similarity to the paralogous protein resulted in a HS interaction resembling the protein of the CW1 sequence origin (B and C). Chromatograms represent mean values ± s.e.m. The protein amounts were quantified using ImageJ software and are given as (%) relative to total recovered protein. Western blots show one representative experiment. n=4, ShhNp$^{K33R/H36P/K38R}$ n=3.

4.1.4.2 Variations in the CW1 sequence composition determine paralog-specific multimer sizes

To elucidate whether the differences between the Shh and Ihh CW1 sequences affect the size of their multimers the wild-type proteins and the CW1-exchange mutants were analyzed by size-exclusion chromatography (Fig. 4. 6, Table 9. 1). Similar to previous studies (Farshi et al., 2011; Ohlig et al., 2011), the size of ShhNp multimers ranged between >660 kDa and less than 200 kDa. In contrast, IhhNp formed solely multimers of >660 kDa. Substitution of the motif with the sCW1 sequence in IhhNp$^{R75K/P78H/R80K}$ increased the size range of the protein clusters, which, similar to ShhNp were observed from >660 to >550 kDa. Interestingly, introducing the extended ShhNp CW1 in IhhNp$^{V71G/V72F/S74\Delta/R75K/P78H/R80K}$ restricted the variety of the multimers, which were detected between ≈660 and >550 kDa. Contrariwise, the

ShhNp$^{K33R/H36P/K38R}$, carrying the iCW1 motif, phenocopied the IhhNp protein and formed mostly multimers of >660 kDa.

Together, these data show that the sequence of the extended Hh CW1 domain defines paralog-specific HS affinity and multimer size.

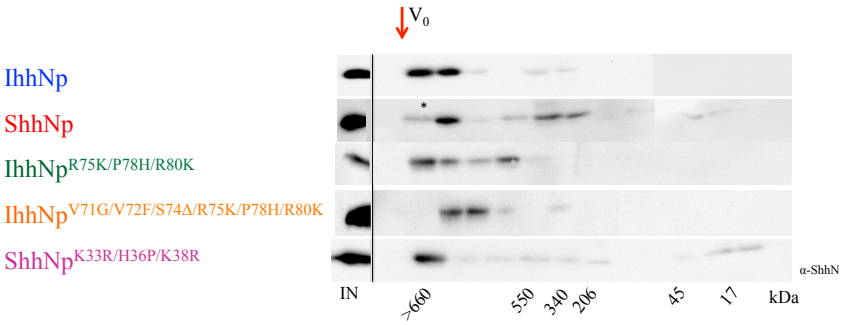

Fig. 4. 6 The composition of the CW1 motif determines a paralog-specific multimer size. Size-exclusion chromatography of conditioned medium derived from HEK-293Ebna cells expressing wild-type ShhNp and IhhNp, and CW1-exchange mutant proteins. The IhhNp$^{R75K/P78H/R80K}$ mutant (dark green) carrying the sCW1 motif formed clusters with similar size distribution to ShhNp, while the variety of IhhNp$^{V71G/V72F/S74\Delta/R75K/P78H/R80K}$ (orange) multimers was restricted. Conversely, introducing the iCW1 motif into ShhNp resulted in multimer sizes similar to IhhNp. The levels of the mutant proteins and ShhNp at each molecular size were compared to IhhNp. Statistical analyses were carried out using two-tailed, unpaired Student's *t*-test, * $p < 0.05$. The sizes of molecular weight standards and V_0 are indicated. One representative experiment is shown. n≥3.

4.1.5 HS-binding motifs are required for Ihh signaling activity

Previous studies of Shh have implicated that the CW1 motif integrity influences the signaling activity of the protein (Farshi et al., 2011). For this reason, the biological activity of Hh mutant proteins was assessed using the Hh-dependent osteoblast differentiation of C3H10T1/2 cells (Fig. 4. 7). The osteoblast precursor cells were cultured for five days in medium supplemented with equal amounts of the analyzed proteins. The activity of the alkaline phosphatase (AP), which is upregulated during osteoblast differentiation, was used as a read-out for the Hh induced differentiation of C3H10T1/2 cells, and hence for the biological activity of the mutant proteins (Nakamura et al., 1997). Treatment with purmorphamine (PA), a Hh agonist, was used as a positive control, while cyclopamine (CA), given in parallel to the analyzed protein, was used to block the Hh pathway and served as a negative control, together with medium from mock-transfected cells.

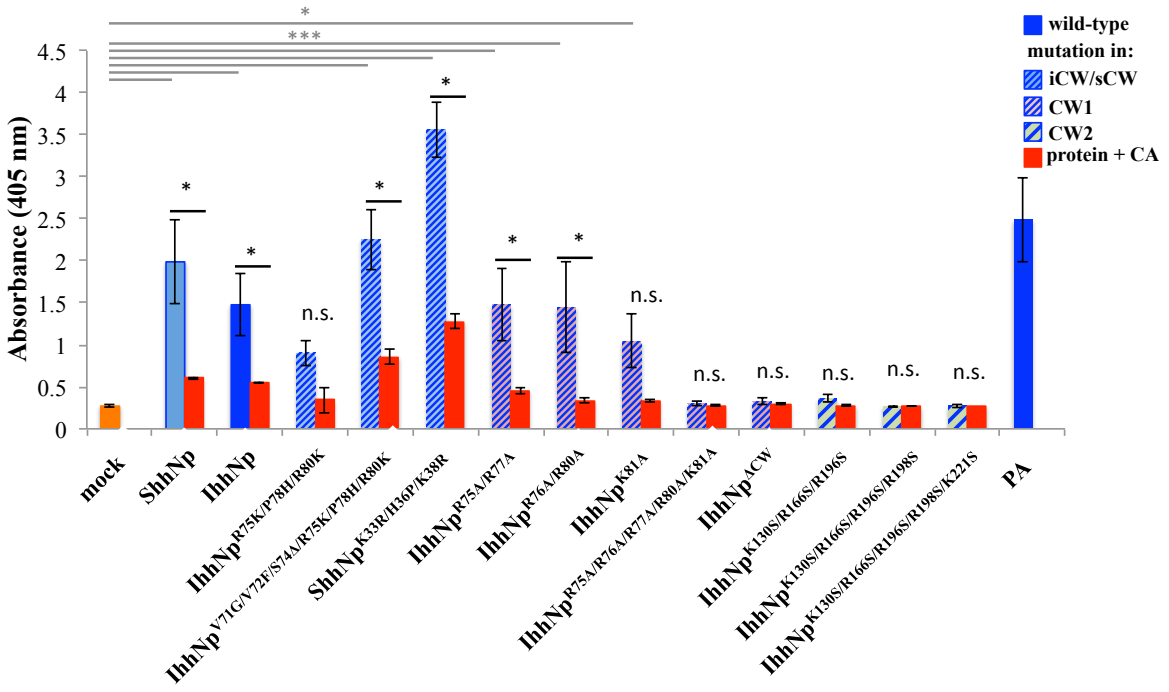

Fig. 4. 7 The CW motifs are required for the signaling activity of Hh proteins.
C3H10T1/2 osteoblast precursor cells were incubated for five days with equal amounts of wild-type and mutant Hh proteins expressed in HEK-293Ebna cells. The Hh-induced AP activity was used as a read-out for C3H10T1/2 differentiation and, hence for biological activity of wild-type and mutant Hh proteins. Cyclopamine (CA) treatment and medium from mock-transfected cells were used as a negative control; purmorphamine (PA) treatment served as a positive control. The analysis showed preserved biological activity for most of the CW1 mutants, while any mutation in CW2 motif resulted in loss of signaling activity of the mutant proteins. Values are mean ± s.e.m, n=4. Statistical analysis was performed using two-way ANOVA with Bonferroni post-test. * p <0 .05, *** p < 0.001.

The majority of the IhhNp and ShhNp CW1 mutants preserved their biological activity and induced significantly more AP activity compared to the control or CA treated cells. Loss of IhhNp signaling activity was observed when the complete CW1 motif was deleted or mutated to alanine (IhhNp$^{\Delta CW}$ and IhhNp$^{R75A/R76A/R77A/R80A/K81A}$) (Fig. 4. 7). Importantly, all Ihh CW2 mutants failed to induce osteoblast differentiation of C3H10T1/2 cells, further underlining the importance of the HS-binding motifs for Ihh signaling.

4.1.6 Loss of *N*- and 2-*O*-sulfation enhances the binding of IhhNp and ShhNp to HS

Another important question concerning the Hh interaction with HS is if and how the HS sulfation pattern impacts protein binding. To address this question, the role of *N*- and 2-*O* sulfation catalyzed by the enzymes Ndst1 and Hs2st, respectively, was investigated. To confirm a skeletal phenotype, the cartilage morphology of E16.5 *Ndst1*$^{-/-}$, *Hs2st*$^{-/-}$ and control mice was analyzed on Safranin-Weigert stained forelimb sections. While wild-type forelimb cartilage displayed well-organized zones of proliferating and hypertrophic chondrocytes

(Fig. 4. 8 A, B), the *Ndst1*$^{-/-}$ and *Hs2st*$^{-/-}$ mutants were characterized by an increased zone of proliferating chondrocytes indicating upregulated Ihh signaling (Fig. 4. 8 A', B').

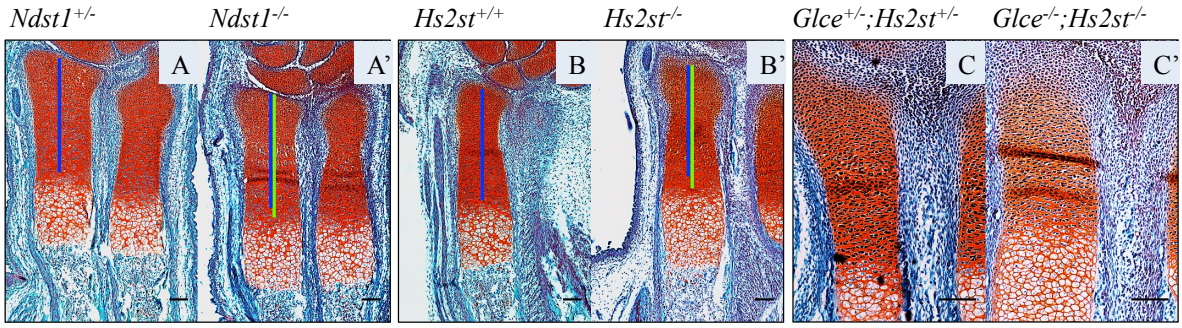

Fig. 4. 8 Mouse mutants of HS modifying enzymes are characterized by mild bone phenotypes.
Limb sections of E16.5 *Ndst1*$^{-/-}$ (A), *Hs2st*$^{-/-}$ (B) and E14.5 *Glce*$^{-/-}$*;Hs2st*$^{-/-}$ (C) mutants and control littermates (A', B', C') were stained with Safranin-Weigert. *Ndst1*$^{-/-}$ and *Hs2st*$^{-/-}$ limbs were characterized by elongated zones of proliferating chondrocytes (green lines) compared to wild-type limbs (blue lines). Analysis of *Glce*$^{-/-}$*;Hs2st*$^{-/-}$ cartilage showed an irregular chondrocyte organization (see section 4.1.7). Scale bars = 100 µm.

To investigate whether *N*- and 2-*O*-sulfate deficient HS exhibits an altered affinity to Hh proteins, HS purified form E16.5 *Ndst1*$^{-/-}$ and *Hs2st*$^{-/-}$ and control embryos was coupled to chromatography columns and employed in affinity chromatography experiments.

IhhNp and ShhNp expressed in HEK-293Ebna cells bound in a similar manner to HS purified from *Ndst1* and *Hs2st* wild-type littermates, eluting between 0.2-0.5 mol/L NaCl. The difference in the elution profiles between the wild-type HS columns (Fig. 4. 9) is most likely an effect of small variations in the composition of the HS, which was purified from different mouse lines.

Unexpectedly, loss of Ndst1 did not decrease the affinity of the mutant HS to IhhNp and ShhNp. Instead, a second peak of high affinity binding protein (at 0.5-0.6 mol/L NaCl) was observed in addition to the bulk protein, which interacted with similar affinity with the wild-type HS (between 0.2-0.5 mol/L NaCl). This shows that the *Ndst1*$^{-/-}$ embryo-derived HS binds ShhNp and IhhNp with higher affinity compared to wild-type HS (Fig. 4. 9 A, B).

In contrast, no difference was observed when the affinity of Ihh to 2-*O*-sulfate deficient HS was analyzed, demarcated by the protein elution between 0.2-0.6 mol/L NaCl for both, mutant and control HS (Fig. 4. 9 D). Interestingly, the affinity of ShhNp to HS deficient on 2-*O*-sulfation was increased, as shown by the protein recovery at 0.5-0.6 mol/L NaCl (Fig. 4. 9 C). Taken together this data strongly support the idea that both–the CW motifs on the protein and the HS sulfation pattern, determine the Hh-HS interaction.

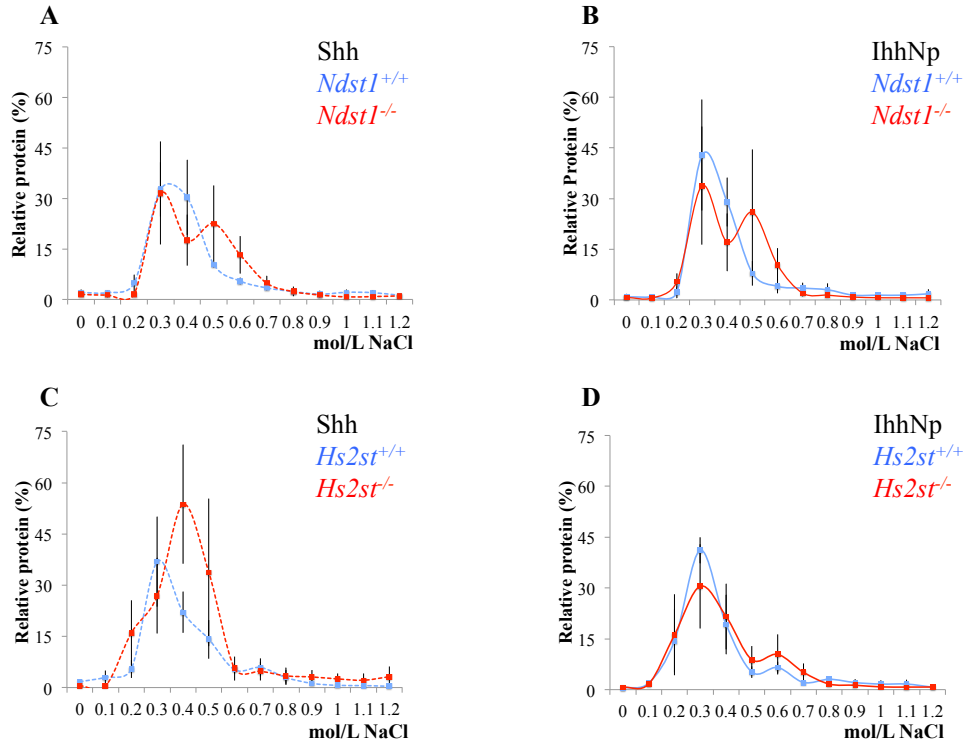

Fig. 4. 9 Distinct alterations in HS sulfation pattern alter Ihh and Shh binding.
HS purified from E16.5 *Ndst1*$^{-/-}$, *Hs2st*$^{-/-}$ and wild-type mouse embryos were coupled to affinity matrix, and applied in affinity chromatography experiments with ShhNp or IhhNp expressed in HEK-293Ebna cells. Loss of *N*-sulfation (*Ndst1*$^{-/-}$) slightly increased the affinity of ShhNp and IhhNp (A, B). IhhNp interaction with HS deficient on 2-*O*-sulfates HS (*Hs2st*$^{-/-}$) did not differ from the control. In contrast, Shh bound stronger to HS purified from *Hs2st*$^{-/-}$ embryos then to the wild-type. Protein amounts are given as (%) relative to total recovered protein. Chromatograms represent mean values ± s.e.m. n=3.

4.1.7 An altered HS level or sulfation pattern does not affect the size of Ihh multimers in primary chondrocytes

The data obtained so far indicate that the HS-binding motifs in Ihh, and likely their interaction with HS, regulates the multimerization of Ihh expressed in HEK-293Ebna cells. To investigate how the HS of chondrocytes affects the process of endogenous Ihh multimerization, primary chondrocytes were isolated from E13.5 embryos and differentiated. The size of the endogenous Ihh multimers released into the medium was analyzed by size-exclusion chromatography. To evaluate the role of HS levels and sulfation in the multimerization, Ihh expressed in primary chondrocytes of two HS mutant strains were analyzed in parallel. These include the *Ext1*$^{gt/gt}$ mice, producing about 18% of the wild-type HS (Koziel et al., 2004) and the *Glce*$^{-/-}$*;Hs2st*$^{-/-}$ mice, which lack C5-epimerase and Hs2st, and therefore synthesize HS with altered modification pattern.

To evaluate the role of these modification during bone development, a morphological analysis on E14.5 *Glce*$^{-/-}$;*Hs2st*$^{-/-}$ and wild-type mouse forelimb sections following Safranin-Weigert staining was performed (Fig. 4. 8). While in the control forelimbs the zones of hypertrophic and proliferating chondrocytes were well organized, in the mutant limbs the proliferating chondrocytes appeared round and their columnar organization was disturbed, indicating an altered Ihh signaling (Fig. 4. 8 C, C').

The analysis of Ihh multimer size in primary chondrocytes gave several surprising results. First, size analysis showed that the Ihh complexes produced in primary chondrocyte were remarkably smaller than those of HEK-293Ebna cells overexpressing IhhNp. While the recombinant IhhNp protein had a molecular size of >660 kDa (Fig. 4. 4), endogenously formed multimers were of size between 200-550 kDa (Fig. 4. 10) Moreover, immunoblot analysis of the protein fraction obtained after size-exclusion chromatography indicated the presence of a ≈40 kDa protein complex (red arrow), representing most likely Ihh dimers, in addition to the 19 kDa Ihh monomers (blue arrow). These complexes were not denatured under the reducing conditions of SDS-PAGE indicating an increased stability (Fig. 4. 10 A, B). Thus, primary chondrocytes synthesize Ihh, which forms very stable, small complexes of ≈40 kDa, organized in larger clusters, which however do not exceed 550 kDa.

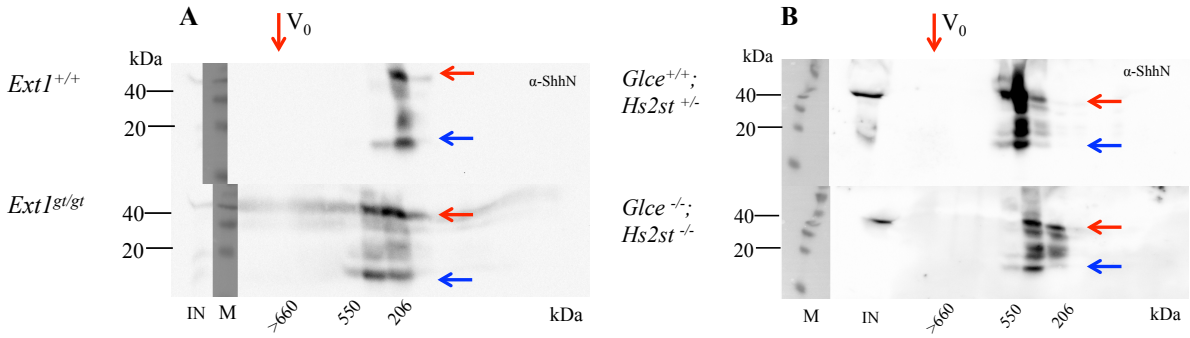

Fig. 4. 10 HS level and sulfation pattern do not determine the multimer size of Ihh in differentiated chondrocytes.
Primary chondrocytes were isolated from fore- and hindlimbs of E13.5 *Ext1*$^{gt/gt}$, *Glce*$^{-/-}$;*Hs2st*$^{-/-}$ and control embryos. The cells were differentiated for ten days. The size of the Ihh multimers, secreted into the conditioned medium, was determined by size-exclusion chromatography. Ihh formed clusters between 200 and 550 kDa. The multimer size was not altered in the mutant cells. A stable Ihh multimer, likely a dimer was observed at ≈40 kDa (red arrow). Blue arrow indicates Ihh monomer. *Glce*$^{-/-}$;*Hs2st*$^{-/-}$, n=2; *Ext1*$^{gt/gt}$, n=3. M–protein marker, IN=20% of the input. One representative experiment is shown.

Surprisingly, the chondrocytes of both HS mutants produced the same stable clusters of ≈40 kDa size and larger multimers of similar molecular weight as the control cells, indicating that the size of Ihh multimers produced in chondrocytes is not determined by the HS level or sulfation pattern.

4.2 CS levels are enriched in embryos with reduced or altered HS biosynthesis

The previous experiments showed that although the Ihh-HS interaction seems to be critical in determining the multimer size of IhhNp expressed in HEK-293Ebna cells, neither the HS level nor the sulfation pattern affected the protein multimerization in chondrocytes (Fig. 4. 10). This could mean that either HS binding is not critical for the formation of multimers in general or that chondrocytes compensate for the altered HS structure. It is important to note, that HS mutants are characterized by relatively mild bone phenotypes (Fig. 4. 8 and (Dierker et al., 2016; Koziel et al., 2004)), while other organs are severely affected by the altered HS structure (Bullock et al., 1998; Grobe et al., 2005; Li et al., 2003). This supports the hypothesis that in chondrocytes unknown mechanisms compensate for the impaired HS functions. In contrast to other tissues, chondrocytes are specifically rich in CS, which has similar biochemical properties as HS. To test if CS might compensate for HS in the developing skeleton, the GAG composition was analyzed in HS mutants.

4.2.1 Increased CS levels in chondrocytes producing decreased HS levels

4.2.1.1 The ECM of *Ext1*$^{gt/gt}$ mutants is enriched in CS

To test whether the HS deficiency is compensated by CS in cartilage, the CS levels were initially analyzed on E15.5 *Ext1*$^{gt/gt}$ and wild-type limb sections by immunofluorescence analysis using antibodies against CS neoepitopes generated upon chondroitinase ABC digestion. These antibodies recognize an unsaturated GlcA residue at the non-reducing end, adjacent to a GalNAc residue, which can be either unsulfated (C-0-S, 1B5 antibody), 4-*O*-sulfated (C-4-S, 2B6 antibody) or 6-*O*-sulfated (C-6-S, 3B3 antibody) (Caterson, 2012; Hayes et al., 2008).

In wild-type cartilage, the unsulfated and sulfated CS neoepitopes were ubiquitously expressed throughout the tissue producing a strong signal in the extracellular matrix (Fig. 4. 11 A, B, C). In line with the hypothesis mentioned above, E15.5 *Ext1*$^{gt/gt}$ cartilage displayed an increased staining for all three antibodies compared to wild-type littermates (Fig. 4. 11 A', B', C'). To quantify the intensity of the fluorescence staining produced by the CS-specific antibodies, the fluorescence signal was measured in the zone of columnar

chondrocytes using ImageJ software and was normalized to the nuclear DAPI signal of the same region. The quantification of the relative fluorescence signal confirmed increased levels for the unsulfated, 4-*O*- and 6-*O*-sulfated neoepitopes (Fig. 4. 11 D). This indicates that the HS deficiency is compensated by an enrichment of the cartilage ECM with CS.

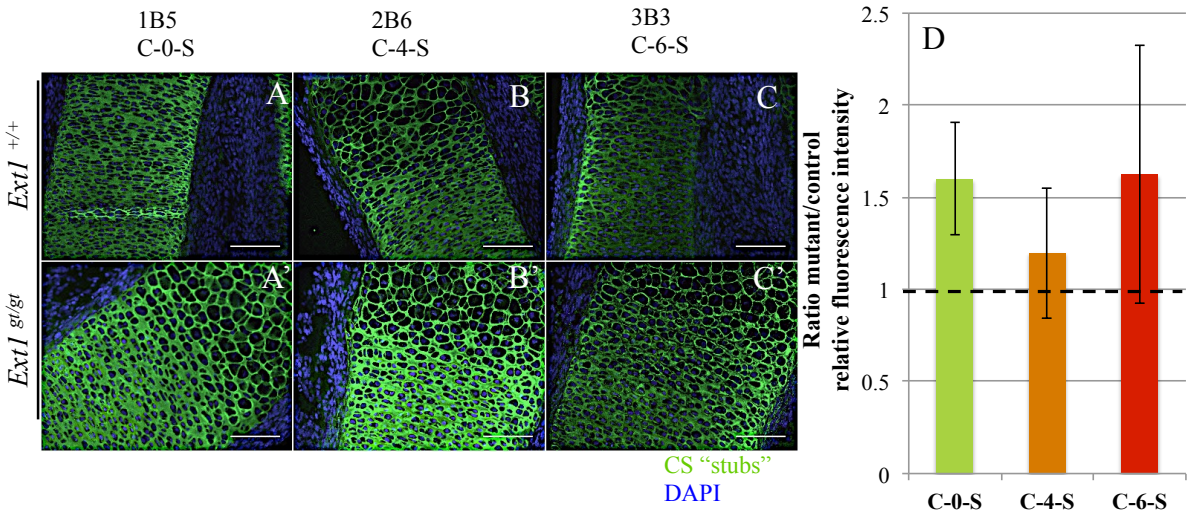

Fig. 4. 11 Increased CS levels in *Ext1*$^{gt/gt}$ embryonic cartilage.
Immunofluorescence staining of E15.5 *Ext1*$^{gt/gt}$ (A'-C') and control littermates (A-C) limb sections showed an increased level of sulfated (B, B', C, C') and unsulfated (A, A') neoepitopes in the mutant mice. Quantification of the fluorescence signal, normalized against the nuclear DAPI (D). Data are mean values ± s.e.m., relative to the control sample set as 1. Scale bar = 100 µm. n=3.

4.2.1.2 The reduced HS levels of *Ext1*$^{gt/gt}$ chondrocytes are compensated by an increased CS amount

In the previous experiment, the alterations in CS levels and sulfation in HS deficient mutant were detected by an antibody staining, a method, which is characterized by a relatively high experimental variability. To verify an alteration in GAG levels, HS and CS purified from E15.5 Ext1$^{gt/gt}$ and control skeletons were subjected to disaccharide analysis by Reversed-phase ion-pairing high-performance liquid chromatography (RPIP-HPLC) and compared to control littermates. This analysis was performed in collaboration with Dr. Tabea Dierker and Prof. Dr. Lena Kjellen, University of Uppsala.

In agreement with earlier studies, the disaccharide analysis showed that the *Ext*$^{gt/gt}$ skeletons contain 20% of the HS detected in control littermates (Mitchell et al., 2001) (Fig. 4. 12 A, Table 9. 2).

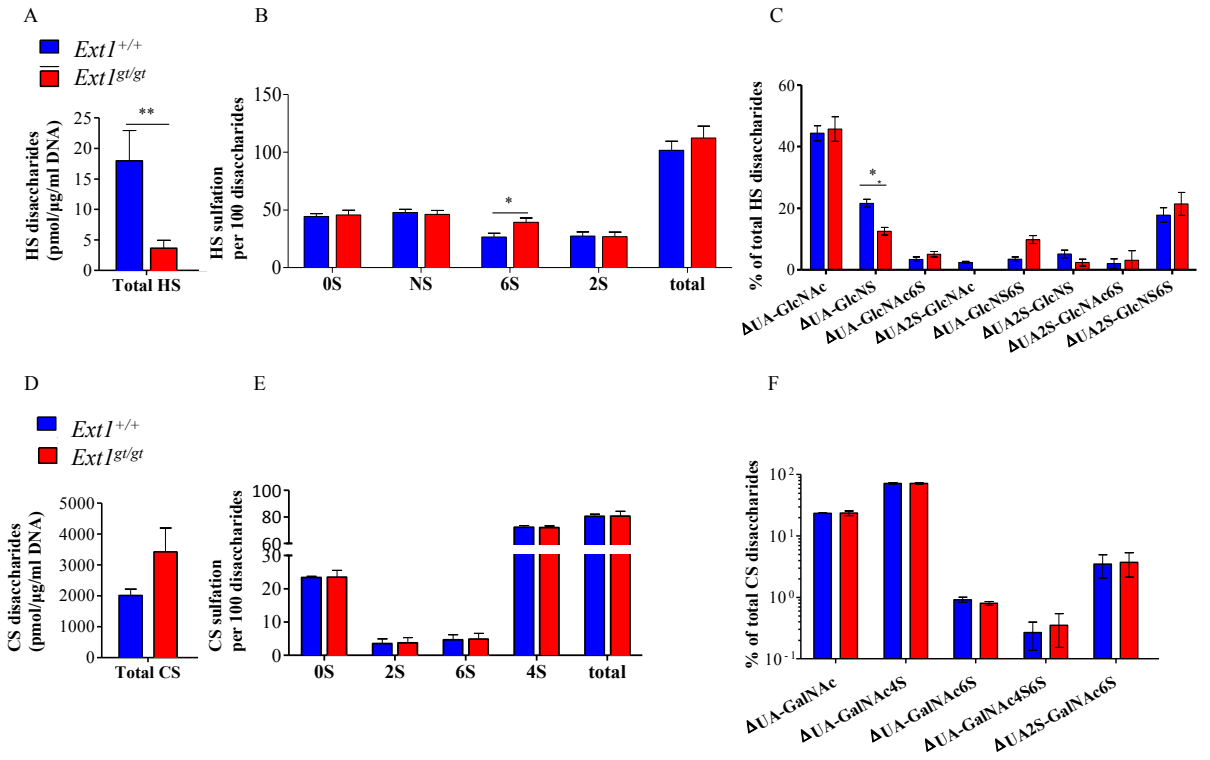

Fig. 4. 12 Increased CS levels in *Ext1*$^{gt/gt}$ cartilage.
The disaccharide composition of HS and CS, purified from E15.5 *Ext1*$^{gt/gt}$ and control skeletons, was analyzed by RPIP-HPLC. The HS in the mutant was reduced to 20% of the wild-type levels (A), but maintained normal total sulfation levels (A, B). Disaccharide analysis (C) showed reduced levels of ΔUA-GlcNS, but no other significant alterations in disaccharide distribution. CS structure analysis revealed a 70% elevated CS amount in *Ext*$^{gt/gt}$ mutants (D), while the sulfation levels and disaccharide composition were not altered (E, F). Values in (B, C, E, F) are given in (%) of total disaccharides and are the mean ± s.e.m. Total amounts (A, D) are given as pmol/µg/ml DNA of the starting material Statistical significance was calculated by two-way ANOVA with Bonferroni post-test. * p <0.05, ** p <0.01, *** p <0.001, n=6.

Analysis of the HS sulfation revealed that the wild-type HS was predominated by similar levels of *N*-sulfated and unsulfated species, followed by sulfation at 2-*O*- and 6-*O*- positions, which were equally represented. Except for the significantly increased 6-*O*-sulfation in *Ext1*$^{gt/gt}$ mice, no other alterations were observed (Fig. 4. 12 B, and Table 9. 2). A detailed disaccharide analysis (expressed as disaccharide species per 100) revealed that in the control littermates the unsulfated disaccharides were the largest group (≈44%), followed by tri-sulfated disaccharides, which remained unaltered in the mutants. Significantly decreased in the mutants were only the monosulfated ΔUA-GlcNS disaccharides (Fig. 4. 12 C).

In line with the immunofluorescence analysis, the quantification of CS levels showed that wild-type skeletons contained 2011 ± 208.7 pmol/µg/ml DNA CS against 3423.1 ± 773 pmol/µg/ml DNA in *Ext1*$^{gt/gt}$ samples, indicating an increase in CS amount by 70% in the mutant skeletons (Fig. 4. 12 D, Table 9. 3). Evaluation of the relative CS sulfation levels

showed that in the controls the most common modification was 4-*O*-sulfation followed by unsulfated, and 6-*O* and 2-*O* sulfated species (Fig. 4. 12 E). This distribution was similar in the mutants. In addition, detailed analysis of the disaccharide composition showed no shift in the disaccharide species, indicating that upon HS depletion mutant chondrocytes synthesize more CS, which retains a normal sulfation status (Fig. 4. 12 E, F). Nevertheless, due to the massive increase in CS levels the total 4-*O*-sulfated disaccharides were enriched in the mutants (Table 9. 4). Taken together, these data demonstrate that embryonic chondrocytes respond to reduced HS amounts with an increase in HS 6-*O*-sulfation and a substantial enrichment in CS levels, which maintains a normal sulfation status.

4.2.2 Chondrocytes respond to changes in HS pattern by alteration in CS levels and structure

4.2.2.1 Increased propagation of CS neoepitopes in HS sulfation mutants

The increased CS levels observed in the *Ext1*$^{gt/gt}$ mice lead to the question whether chondrocytes respond with alterations in CS levels not only to HS deficiency, but also to changes in HS sulfation pattern. To test this, E16.5 forelimb sections of *Ndst1*$^{-/-}$ and *Hs2st*$^{-/-}$ mice were subjected to immunofluorescence analysis using antibodies against the CS neoepitopes. Strong and ubiquitous CS neoepitope expression throughout the tissue was observed in the control littermates (Fig. 4. 13 A-C, E-G). Similar to the *Ext1*$^{gt/gt}$ mice, the HS sulfation mutants were characterized by an increase in the relative fluorescence intensity for the three antibodies, revealing augmented CS neoepitope levels in the tissue (Fig. 4. 13 A'-C', E'-G', D, H). The immunofluorescence signal was particularly stronger and consistently increased for the C-4-S and C-6-S neoepitopes in both *Ndst1*$^{-/-}$ and *Hs2st*$^{-/-}$ mice. Nonetheless, these data indicate that, similar to the *Ext1*$^{gt/gt}$ mice, the CS level rather than CS sulfation pattern were altered in the HS modification mutants.

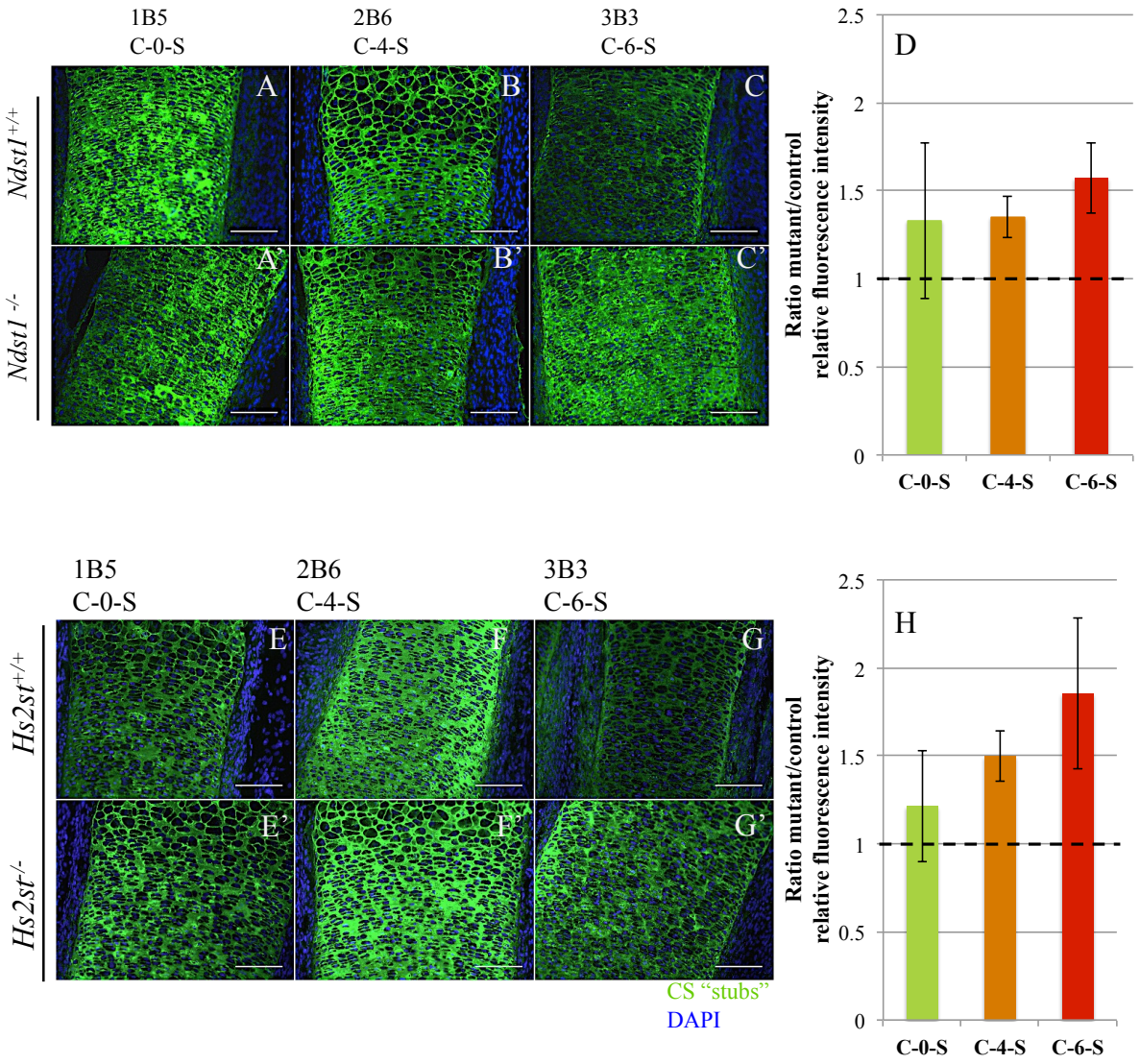

Fig. 4. 13 Increased CS levels in mutants with altered HS sulfation pattern.
Immunofluorescence analysis of embryonic limb sections of E16.5 *Ndst1*$^{-/-}$ (A'-C'), *Hs2st*$^{-/-}$ (E'-G') and control littermates (A-C, E-G) revealed increased CS neoepitopes levels in both HS mutant strains (D, H). Quantification of the fluorescence signal, normalized against the nuclear DAPI (D, H). Data are mean values ± s.e.m relative to the control sample, set as 1. Scale bar = 100 µm. n=3.

4.2.2.2 *Hs2st*$^{-/-}$ skeletons are characterized by an undersulfated HS and augmented CS levels

In order to verify the results obtained by immunofluorescence analyses, the disaccharide composition of CS and HS purified from E15.5 *Hs2st*$^{-/-}$ and control skeletons was analyzed by RPIP-HPLC. In contrast to the *Ext*$^{gt/gt}$ cartilage, the Hs2st deficient mice did not show alterations in the amount of HS (Fig. 4. 14 A, Table 9. 2). Analysis of the sulfation, however, revealed reduced total HS sulfation levels in the *Hs2st*$^{-/-}$ mice. Surprisingly, besides the expected depletion on 2-*O*-sulfation in *Hs2st*$^{-/-}$ mice, 6-*O*-sulfation was also decreased by 42% (Fig. 4. 14 B, Table 9. 2).

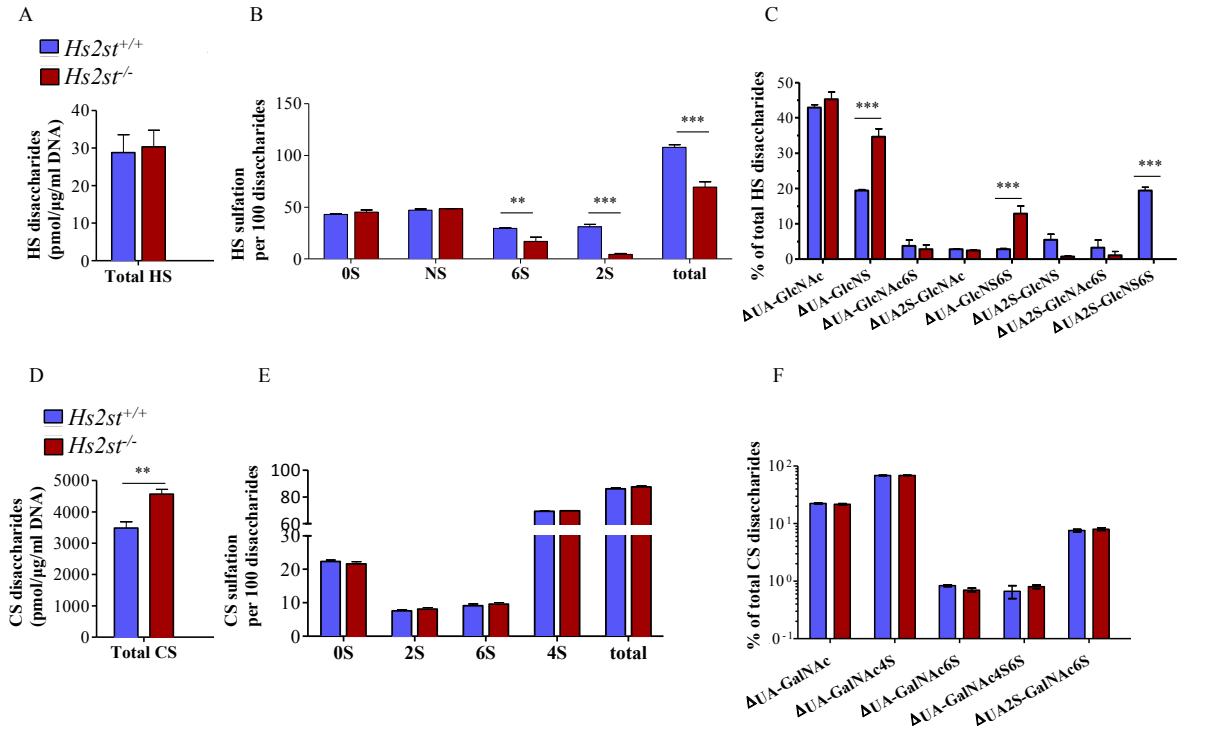

Fig. 4. 14 Hs2st deficiency in chondrocytes leads to an alteration in HS sulfation pattern and increased CS levels.
Structural analysis of HS purified from E15.5 *Hs2st*$^{-/-}$ and control cartilage by RPIP-HPLC indicated similar HS levels as in wild-type controls (A). *Hs2st*$^{-/-}$ HS was characterized by significantly reduced 2-*O*, 6-*O* and total HS sulfation (B) Mono-sulfated disaccharides carrying *N* and 6-*O* sulfation were increased in the mutant, while three-sulfated disaccharides were reduced (C). Analysis of CS structure revealed that *Hs2st*$^{-/-}$ skeletons contain 35% more CS compared to the controls (D), while CS sulfation and disaccharide composition were unaltered (E, F). Values in (B, C, E, F) are given in % of total disaccharides and are the mean ± s.e.m. The degree and type of sulfation are calculated from disaccharides species. Total amounts (A, D) are given as pmol/µg/ml DNA of the starting material Statistical significance was calculated by two-way ANOVA with Bonferroni post-test. * $p < 0.05$, ** $p < 0.01$, *** $p < 0.001$, n=3.

In line with this, the tri-sulfated disaccharides containing 2-*O* and 6-*O* sulfation (ΔUA2S-GlcNS6S) were lost in the mutant samples, while the amount of mono and di-sulfated disaccharides carrying *N*-sulfation (ΔUA-GlcNS and ΔUA-GlcNS6S) were higher, partially compensating for the low 2-*O* and 6-*O* sulfation (Fig. 4. 14 C).

In addition to the altered HS sulfation pattern, the *Hs2st*$^{-/-}$ cartilage was characterized by 31% elevated CS amount (Fig. 4. 14 D). Similar to the *Ext1*$^{gt/gt}$ mice, the degree of CS sulfation and the disaccharide distribution showed no apparent alterations (Fig. 4. 14 E, F), indicating that *Hs2st*$^{-/-}$ mutants synthesize more CS, which maintains a wild-type sulfation pattern. Importantly, due to the higher CS levels in the mutant cartilage, the total amount of ΔUA-GalNAc4S disaccharides was also increased, correlating with the augmented C-4-S neoepitope levels detected via immunofluorescence analysis (Table 9. 4).

These data show for first time that cells, and specifically chondrocytes react not only to quantitative, but also to qualitative alteration in the HS structure by increased the levels of CS.

4.2.2.3 High HS 6-*O*-sulfation is compensated by a reduction in CS levels and sulfation

As the data obtained so far support an interplay between HS and CS synthesis I asked whether high HS sulfation would be balanced by a reduction in CS level as well. To test this possibility, *Sulf1*$^{gt/gt}$;*Sulf2*$^{gt/gt}$ mice, which carry hypomorphic alleles for the HS 6-*O*-endosulfatase 1 and 2, and therefore produce HS with increased 6-*O*-sulfation levels (Lamanna et al., 2008) were included in the study.

Analysis of the E16.5 cartilage morphology after Safranin-Weigert staining showed that *Sulf1*$^{gt/gt}$;*Sulf2*$^{gt/gt}$ mutants are characterized by accelerated hypertrophic differentiation and reduced chondrocyte proliferation, demarcated by the shorter zones of columnar and hypertrophic chondrocytes in the mutant mice (Fig. 4. 15 E, E') (Ratzka et al., 2008). An antibody staining for the CS neoepitopes and a quantification of the fluorescence signals showed decreased levels of C-4-S epitopes in the compound *Sulf1*$^{gt/gt}$;*Sulf2*$^{gt/gt}$ mice (Fig. 4. 15 B, B', D), while the C-6-S epitope expression remained similar to the control (Fig. 4. 15 C, C', D). Interestingly, in *Sulf1*$^{gt/gt}$;*Sulf2*$^{gt/gt}$ limb sections an increased degree of unsulfated CS neoepitope (C-0-S) was detected (Fig. 4. 15 A, A') suggesting that the high HS 6-*O*-sulfation levels in these mice are compensated by an alternative mechanism, involving an alteration of CS sulfation rather than a reduction of the total CS amount.

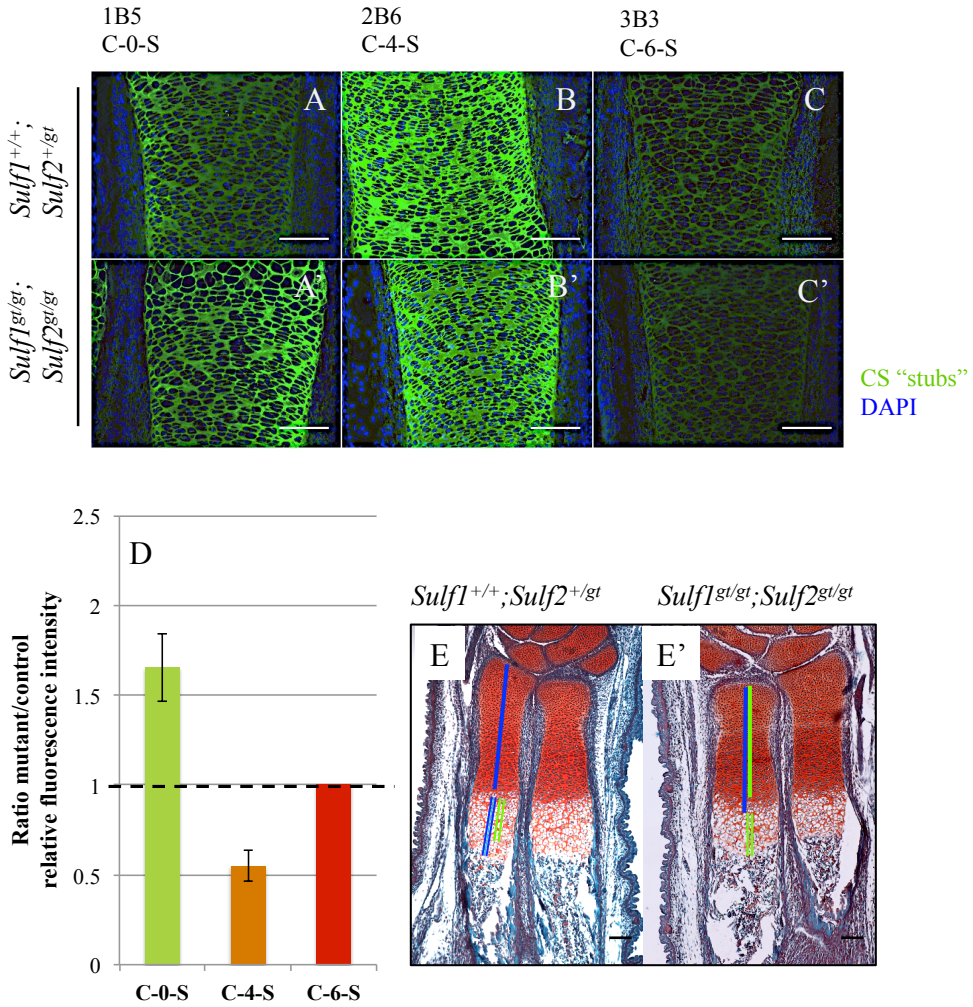

Fig. 4. 15 Increased HS 6-O-sulfation in *Sulf1*$^{gt/gt}$;*Sulf2*$^{gt/gt}$ mice results in the synthesis of lower sulfated CS.

Immunofluorescence staining for CS neoepitopes of E16.5 *Sulf1*$^{gt/gt}$;*Sulf2*$^{gt/gt}$ (A'-C') and control (A-C) limb sections revealed an increased level of unsulfated C-0-S CS neopitopes in the mutants, while the amount of the 4-*O*- (B, B') and 6-*O*- (C, C') sulfated CS neoepitope were decreased or unaltered, respectively. Quantification of the fluorescence signal normalized to the nuclear DAPI (D). Limb section of E16.5 *Sulf1*$^{gt/gt}$;*Sulf2*$^{gt/gt}$ (E') and control littermates were stained with Safranin-Weigert. The mutant limbs were characterized by a shortened zone of proliferating chondrocytes (green line) and hypertrophic chondrocytes (double green line) compared to the control (blue lines) mice. Data are presented as mean values ± s.e.m., relative to the control sample, set as 1. n=3 for C-0-S and C-4-S, n=1 for C-6-S. Scale bar = 100 µm.

4.2.3 CS chains length is altered in *Ext1* and *Hs2st* mutants

The increased CS level identified in HS mutants could be attained by synthesis of either more or longer CS chains, or a combination of both. To test whether the length of the CS chains was altered, ^{35}S labeled GAGs, produced by primary chondrocytes were analyzed using size-exclusions chromatography.

In short, the cell surface associated and secreted in the conditioned medium PGs of E13.5 primary chondrocytes were labeled metabolically with ^{35}S in culture and purified via ion-exchange chromatography. The purified, labeled material was separated by size-exclusion chromatography on a Superose 6 column to identify the high molecular weight PG population and purify it from heparanase degradation products (preparative separation). Following an alkali treatment to remove the core proteins, total GAGs, HS or CS were separated by size using size-exclusion chromatography. An enzymatic digest of the total GAGs by chondroitinase ABC was performed when HS chain length comparison was intended. HS is expected to elute in a broad polymer peak, while the susceptible to the enzymatic activity CS are observed in an elution peak (disaccharide (dp2)) before V_t (total column volume). To compare the length of the CS chains, the HS in a GAG mixture was cleaved using nitrous acid treatment, which results in CS elution as large polymers, while HS degradation products will be detected in a dp2 peak (Dagalv et al., 2015).

In line with the fact that distinct members of the PG family are found in the cell surface-associated and in the secreted PG population, differences in the elution profiles of these two fractions were already detected during the preparative PGs separation (Fig. 4. 16). While the cell surface-bound PGs eluted in a single peak (red square), the secreted PG population was divided into two distinct populations (yellow and green square), both corresponding to high molecular weight molecules. Each PG fraction was analyzed separately.

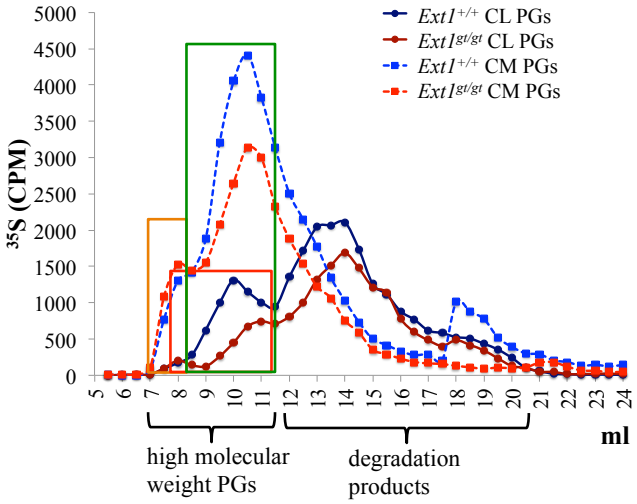

Fig. 4. 16 The PGs associated with plasma membrane and secreted in the ECM differ in their size.
^{35}S labeled PGs were purified from cell lysate and conditioned medium of *Ext1*$^{gt/gt}$ and control chondrocytes, and separated by size-exclusion chromatography on Superose 6 column. Secreted PGs were detected between 7-11.5 ml elution volume, forming two fractions (orange and green rectangles), which correspond to high molecular weight molecules. Cells lysate PGs eluted in a single fraction between 8-11.5 ml elution volume (red rectangle). Values are given as absolute cpms. CL–cell lysates, CM–conditioned medium.

4.2.3.1 *Ext1*$^{gt/gt}$ chondrocytes produce more cell surface-associated CS chains with lower molecular weight

Total GAGs, HS and CS purified from *Ext1*$^{gt/gt}$ and wild-type differentiated chondrocyte were separated by size-exclusion chromatography. The wild-type GAGs eluted in a broad peak and had a molecular weight between 70 and 15 kDa, predominated by GAG chains of ≈33 kDa. A HS digest with nitrous acid allowed to determine the CS chains length, which corresponded to ≈33 kDa, while the HS chains (CSaseABC) appeared shorter and had a molecular weight of ≈24 kDa (Fig. 4. 17 A). In contrast, in *Ext1*$^{gt/gt}$ chondrocytes the total GAGs chains had an average size of ≈25 kDa (Fig. 4. 17 B). Moreover, a direct comparison of the chromatograms of *Ext1*$^{gt/gt}$ and wild-type total GAGs size demonstrated increased levels of shorter chains in the mutant (≈15 kDa), while fewer chains corresponding to ≈33 kDa were detected (Fig. 4. 17 C). These data indicate that *Ext1*$^{gt/gt}$ chondrocytes produce GAGs of a reduced length compared to the wild-type cells.

A quantification of HS and CS recovered in size-exclusion experiments (expressed as (%) relative to the total PGs in the high molecular weight fraction) showed that *Ext1*$^{gt/gt}$ chondrocytes contained ≈38% less cell surface-associated HS, which had a molecular weight of ≈20 kDa (Fig. 4. 17 E, Table 9. 5).

Importantly, a quantification of the CS levels revealed an elevation by ≈42% in the mutant cells (Table 9. 5). Interestingly, a direct comparison of the chromatograms of wild-type and mutant chondrocyte-derived CS demonstrated the presence of more, but shorter CS chains, ranging between 18 kDa to 33 kDa in the mutant samples (Fig. 4. 17 D). Moreover, while in the wild-type cells the membrane associated HS and CS chains were detected in similar proportions, the vast majority of GAGs in *Ext1*$^{gt/gt}$ cells were CS (Fig. 4. 17 A, B; Table 9. 5). This indicates that *Ext1*$^{gt/gt}$ cells compensate for the low HS levels by carrying more CS chains on cell surface bound PGs.

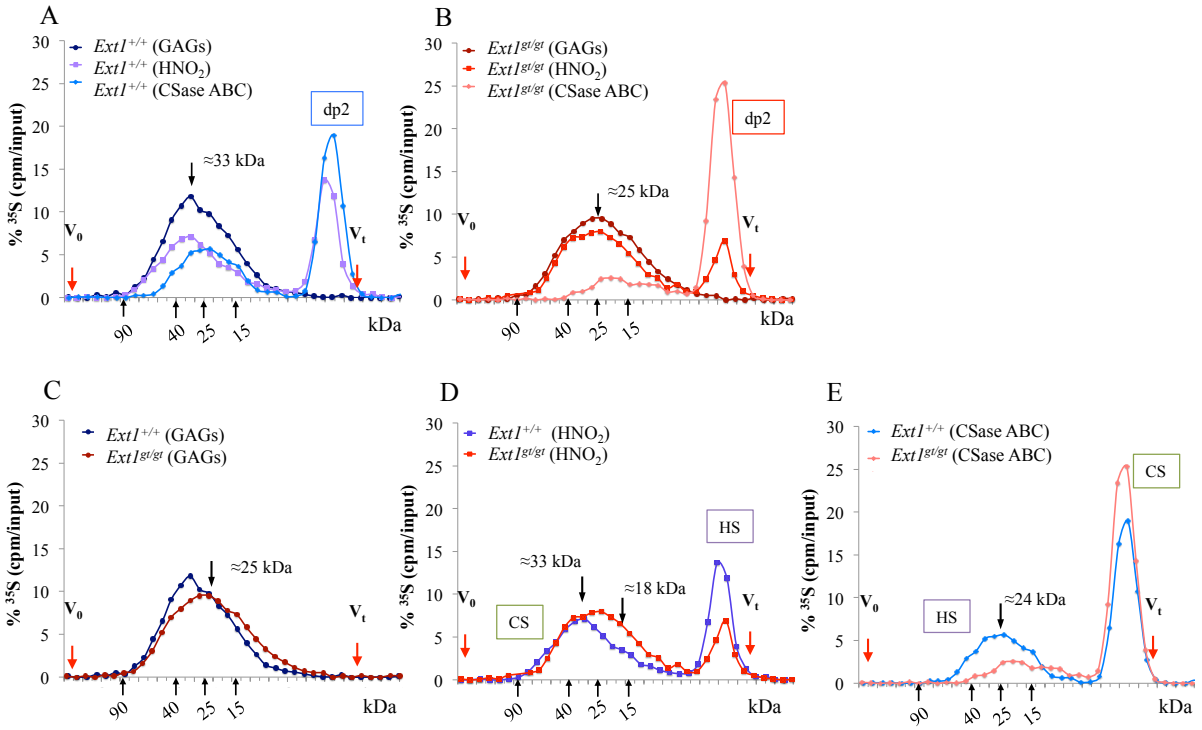

Fig. 4. 17 *Ext1*$^{gt/gt}$ chondrocytes produce more, but shorter CS chains.
The chain length of ^{35}S metabolically labeled total GAGs, HS (CSase ABC) and CS (HNO_2), purified from primary differentiated *Ext1*$^{gt/gt}$ (A) and control chondrocytes (B), was compared by size-exclusion chromatography. While in wild-type chondrocytes HS and CS are represented in comparable amounts in the cell lysates (A), CS chains were the major GAGs in *Ext1*$^{gt/gt}$ cells (B). Direct comparison by size of wild-type and mutant GAGs revealed an increased fraction of short CS chains in the *Ext1* mutant cells (D). Data are presented as % cpm relative to the input. n=3. One representative experiment is shown. dp2–disaccharides, V_0–void volume, V_t–total column volume. The sizes of molecular weight standards are indicated.

A quantification of the GAGs secreted into the conditioned medium revealed that in wild-type cells ≈9% of the total GAGs were HS chains, while the HS amount was further decreased to ≈4% in *Ext1*$^{gt/gt}$ chondrocytes. Moreover, in *Ext1*$^{gt/gt}$ chondrocytes CS levels were additionally increased compared to wild-type cells, specifically in fraction one of secreted PGs (Table 9. 5).

A direct comparison of the total GAG and CS chains length revealed small difference between the sizes of the wild-type chains identified in each PG fraction. While the GAG and the CS chains of fraction 1 had a molecular size of ≈43 kDa, their average size was reduced to ≈35 kDa in fraction 2 (Fig. 4. 18 A, C; Fig. 9. 1).

Similar to the cell lysate, the secreted *Ext1*$^{gt/gt}$ CS chains of Fraction 1 were shorter compared to the controls and were characterized by an increased proportion of chains with molecular weight of ≈30 kDa. No alteration in the secreted *Ext1*$^{gt/gt}$ chains was observed when analyzing the GAGs detected in fraction 2 (Fig. 4. 18 B, D).

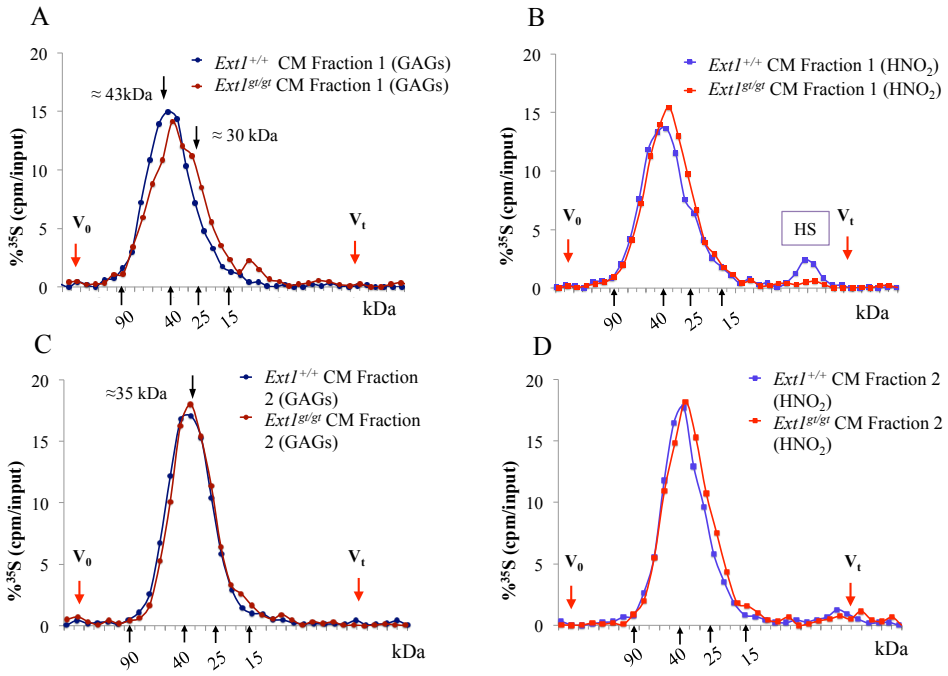

Fig. 4. 18 Secreted PGs of *Ext1*$^{gt/gt}$ and control chondrocytes carry mostly CS.
^{35}S labeled total GAGs (A, C) and CS (HNO_2) (B, D) chains of *Ext1*$^{gt/gt}$ and wild-type chondrocytes, recovered in the secreted PG fractions were separated by size-exclusion chromatography. Size determination showed a decreased length of the mutant chains in fraction 1 (A, B), while no alteration in the size of fraction 2 GAG/CS were observed (C, D). Data are shown as % cpm relative to the input. n=3. One representative experiment is shown. V_0–void volume, V_t–total column volume. The sizes of molecular weight standards are indicated.

4.2.3.2 Alteration in HS and CS chain length during chondrocyte differentiation

To evaluate whether the changes in HS and CS chain length are specific for differentiated chondrocytes, the GAGs produced by primary undifferentiated *Ext*$^{gt/gt}$ and control chondrocytes were analyzed by size-exclusion chromatography. Wild-type total GAGs in these cells had a molecular weight of ≈40 kDa–slightly larger than the GAGs purified from differentiated chondrocytes (Fig. 4. 17 A, Fig. 4. 19 A). Interestingly, analysis of HS chains,

following chondroitinase ABC digest, showed that in undifferentiated control cells the cell surface PGs carried mainly chains with a molecular weight of ≈35 kDa–larger than the HS molecules identified in differentiated chondrocytes (Fig. 4. 19 C). CS was detected at low levels, as indicated by the relatively low dp2 peak observed after chondroitinase ABC digest (Fig. 4. 19 C). The flat CS polymer elution profile upon HS degradation confirmed these observations (Fig. 4. 19 B).

In line with the data obtained for differentiated chondrocytes, comparison of the total wild-type and *Ext*$^{gt/gt}$ GAGs revealed an increase of small molecular weight chains in *Ext*$^{gt/gt}$ cells (Fig. 4. 19 A). Remarkably, in the mutant cells, the cell surface-associated GAGs contained very low amounts of HS, but were enriched on CS, which comprised almost the complete GAG population (Fig. 4. 19 B, C and Fig. 9. 2 B).

Taken together, these data demonstrate that an augmentation of CS levels due to HS depletion is not specific to differentiated chondrocytes, but is initiated during early stages of chondrocytes differentiation.

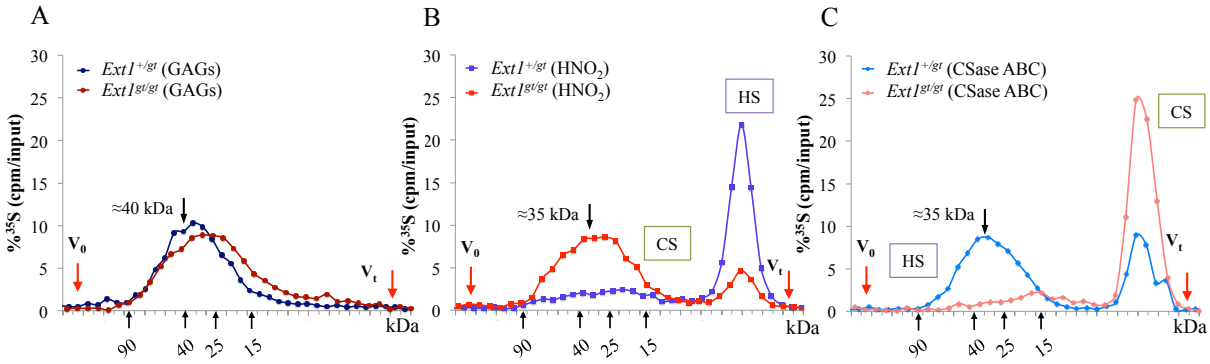

Fig. 4. 19 Primary undifferentiated *Ext1*$^{gt/gt}$ chondrocytes upregulate CS.
The chain length of ^{35}S labeled total GAG (A), CS (HNO_2 (B)) and HS (CSase ABC (C)) of primary undifferentiated *Ext1*$^{gt/gt}$ and control chondrocytes was compared by size-exclusion chromatography. The size of the total GAG and HS chains were decreased in *Ext1*$^{gt/gt}$ cells compared to the control samples (A, C). Comparison of the CS chain length showed increased levels of CS the *Ext1*$^{gt/g}$ chondrocytes, but no alteration in chain length (B). Data are given as (%) cpm relative to the input. n=2. One representative experiment is shown. V_0–void volume, V_t–total column volume. The sizes of molecular weight standards are indicated.

4.2.3.3 Secreted CS chains of *Hs2st*$^{-/-}$ chondrocytes are elongated

To investigate whether an alteration of the HS sulfation pattern is compensated by changes in GAG chain length, ^{35}S labeled total GAGs, HS and CS produced by primary differentiated *Hs2st*$^{-/-}$ and control chondrocytes were analyzed by size-exclusion chromatography. In wild-type cells the total GAGs, CS and HS were of similar size as described in section 4.2.3.1.

Importantly, the total cell surface GAGs comprised equal portions HS and CS (Table 9. 6). In contrast to the *Ext1*$^{gt/gt}$ cells, direct comparison of the total GAG elution profiles showed an increased amount of high molecular weight chains with a size of ≈43 kDa in the mutants (Fig. 4. 20 A). Moreover, different to Ext1 deficient cells, in *Hs2st*$^{-/-}$ chondrocytes the cell surface-associated HS was increased by ≈34%, as shown by the higher HS polymer peak observed after CSase ABC digestion (Fig. 4. 20 C, Fig. 9. 3, Table 9. 6). Importantly, chain length analysis did not show any alterations for CS or HS size produced by the mutant cells.

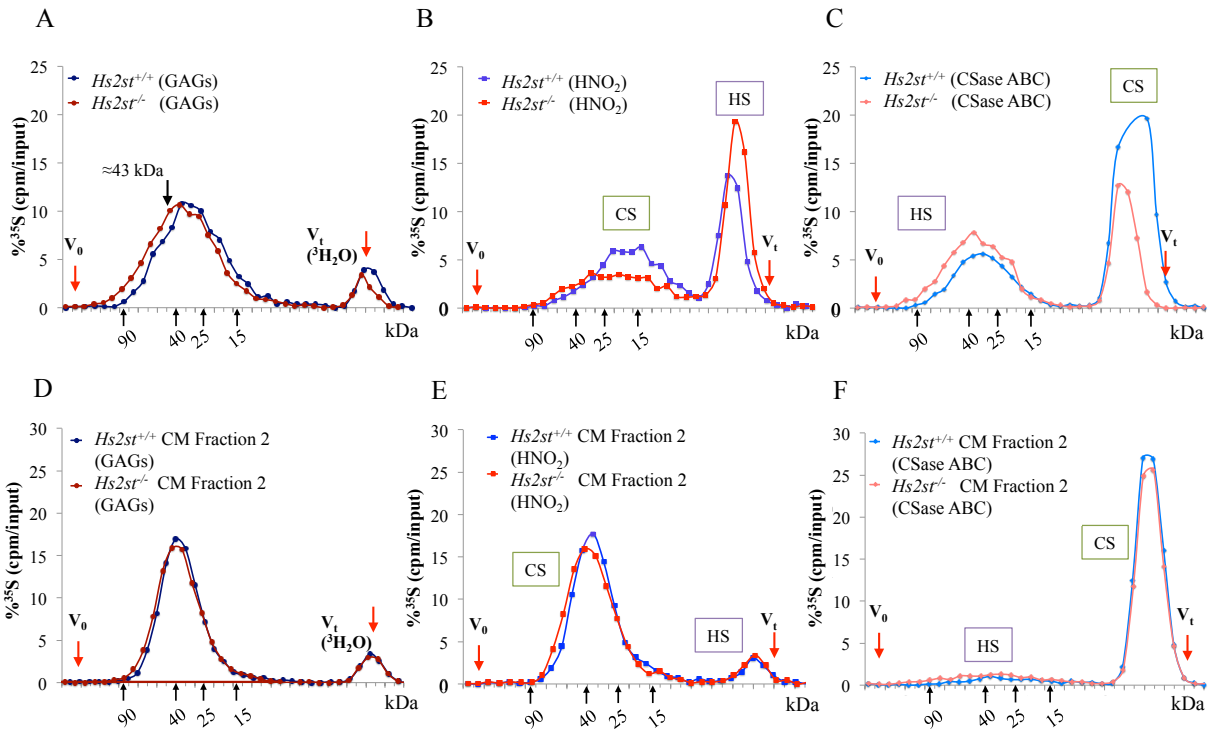

Fig. 4. 20 *Hs2st*$^{-/-}$ chondrocytes upregulate cell surface-associated HS and length of secreted CS chains.
Cell surface-associated (A, B, C) and secreted GAGs (D, E, F) of primary differentiated *Hs2st*$^{-/-}$ and control chondrocytes were metabolically labeled with ^{35}S, and analyzed by size-exclusion chromatography. *Hs2st*$^{-/-}$ chondrocytes contained longer GAG chains (A), more HS (C) and less CS (B) compared to wild-type cells. In the secreted fractions CS was the predominant sulfated GAG (E, F). The length of the secreted GAG (D) and CS ((E) HNO_2 digest) chains was moderate elongation in the mutant. Data are shown as (%) cpm relative to the input. n=3. One representative experiment is shown. V_0–void volume, V_t–total column volume.

Analysis of the secreted PGs of fraction 1 indicated a molecular weight of ≈45 kDa for the total GAGs, while the size of CS was ≈40 kDa for both, wild-type and mutant cells (Fig. 9. 4). Nevertheless, a slight elongation of the chain length of the GAGs purified from *Hs2st*$^{-/-}$ was observed in fraction 2 of the extracellular PGs (Fig. 4. 20 D). Individual analyses of CS and HS revealed a slightly increased molecular weight of CS, but no alterations of the HS

polymer size (Fig. 4. 20 E). Nevertheless, this difference was quite small and estimated as ≈5 kDa larger CS chains in the mutant cells.

In summary, the obtained data show that chondrocytes compensate for the altered HS structure not only by increasing CS levels, but also by distinct alterations in HS amount and modification. Importantly, this compensatory mechanism affects both, the cell surface-associated and the secreted PG populations, which moreover are affected in a distinct manner.

5 Discussion

The secreted protein Ihh is one of the main regulators of endochondral ossification, controlling the proliferation and differentiation of chondrocytes and osteoblast differentiation. It has been established that Ihh activity is dependent on the composition of the ECM in the tissue and that alterations cause deregulation of the signaling pathway and bone development. In this context HSPGs, a major component of the ECM, have been shown to modulate the multimerization of Shh (Dierker et al., 2009a; Farshi et al., 2011; Vyas et al., 2014), its distribution and signaling activity. Despite the extensive research, the precise molecular mechanisms, by which HSPGs and other ECM molecules regulate this wide spectrum of events, are not fully understood.

The current work characterizes two conserved HS-binding motifs in the Ihh molecule and demonstrates an interaction with HS via each motif. Importantly, these binding sites differ in their affinity to HS, indicating that an interaction via each motif mediates binding to specifically sulfated HS, and perhaps regulates distinct aspect of Ihh biology. Additionally, the data reported here show that functional CW motifs, and possibly an interaction with HS, are necessary for Ihh multimerization in HEK-293Ebna cells. Despite this, analysis of the endogenous Ihh, produced by *Ext1*$^{gt/gt}$ and *Glce*$^{-/-}$*;Hs2st*$^{-/-}$ chondrocytes showed no differences in the multimer size compared to the Ihh produced by wild-type cells, indicating that either: 1) GAGs do not play a crucial role in the multimerization, 2) another GAG drives the multimeric organization or 3) HS cooperates with another GAG, which compensates for the hindered HS functions in this process. In line with the later hypothesis an upregulation of CS was observed in embryonic cartilage of several mouse strains with impaired HS synthesis. These data combined with the mild bone phenotype of HS mutants and an altered Ihh signaling observed in various CS mutants (Cortes et al., 2009; Kluppel et al., 2005) indicate that both GAGs are involved in the regulation of Ihh multimerization, distribution and signaling, likely controlling different aspects of these events, but able in part to substitute for each others functions.

5.1 Ihh motifs involved in interaction with HS

5.1.1 The CW1 motif defines the interaction of Ihh with HS

A role of HSPGs in Ihh distribution has been proposed for the first time with the identification of *Tout-velu*, the homolog of *Ext1* in *Drosophila* (Bellaiche et al., 1998; The et al., 1999). In these studies, the *Drosophila* Hh could activate target genes in clones of HS deficient cells flanking the Hh expression domain, but not in cells located several cell

diameters away from the Hh source. In line with this, an altered Hh diffusion has been observed in mutants with loss of function of other genes involved in the synthesis of HS (Han et al., 2004a; Takei et al., 2004) or the HSPG core protein (Ayers et al., 2010; Han et al., 2004b; Takeo et al., 2005; Williams et al., 2010). An evidence for a direct interaction with HS has been acquired with the identification of a HS-binding domain, a CW motif, within the N-terminal extended tail of Shh (Rubin et al., 2002). Mutation of two positively charged residues (K34 and K38) to alanine in this motif was shown to impair the HS interaction *in vitro*. Surprisingly, a mouse mutant, the Shh^{Ala} mouse, bearing the same mutation did not exhibit patterning defects, but a reduced proliferation and apoptosis (Chan et al., 2009). A more detailed analysis of the Shh CW sequence, performed by Farshi and colleagues, proposed that each CW residue contributes in distinct manner to the interactions with HS (Farshi et al., 2011). According to this work, the residues within the motif are organized into two groups, which are oriented to opposite directions in the N-terminal peptide, contributing either to the interaction with the adjacent molecule to form a multimer or mediating an interaction with HS. Thus, the residues K34 and K38 (mutated in the Shh^{Ala} mouse) were shown to mediate protein multimerization, while the residues K33, R35 and K39 were described to facilitate an interaction with HS (Farshi et al., 2011). Nevertheless, it is unlikely that such flexible, random coil-like structure as the N-terminal Hh peptide can maintain a strict orientation under physiological condition. In contrast to the findings for Shh, the current study shows that in Ihh, comparable groups of CW residues–R76/R80; R75/R77 and K81, reduced the affinity of Ihh to HS to a similar degree, indicating an equal contribution to HS binding (section 4.1.2.2). Another discrepancy with the results reported in Farshi et al., is the fully abolished interaction of Shh with HS observed after deletion of the CW motif or mutation of all residues to alanine. As reported here, the corresponding Ihh mutants ($IhhNp^{\Delta CW}$, $IhhNp^{R75A/R76A/R77A/R80A/K81A}$) were still able to bind to embryonic HS, although with lower affinity than the wild-type protein. It is worth noting that the experiments in both studies were performed using HS purified from mouse embryos, which is highly diverse and changes its composition during development. Thus, small differences in the composition of HS used in each study might be age-related, thereby leading to the observed differences in protein binding. This, together with the variations in the CW1 motifs of the studied paralogous proteins is a possible explanation for the apparent discrepancies in this study and the previously reported data by Farshi and colleagues. Nevertheless, the preserved HS binding of the Ihh CW1 deletion mutant ($IhhNp^{\Delta CW}$) indicates a contribution of more residues, beside those of the CW1 motif, to the interaction with HS.

5.1.2 Role of the CW2 motif in the interaction with HS

This work demonstrated for first time an interaction of Ihh with HS via a second CW site–the CW2 motif, which further challenges the previously described loss of HS interaction due to a deletion of the CW1 motif in Shh (Farshi et al., 2011). This motif is non-linear and less critical in determining the binding of the protein to HS than the CW1 motif. A perturbed HS-Ihh interaction was observed when at least three CW2 residues were mutated. Importantly, mutating the entire CW2 sequence in the $IhhNp^{K130SR166SR196SR198SK221S}$ mutant resulted in a dramatic decrease in the detected Ihh levels after an interaction with HS. Nevertheless, this effect is possibly due to a decreased protein stability, suggesting that an interaction with HS through the CW2 domain is likely required for protein stabilization.

The identification of an additional HS binding residue in Shh–K178 (corresponding to K221 in murine Ihh) is in agreement with the findings reported here and reinforces the idea that Hh proteins interact with HS via more than one binding domain (Chang et al., 2011). In the later work, loss of positive charge at K178, K37 and K38 in Shh abolished the interaction with heparin. It is worth noting that the recombinant Shh protein, analyzed in this study, was a bacterially produced monomeric form, which does not carry lipid modifications and has previously been shown to bind HS with different affinity compared to dual-lipidated, multimeric Shh (Chang et al., 2011; Farshi et al., 2011). This likely contributes to the prominent destabilization of the heparin interaction caused by the loss of only three positively charged residues. Further research on the subject identified four additional HS interacting residues in the globular domain of Shh, which together with K178 form a second HS-binding site–the CW2 motif (Whalen et al., 2013). Notably, the CW2 motif overlaps with the binding sites of the Hh receptor Ptch1 and other co-receptors, indicating a direct role of HS in regulating the Hh interaction with these proteins. This hypothesis is supported by the loss of biological activity of all analyzed Ihh CW2 mutants.

According to the findings reported here and in studies of Shh (Chang et al., 2011; Whalen et al., 2013), the HS interaction of mammalian Hh proteins is mediated by at least two clusters of positively charged residues.

5.1.3 Distinct roles of the CW1 and CW2 motifs in Ihh biology

The current work shows that Ihh binding to HS is mediated by the CW1 and CW2 motifs. An exciting finding described for first time in this work is that each Ihh CW motif binds preferably to particularly sulfated HS. While alterations in the CW1 motif showed greater influence on the interactions with HS, a perturbation in CW2 had only a moderate effect on

HS binding, but a stronger impact on the interactions with heparin. This may suggest that distinct aspects of Hh signaling are regulated by each HS-binding domain. Such possibility is supported by a study in *Drosophila* describing a requirement for particular HS sulfation patterns in the producing and receiving cells (Wojcinski et al., 2011). In that study, loss of function of the extracellular 6-*O*-endosulfatase *DSulf*, leading to higher HS 6-*O*-sulfation in producing and responding cells, had opposite effect on Hh signaling. While loss of function of *DSulf* in the responding cells promoted Ihh signaling, the same mutation in producing cells inhibited the signaling. It is possible that low sulfated HS interacts preferably with the CW1 motif in the producing cells to promote protein release, while high sulfated HS, interacting with CW2 domain, is required at the responding compartment to bind and restrict the protein, or promote an interaction with Ptch1. This hypothesis is further supported by the low *N*-sulfation, observed in prehypertrophic, Ihh producing chondrocytes (Fig. 9. 5). Finally, a scenario in which HS regulates different aspects of Hh signaling by interacting with one or the other binding motif could explain the mild phenotype of the Shh^{Ala} mouse.

5.2 HS-binding motifs define Ihh multimerization *in vitro*

The organization of Hh proteins in high order structure has been observed *in vivo* (Vyas et al., 2008) and implemented as a possible mechanism for protein distribution in the tissue. More importantly, it has been stated that an interaction with HS is a prerequisite for multimerization (Chang et al., 2011; Farshi et al., 2011; Vyas et al., 2008). Therefore, the capacity of Ihh CW1 and CW2 mutants to form multimers was investigated. The data presented here indicate that in HEK-293Ebna cells each site is required for IhhNp multimer formation to a certain degree, which correlates with their respective influence on HS binding. The CW1 motif, which has a strong effect on the interaction with HS, has a more pronounced impact on the diversification of the IhhNp cluster sizes than the CW2 domain. This indicates that HS interaction and protein multimerization are linked. In contrast to Shh (Farshi et al., 2011), the CW1 mutants $IhhNp^{R75A/R77A}$ and $IhhNp^{R76A/R80A}$ had a similar effect on protein multimerization. This further questions the previously suggested special orientation of the CW1 residues to support either multimerization or HS binding, and argues for a role of each residue in both processes. Interestingly, $IhhNp^{\Delta CW}$ formed multimers of similar size as the wild-type protein. This could be a result of other positively charged residues that alter their orientation and become available for an interaction if the CW1 motif is not present.

In agreement with its limited role in HS interaction the CW2 motif had a moderate effect on protein multimerization. Importantly only mutants with decreased affinity to HS formed

clusters of reduced size. Additionally, only a substitution of four CW2 residues to serine reduced the size of the multimers below 350 kDa. These data further support a crucial role of HS in the formation of multimers. Whether HS is a component of the multimer, how the monomers are organized in the clusters, and whether each CW motif has a different function in the process needs to be further analyzed.

5.3 The HS pattern has limited effect on Ihh binding and multimerization

5.3.1 Alterations in Hh sulfation pattern have diverse effects on the affinity of Hh proteins

Previous analyses of *Glce*$^{-/-}$ mice have shown that loss of C5-epimerization and subsequently reduced 2-*O*-sulfation results in decreased binding of IhhNp to the mutant HS. In these mice, the total HS sulfation remains unaltered due to an increased *N*- and 6-*O*-sulfation, but the HS disaccharide distribution is altered. Moreover, the loss of IdoA creates a chain with restricted flexibility, which may limit the domains accessible for Ihh binding (Dierker et al., 2016). An earlier study reported that HS purified from *Ndst1*$^{-/-}$ mice had an unaltered affinity, but a decreased binding capacity to a monomeric recombinant Shh protein in comparison to wild-type HS (Grobe et al., 2005). Differently to this, the analysis of dual-lipidated multimeric Shh and Ihh showed an increased affinity to *Ndst1*$^{-/-}$ HS compared to the control (section 4.1.6), supporting previous reports that multimeric and monomeric Shh forms differ in their interaction with HS (Farshi et al., 2011). It is possible that loss of *N*-sulfation is compensated by an increase in 6-*O*-sulfation, which may generate alternative binding domains mediating altered, but not decreased Hh binding to HS. Additionally, the HS used in these experiments was purified from whole mouse embryos. Four mouse *Ndst* genes with wide tissue expression during embryonic development have been described. The mouse mutants with loss of function in the other three *Ndst* genes have mild phenotypes, limited to undersulfated heparin in mast cells (*Ndst2*$^{-/-}$), hematological and behavior abnormalities (*Ndst3*$^{-/-}$) or colon defects (*Ndst4*$^{-/-}$) (Dagalv et al., 2011; Jao et al., 2016; Pallerla et al., 2008). Nevertheless, it is possible that Ndst1 loss in mice could be at least partly compensated by the activity of the other three Ndst enzymes, resulting in a pool of relatively normal or even high sulfated HS chains.

Similarly, the unaltered Ihh affinity to HS deficient in 2-*O*-sulfation might be a result of an increased *N*-sulfation, generating compensatory binding motifs, which could interact with Ihh. In agreement with a previous study of Shh (Witt et al., 2013), loss of 2-*O*-sulfation altered the

affinity of Shh to a certain extent. Such effect was not observed for Ihh, suggesting that different sulfation motifs might be preferred as a binding platform for each paralog.

5.3.2 ECM composition defines the size of Ihh multimers

A surprising finding of this study is that the Ihh multimers produced in HEK-293Ebna cells and primary chondrocytes differ dramatically in their size. While Ihh overexpressed in HEK-293Ebna cells produced clusters of >660 kDa, the endogenous multimers of the ECM-rich chondrocytes did not exceed 550 kDa indicating that the ECM composition regulates the size of the Ihh complexes. Moreover, the multimers formed by chondrocytes were characterized by an increased stability (Fig. 4.7 1). Such stable multimers, produced by primary chondrocytes have been reported before (Dierker et al., 2009a). Interestingly, in that study lower sulfated HS was shown to mediate the formation of stable multimers more efficiently than a higher sulfated HS *in vitro* (Dierker et al., 2009a). This, together with the requirement of low 6-*O*-sulfated HS in the Hh producing cells reported in (Wojcinski et al., 2011) suggests that low sulfated HS might be necessary for the formation of multimers *in vitro*. The process might be dependent on interaction of HS via the CW1 sequence, which, in the current work, was found to bind the relatively low sulfated HS more efficiently than heparin.

Surprisingly, the Ihh multimer size in chondrocytes was unaffected by alteration of the HS levels ($Ext1^{gt/gt}$) and pattern of sulfation ($Glce^{-/-};Hs2st^{-/-}$). This might mean that the sulfation and amount of HS produced by these mutant cells were sufficient to meet the requirements for multimer organization. Alternatively, the upregulated CS in $Ext1^{gt/gt}$ mutants might compensate for the low HS levels and support the formation of multimers. Independent on the mechanism by which the multimers are formed, these data indicated that the extended Ihh propagation in the $Ext1^{gt/gt}$ and $Glce^{-/-};Hs2st^{-/-}$ ((Koziel et al., 2004) and data not shown) mouse mutants is a result of a disturbed interaction of correctly formed multimers with the altered ECM. Moreover, the fact that CS upregulation is not sufficient to compensate for HS strongly support overlapping, but distinct functions of the two GAGs in regulating Ihh signaling.

5.4 Ihh and Shh differ in their interaction with HS and multimer size

The vertebrate Hh genes emerged as a result of the two Whole-Genome Duplications that took place prior to the development of chordates. The current hypothesis is that the first duplication of the Hh gene led to the ancestral Ihh/Shh and Dhh genes, that likely evolved independently prior the second genome duplication, which generated the three paralogs and a

fourth gene that was quickly lost. Comparative analyses have shown that Dhh is closer to the Drosophila Hh, while Shh and Ihh are more closely related to each other and share a high percentage of identity in their N-terminal signaling domain (Ingham and McMahon, 2001; Pereira et al., 2014). Strikingly, Shh and Ihh differ in their N-terminal CW1 motif by the higher total number of R residues in the Ihh sequence, which may lead to a stronger affinity to HS. Due to the geometric structure of the R residue such composition would provide more stability to the Ihh CW1 sequence. In addition, the guanidinium group of R allows the formation of more electrostatic interactions and hydrogen bonds compared to the basic functional group of K residue (Borders et al., 1994). This effect is partly balanced by the presence of P instead of the positively charged H residue found in Shh. Consequently, introducing the Shh CW1 motif into Ihh ($IhhNp^{R75KP78HR80K}$) resulted in a decreased affinity of the mutant protein to HS mimicking that of ShhNp. It can thus be concluded that the residues in the CW1 domain shape the HS interaction of each paralog. Interestingly, the Ihh V^{71}, V^{72} and S^{74} seem to contribute to the higher affinity of Ihh to HS, although it is highly unlikely that this effect is direct. The only partially reproduced Ihh elution profile by Shh bearing the iCW motif is somewhat surprising. Nevertheless, the number of total R residues in the sequence led to an extended elution profile and an increased affinity, partly reproducing the Ihh elution profile.

Shh and Ihh differ more significantly in their multimer size. Importantly, the paralog-specific multimer size-range can be successfully inverted by switching the CW motifs of the two proteins. Interestingly, $IhhNp^{V71GV72FS74\Delta R75KP78HR80K}$, carrying the extended Shh N-terminus formed multimers of similar size as Ihh. It is possible that the residues at position 71-74 in the mutant Ihh protein come in contacts with hydrophobic pockets of other components of the cluster, which supports multimer formation.

As shown by the distinct affinities of Shh and Ihh to 2-*O*-sulfate deficient HS, the binding of each paralog is further defined by the tissue-specific HS sulfation pattern. Interestingly Ihh, which operates in a tissue dominated by CS, contains the largest number of R residues in the CW1 motif, while the *Drosophila* Hh has only three out of the seven CW1 residues and interacts with highly sulfated HS, resembling heparin by its structure (Kusche-Gullberg et al., 2012). Thus, the Hh CW1 motifs most likely have evolved to secure an appropriated binding with the corresponding extracellular components for optimal release, transport and signaling. In contrast to the variation in CW1, the CW2 domain is much more conserved, which is consistent with the overlap of this motif with the binding domain of the receptor Ptch1.

5.5 Low levels of HS or an altered sulfation is compensated by an increase in CS level

CS and HS have a common tetrasaccharide primer, which raises the question whether interplay between their syntheses is possible. The current work provides strong *in vivo* evidence that reduced HS levels lead to an upregulation of CS in vertebrates. Several lines of evidence support this data. In zebrafish, for instance, loss of Extl3, which initiates assembly of HS chains, results in upregulation of CS synthesis, while inhibition of CSgalnact 1 and 2, necessary for CS chain initiation, boosts the synthesis of HS (Holmborn et al., 2012). Similar to this, loss of HS in *Ext1*$^{-/-}$ embryoid bodies results in increased CS levels, which compensates for the loss of HS and supports Vegf in induction of sprouting angiogenesis (Le Jan et al., 2012).

In addition, the current work provides for first time evidence for an alteration of CS levels not only due to decreased HS amount, but also as a result of an altered HS sulfation pattern. Such effect was observed for several HS mutant strains–*Hs2st*$^{-/-}$, *Ndst1*$^{-/-}$ and *Sulf1*$^{gt/gt}$*;Sulf2*$^{gt/gt}$. Notably, while in mutants characterized by decreased levels or sulfation of HS, CS was upregulated, in *Sulf1*$^{gt/gt}$*;Sulf2*$^{gt/gt}$ mutants, characterized by high HS 6-*O*-sulfation, the levels of sulfated CS were decreased. This indicates a mechanism, which monitors and regulates the levels and quality of the HS chains. Analysis of the GAG composition in *Ext1*$^{gt/gt}$ and *Hs2st*$^{-/-}$ cartilage confirmed an increase in CS levels, however, no alterations in CS sulfation were observed, which shows that mutant chondrocytes synthesize more chains with a normal sulfation pattern. Thus, the increased staining of CS neoepitopes is due to the presence of more CS chains and, consequently, more sulfated and unsulfated "stubs". In agreement with this, chain length analysis in *Ext1*$^{gt/gt}$ cells showed that the HS deficiency was compensated by synthesis of more, but shorter CS chains, carried by cell surface-associated and secreted PGs. Importantly, this effect is not restricted to differentiated cells and CS enrichment was observed in primary undifferentiated chondrocytes as well. An interesting observation was made when the HS and CS levels in primary, undifferentiated and differentiated cells were compared. The cell surface PGs in undifferentiated cells contained predominantly HS, while CS was poorly represented. At later stage, however, CS levels are increased and both GAGs are equally represented on the cell surface indicating that each GAG is required at distinct levels in a particular chondrocyte population. Nevertheless, the HS functions in *Ext1*$^{gt/gt}$ chondrocytes seem to be in part compensated by CS, which reaches levels comparable to those of HS in wild-type cells. Importantly, the length of the CS chains in undifferentiated

cells was also not increased, indicating that at both cell differentiation stages the augmented CS levels are attained by the synthesis of more, but shorter chains.
Differently to the *Ext1*$^{gt/gt}$ mutants, the increased CS of the *Hs2st*$^{-/-}$ mutants resulted in slightly longer CS chains, which were detected in the secreted PG population. Interestingly, these mutants also produced more HS on the cell surface, indicating that the sulfation insufficiency in *Hs2st*$^{-/-}$ cells is compensated by an increase in both, HS and CS syntheses.

5.5.3 CS as a regulator of bone development

HS has been shown to play crucial roles in embryonic bone development (reviewed in (Jochmann et al., 2014). In addition, the importance of CS levels in this process has been demonstrated in number of studies. In CSgalnact1 and ChSy1 mutant mice, the reduced CS levels caused skeletal abnormalities including short stature, disorganized growth plate, digit-patterning deffects, reduced bone density, combined with disturbed Ihh distribution and reception (Sato et al., 2011; Watanabe et al., 2010; Wilson et al., 2012).
Moreover, analyses of the brachymorphic (bm) mouse underlined the importance of CS sulfation for Ihh signaling and bone growth. The bm mouse bears a mutation in the *PAPS synthetase 2* (*Papss2*) gene, which encodes an enzyme responsible for the synthesis of 3′-phosphoadenosine 5′-phosphosulfate (PAPS)–the sulfate donor for HS and CS (Cortes et al., 2009; Sugahara and Schwartz, 1979). While HS levels and sulfation in these mice appear normal, CS is severely undersulfated, causing decreased Ihh expression and restricted distribution. In line with this, CS undersulfation in the mouse model for Diastrophic dysplasia (dtd mouse) results in skeletal defects, which were linked to a reduced Ihh diffusion through the tissue (Gualeni et al., 2013; Gualeni et al., 2010). Nevertheless, this mouse carries a mutation in the diastrophic dysplasia sulfate transporter (SLC26A2) and an alteration of HS sulfation were not excluded as possible cause of the phenotype.
In agreement with the studies in mutant mice, loss of function mutations in genes encoding CS synthesizing enzymes were identified in number of human syndromes as adducted thumb-clubfoot syndrome (ATCS), EDS Koshotype (EDSKT) syndromes and a subset of kyphoscoliosis type EDS without lysyl hydroxylase deficiency (EDS VIB) (Dundar et al., 2009; Malfait et al., 2010; Miyake et al., 2010). Thus, levels and accurate sulfation pattern of CS in the cartilage have an essential role for proper activity of the regulators of bone development, including Ihh. Whether HS and CS have overlapping functions or regulate different aspects of Ihh pathway activation needs to be further analyzed. Yet, the possibility of

functional overlap between HS and CS in Ihh signaling is supported by the identification of a putative CS binding site in Shh, which overlaps with the CW2 motif (Whalen et al., 2013).

5.5.4 Balancing the CS and HS levels during development

The dynamic balance between CS and HS levels reported here raises the question of how the synthesis is directed to either HS or CS chains, and how their levels of sulfation are controlled. It has been shown that specific domains of the PG core protein define which type of GAG chain will be attached and how it will be sulfated. The N-terminal globular domain of Glypicans, for instance, promotes attachment of HS chains via a mechanism involving the inhibition of CS chain assembly (Chen and Lander, 2001). Additionally, HS synthesis is promoted by clustering of acidic residues and adjacent tryptophan residues near the chain attachment site (Zhang and Esko, 1994). Nonetheless, it remains unclear how this information is transmitted from the core protein to the GAG synthesizing enzymes.

Another study suggests that phosphorylation and sulfation of the units of the tetrasaccharide primer are involved in this regulation (Gulberti et al., 2012; Gulberti et al., 2005). Thus, the increased synthesis of CS may be achieved by modifications in the linker, which will promote assembly of CS over HS. This could be the case for the *Ext1*$^{gt/gt}$ mutants, for which ≈40% more CS was observed on the cell surface of mutant chondrocytes. An altered expression of specific GAG carriers may also be involved in this regulatory mechanism, which likely is the case for both, *Hs2st*$^{-/-}$ and *Ext1*$^{gt/gt}$ mutants.

A critical role for the regulation of the GAG synthesis and sulfation pattern has the transport of nucleotide sugars and the universal sulfate donor PAPS. Thus, the decreased HS synthesis and sulfation might lead to larger pools of available PAPS and UDP-sugars that are directed to the synthesis of CS.

A striking effect was observed for the *Sulf1*$^{gt/gt}$*;Sulf2*$^{gt/gt}$ mutants, which have reduced CS sulfation and, possibly, amount. Since the Sulf enzymes operate extracellularly, but affect the CS pattern, these results strongly indicate a feed back mechanism, which monitors the quality of the extracellular GAG chains and induces intracellular compensatory mechanism. Further analyses have to be conducted to identify the factors and mechanisms, which fine-tune the composition of GAGs in the individual tissues.

6 Summary

Indian hedgehog (Ihh), which belongs to the conserved family of Hedgehog proteins, is one of the key regulators of embryonic bone development. Several lines of evidence indicate that the distribution and activity of Ihh in the cartilage tissue are dependent on the extracellular matrix (ECM) composition and, particularly, on the level and sulfation pattern of Heparan sulfate (HS) (Dierker et al., 2016; Koziel et al., 2004; Ratzka et al., 2008; Yasuda et al., 2010).

This work investigates the properties of the HS-Ihh interaction and the role of HS in the multimerization of Ihh. Moreover, the changes in GAG composition of mice with an altered HS structure were analyzed.

In the closely related Sonic Hedgehog (Shh), two conserved HS-binding sequences, called Cardin-Weintraub (CW) motifs, which support a direct interaction with HS, have been proposed. (Chang et al., 2011; Farshi et al., 2011; Ohlig et al., 2011; Whalen et al., 2013). The current work demonstrates that Ihh, like Shh, also contains two CW motifs (CW1 and CW2). Both domains are highly conserved, but the CW1 sequence is not identical between Shh and Ihh.

Mutation analysis revealed that the binding of Ihh, expressed in HEK-293Ebna cells to HS is mediated by both motifs, which, however, interact to specifically sulfated HS in distinct manners. Moreover, analysis of the Ihh multimerization showed that the CW1 and CW2 domains are essential, but–correlating with their HS affinity–distinctly important for multimer formation.

Surprisingly, analysis of the role of the HS modification pattern on the binding affinity of Shh and Ihh showed that loss of *N*-sulfation leads to an increased affinity of both proteins. 2-*O*-sulfate deficient HS bound Ihh with similar, but Shh with higher affinity than wild type HS.

To better understand how the differences between the Shh and Ihh CW1 sequences impact their HS binding, the affinities of the two paralogs to HS were compared. By exchanging the HS-interacting regions, this work demonstrates that these variations result in distinct affinities to HS and multimer size of the paralogous proteins.

Although the interaction with HS seems to mediate the Ihh multimerization in HEK-293Ebna cells, no alterations in multimer size were observed for Ihh expressed in primary chondrocyte of mouse mutants with an altered HS structure. This indicates that another cartilage glycosaminoglycan partly compensates for the HS functions. In line with this, analysis of E16.5 cartilage by immunofluorescence staining indicated that in mice, deficient in HS

synthesizing (*Ext1*$^{gt/gt}$) or modifying enzymes (*Ndst1*$^{-/-}$; *Hs2st*$^{-/-}$ *and Sulf1*$^{gt/gt}$;*Sulf2*$^{gt/gt}$), the altered HS was compensated by changes in the levels of Chondroitin sulfate (CS), the main sulfated glycosaminoglycans in chondrocytes. This finding was confirmed by disaccharide analysis of HS and CS purified from *Ext1*$^{gt/gt}$ and *Hs2st*$^{-/-}$ embryonic skeletons. Moreover, evaluating the chain length of GAGs, produced by primary chondrocytes revealed that the decreased HS levels in *Ext1*$^{gt/gt}$ mice resulted in more, but shorter CS chains, while *Hs2st*$^{-/-}$ cells compensated the altered HS sulfation pattern by an increase of cell surface-associated HS and an elongation of CS chains carried by secreted proteoglycans.

Taken together, these data indicate that the interactions of Ihh with HS are determined by two motifs of positively charged residues. Each motif likely interacts with specifically sulfated HS, and possibly with CS. In addition, these data demonstrate for the first time that not only reduced levels, but also an altered HS structure leads to an increase in CS levels. This underlines the highly adaptable nature of ECM and strongly points to a functional overlap between HS and CS in regulating signaling molecules during bone development.

7 Zusammenfassung

Indian Hedgehog (Ihh), welches zur konservierten Familie der Hedgehog Proteine gehört, ist einer der Hauptregulatoren der embryonalen Knochenentwicklung. Zahlreiche Studien haben gezeigt, dass die Verteilung und Aktivität von Ihh von der Zusammensetzung der extrazellulären Matrix (ECM), insbesondere von der Menge und dem Sulfatierungsmuster von Herparansulfaten (HS) reguliert wird (Dierker et al., 2016; Koziel et al., 2004; Ratzka et al., 2008; Yasuda et al., 2010).

In dieser Arbeit wurden die HS-Ihh Wechselwirkungen und der Einfluss von HS auf die Multimerisierung von Ihh untersucht. Außerdem wurde anhand von Maus-Mutanten, bei denen verminderte HS-Level oder Sulfatierungstufen vorlagen, ein potenzieller Effekt auf die Zusammensetzung der ECM analysiert.

Bei dem Ihh Paralog Sonic Hedgehog (Shh) wurden zwei konservierte HS-Bindungsdomänen beschrieben, die sogenannten Cardin-Weintraub (CW) Motive, die eine direkte Interaktion mit HS vermitteln. In der vorliegenden Arbeit konnte gezeigt werden, dass das Ihh Protein beide Motive (CW1 und CW2) aufweist. Diese Motive sind hoch konserviert, trotzdem gibt es Unterschiede zwischen den CW1 Sequenzen von Shh und Ihh.

Mittels Mutationsanalysen wurde gezeigt, dass Ihh, welches in HEK-293Ebna Zellen exprimiert wurde, über die beiden CW-Motive mit HS interagiert. Dabei interagiert jedes Motiv mit spezifisch sulfatiertem HS mit unterschiedlicher Affinität. Darüber hinaus zeigten weitere Analysen, dass die CW1 und CW2 Domänen essentiell für die Ihh Multimerisierung sind und diese von der HS-Affinität abhängt.

In weiteren Analysen wurde die Bedeutung des HS-Sulfatierungsmusters für die HS-Hh Interaktion untersucht. Interessanterweise zeigte HS mit verringerter *N*-Sulfatierung im Vergleich zur Kontrolle eine erhöhte Affinität zu Ihh und Shh. 2-*O*-Sulfat defizientes HS weist hingegen eine erhöhte Affinität zu Shh, aber eine unveränderte Affinität zu Ihh auf. Um die Unterschiede in den CW1-Sequenzen von Shh und Ihh und deren Einfluss auf die Interaktion mit HS besser verstehen zu können, wurde deren Affinität zu HS untersucht. Durch den Austausch ihrer CW1 Motive konnte gezeigt werden, dass die Protein-spezifische HS-Affinität und die Multimergröße durch dieses Motiv bestimmt wird.

Obwohl die Interaktion mit HS die Bildung von Ihh-Multimeren in HEK-293Ebna-Zellen vermittelt, konnte in primären Chondrozyzen aus Maus-Mutanten mit veränderter HS-Struktur kein Einfluss auf die Multimergröße festgestellt werden. Diese Ergebnisse deuten drauf hin, dass ein anderes Glykosaminoglykan die Funktion von HS im Knorpel teilweise

kompensieren kann. Einen ersten Hinweis darauf lieferten Immunfluoreszenz-Analysen von E16.5 Gliedmaßen von Maus-Mutanten mit einer Defizienz für Enzyme, die an der HS-Synthese (*Ext1*$^{gt/gt}$) oder Modifikation (*Ndst1*$^{-/-}$; *Hs2st*$^{-/-}$ und *Sulf1*$^{gt/gt}$*;Sulf2*$^{gt/gt}$) beteiligt sind. Die resultierenden HS-Veränderungen wurden durch ein erhöhtes Level an Chondroitinsulfat (CS) kompensiert. Diese Ergebnisse konnten mittels Disaccharid-Analysen von HS und CS aus embryonalen Skeletten von *Ext1*$^{gt/gt}$ und *Hs2st*$^{-/-}$ Mutanten bestätigt werden.

Eine Analyse der GAG-Kettenlänge zeigte, dass in primären Chondrozyten von *Ext1*$^{gt/gt}$ Mäusen das verminderte HS Level in einer erhöhten Menge an kürzeren CS Ketten resultiert. Bei *Hs2st*-defizienten Zellen wurde dagegen das veränderte HS-Sulfatierungsmuster durch eine gesteigerte Menge von Zelloberflächen-assoziiertem HS, sowie einer Verlängerung der in die ECM sezernierten CS-Ketten kompensiert.

Zusammenfassend zeigen die Daten, dass die Interaktion von Ihh mit HS über die positiv geladenen Aminosäuren in den zwei konservierten Bindungsdomänen vermittelt wird. Jede Bindungsdomäne interagiert dabei mit unterschiedlicher Affinität mit spezifisch sulfatiertem HS und möglicherweise auch mit CS. Darüber hinaus zeigt diese Arbeit zum ersten Mal, dass nicht nur verringerte HS-Level, sondern auch ein verändertes Sulfatierungsmuster zu einer gesteigerten Menge an CS führen kann. Diese Beobachtung unterstreicht die hohe Kompensationsfähigkeit der Knorpel-ECM hinsichtlich der Zusammensetzung der GAGs und weist auf funktionale Wechselwirkungen zwischen HS und CS in der Regulation von Signalmolekülen während der Knochenentwicklung hin.

8 List of references

Ai, X., Do, A.T., Kusche-Gullberg, M., Lindahl, U., Lu, K., and Emerson, C.P., Jr. (2006). Substrate specificity and domain functions of extracellular heparan sulfate 6-O-endosulfatases, QSulf1 and QSulf2. J Biol Chem *281*, 4969-4976.

Amizuka, N., Warshawsky, H., Henderson, J.E., Goltzman, D., and Karaplis, A.C. (1994). Parathyroid hormone-related peptide-depleted mice show abnormal epiphyseal cartilage development and altered endochondral bone formation. J Cell Biol *126*, 1611-1623.

Ayers, K.L., Gallet, A., Staccini-Lavenant, L., and Therond, P.P. (2010). The long-range activity of Hedgehog is regulated in the apical extracellular space by the glypican Dally and the hydrolase Notum. Dev Cell *18*, 605-620.

Beachy, P.A., Hymowitz, S.G., Lazarus, R.A., Leahy, D.J., and Siebold, C. (2010). Interactions between Hedgehog proteins and their binding partners come into view. Genes Dev *24*, 2001-2012.

Becker, S., Wang, Z.J., Massey, H., Arauz, A., Labosky, P., Hammerschmidt, M., St-Jacques, B., Bumcrot, D., McMahon, A., and Grabel, L. (1997). A role for Indian hedgehog in extraembryonic endoderm differentiation in F9 cells and the early mouse embryo. Dev Biol *187*, 298-310.

Bellaiche, Y., The, I., and Perrimon, N. (1998). Tout-velu is a Drosophila homologue of the putative tumour suppressor EXT-1 and is needed for Hh diffusion. Nature *394*, 85-88.

Billings, P.C., and Pacifici, M. (2015). Interactions of signaling proteins, growth factors and other proteins with heparan sulfate: mechanisms and mysteries. Connect Tissue Res *56*, 272-280.

Birnboim, H.C., and Doly, J. (1979). A rapid alkaline extraction procedure for screening recombinant plasmid DNA. Nucleic Acids Res *7*, 1513-1523.

Bischoff, M., Gradilla, A.C., Seijo, I., Andres, G., Rodriguez-Navas, C., Gonzalez-Mendez, L., and Guerrero, I. (2013). Cytonemes are required for the establishment of a normal Hedgehog morphogen gradient in Drosophila epithelia. Nat Cell Biol *15*, 1269-1281.

Bishop, J.R., Schuksz, M., and Esko, J.D. (2007). Heparan sulphate proteoglycans fine-tune mammalian physiology. Nature *446*, 1030-1037.

Bitgood, M.J., and McMahon, A.P. (1995). Hedgehog and Bmp genes are coexpressed at many diverse sites of cell-cell interaction in the mouse embryo. Dev Biol *172*, 126-138.

Bitgood, M.J., Shen, L., and McMahon, A.P. (1996). Sertoli cell signaling by Desert hedgehog regulates the male germline. Curr Biol *6*, 298-304.

Bitter, T., and Muir, H.M. (1962). A modified uronic acid carbazole reaction. Anal Biochem *4*, 330-334.

Borders, C.L., Jr., Broadwater, J.A., Bekeny, P.A., Salmon, J.E., Lee, A.S., Eldridge, A.M., and Pett, V.B. (1994). A structural role for arginine in proteins: multiple hydrogen bonds to backbone carbonyl oxygens. Protein Sci *3*, 541-548.

Buglino, J.A., and Resh, M.D. (2008). Hhat is a palmitoylacyltransferase with specificity for N-palmitoylation of Sonic Hedgehog. J Biol Chem *283*, 22076-22088.

Buglino, J.A., and Resh, M.D. (2012). Palmitoylation of Hedgehog proteins. Vitam Horm *88*, 229-252.

Bullock, S.L., Fletcher, J.M., Beddington, R.S., and Wilson, V.A. (1998). Renal agenesis in mice homozygous for a gene trap mutation in the gene encoding heparan sulfate 2-sulfotransferase. Genes Dev *12*, 1894-1906.

Bulow, H.E., and Hobert, O. (2006). The molecular diversity of glycosaminoglycans shapes animal development. Annu Rev Cell Dev Biol *22*, 375-407.

Burke, R., Nellen, D., Bellotto, M., Hafen, E., Senti, K.A., Dickson, B.J., and Basler, K. (1999). Dispatched, a novel sterol-sensing domain protein dedicated to the release of cholesterol-modified hedgehog from signaling cells. Cell *99*, 803-815.

Cardin, A.D., and Weintraub, H.J. (1989). Molecular modeling of protein-glycosaminoglycan interactions. Arteriosclerosis *9*, 21-32.

Carlsson, P., and Kjellen, L. (2012). Heparin biosynthesis. Handb Exp Pharmacol, 23-41.

Caterson, B. (2012). Fell-Muir Lecture: chondroitin sulphate glycosaminoglycans: fun for some and confusion for others. Int J Exp Pathol *93*, 1-10.

Chan, J.A., Balasubramanian, S., Witt, R.M., Nazemi, K.J., Choi, Y., Pazyra-Murphy, M.F., Walsh, C.O., Thompson, M., and Segal, R.A. (2009). Proteoglycan interactions with Sonic Hedgehog specify mitogenic responses. Nat Neurosci *12*, 409-417.

Chang, S.C., Mulloy, B., Magee, A.I., and Couchman, J.R. (2011). Two distinct sites in sonic Hedgehog combine for heparan sulfate interactions and cell signaling functions. J Biol Chem *286*, 44391-44402.

Chen, M.H., Li, Y.J., Kawakami, T., Xu, S.M., and Chuang, P.T. (2004). Palmitoylation is required for the production of a soluble multimeric Hedgehog protein complex and long-range signaling in vertebrates. Genes Dev *18*, 641-659.

Chen, R.L., and Lander, A.D. (2001). Mechanisms underlying preferential assembly of heparan sulfate on glypican-1. J Biol Chem *276*, 7507-7517.

Chen, X., Tukachinsky, H., Huang, C.H., Jao, C., Chu, Y.R., Tang, H.Y., Mueller, B., Schulman, S., Rapoport, T.A., and Salic, A. (2011a). Processing and turnover of the Hedgehog protein in the endoplasmic reticulum. J Cell Biol *192*, 825-838.

Chen, Y., Sasai, N., Ma, G., Yue, T., Jia, J., Briscoe, J., and Jiang, J. (2011b). Sonic Hedgehog dependent phosphorylation by CK1alpha and GRK2 is required for ciliary accumulation and activation of smoothened. PLoS Biol *9*, e1001083.

Clause, K.C., and Barker, T.H. (2013). Extracellular matrix signaling in morphogenesis and repair. Curr Opin Biotechnol *24*, 830-833.

Cohen, M.M., Jr. (2003). The hedgehog signaling network. Am J Med Genet A *123A*, 5-28.

Cortes, M., Baria, A.T., and Schwartz, N.B. (2009). Sulfation of chondroitin sulfate proteoglycans is necessary for proper Indian hedgehog signaling in the developing growth plate. Development *136*, 1697-1706.

Creanga, A., Glenn, T.D., Mann, R.K., Saunders, A.M., Talbot, W.S., and Beachy, P.A. (2012). Scube/You activity mediates release of dually lipid-modified Hedgehog signal in soluble form. Genes Dev *26*, 1312-1325.

Dagalv, A., Holmborn, K., Kjellen, L., and Abrink, M. (2011). Lowered expression of heparan sulfate/heparin biosynthesis enzyme N-deacetylase/n-sulfotransferase 1 results in increased sulfation of mast cell heparin. J Biol Chem *286*, 44433-44440.

Dagalv, A., Lundequist, A., Filipek-Gorniok, B., Dierker, T., Eriksson, I., and Kjellen, L. (2015). Heparan sulfate structure: methods to study N-sulfation and NDST action. Methods Mol Biol *1229*, 189-200.

David, G., Bai, X.M., Van der Schueren, B., Cassiman, J.J., and Van den Berghe, H. (1992). Developmental changes in heparan sulfate expression: in situ detection with mAbs. J Cell Biol *119*, 961-975.

Dejana, E., Hirschi, K.K., and Simons, M. (2017). The molecular basis of endothelial cell plasticity. Nat Commun *8*, 14361.

Deligny, A., Dierker, T., Dagalv, A., Lundequist, A., Eriksson, I., Nairn, A.V., Moremen, K.W., Merry, C.L., and Kjellen, L. (2016). NDST2 (N-Deacetylase/N-Sulfotransferase-2) Enzyme Regulates Heparan Sulfate Chain Length. J Biol Chem *291*, 18600-18607.

Dennis, J.F., Kurosaka, H., Iulianella, A., Pace, J., Thomas, N., Beckham, S., Williams, T., and Trainor, P.A. (2012). Mutations in Hedgehog acyltransferase (Hhat) perturb Hedgehog signaling, resulting in severe acrania-holoprosencephaly-agnathia craniofacial defects. PLoS Genet *8*, e1002927.

Dierker, T., Bachvarova, V., Krause, Y., Li, J.P., Kjellen, L., Seidler, D.G., and Vortkamp, A. (2016). Altered heparan sulfate structure in Glce(-/-) mice leads to increased Hedgehog signaling in endochondral bones. Matrix Biol *49*, 82-92.

Dierker, T., Dreier, R., Migone, M., Hamer, S., and Grobe, K. (2009a). Heparan sulfate and transglutaminase activity are required for the formation of covalently cross-linked hedgehog oligomers. J Biol Chem *284*, 32562-32571.

Dierker, T., Dreier, R., Petersen, A., Bordych, C., and Grobe, K. (2009b). Heparan sulfate-modulated, metalloprotease-mediated sonic hedgehog release from producing cells. J Biol Chem *284*, 8013-8022.

Dundar, M., Muller, T., Zhang, Q., Pan, J., Steinmann, B., Vodopiutz, J., Gruber, R., Sonoda, T., Krabichler, B., Utermann, G.*, et al.* (2009). Loss of dermatan-4-sulfotransferase 1 function results in adducted thumb-clubfoot syndrome. Am J Hum Genet *85*, 873-882.

Echelard, Y., Epstein, D.J., St-Jacques, B., Shen, L., Mohler, J., McMahon, J.A., and McMahon, A.P. (1993). Sonic hedgehog, a member of a family of putative signaling molecules, is implicated in the regulation of CNS polarity. Cell *75*, 1417-1430.

Esko, J.D., and Lindahl, U. (2001). Molecular diversity of heparan sulfate. J Clin Invest *108*, 169-173.

Esko, J.D., and Selleck, S.B. (2002). Order out of chaos: assembly of ligand binding sites in heparan sulfate. Annu Rev Biochem *71*, 435-471.

Eugster, C., Panakova, D., Mahmoud, A., and Eaton, S. (2007). Lipoprotein-heparan sulfate interactions in the Hh pathway. Dev Cell *13*, 57-71.

Farshi, P., Ohlig, S., Pickhinke, U., Hoing, S., Jochmann, K., Lawrence, R., Dreier, R., Dierker, T., and Grobe, K. (2011). Dual roles of the Cardin-Weintraub motif in multimeric Sonic hedgehog. J Biol Chem *286*, 23608-23619.

Fic, E., Kedracka-Krok, S., Jankowska, U., Pirog, A., and Dziedzicka-Wasylewska, M. (2010). Comparison of protein precipitation methods for various rat brain structures prior to proteomic analysis. Electrophoresis *31*, 3573-3579.

Frantz, C., Stewart, K.M., and Weaver, V.M. (2010). The extracellular matrix at a glance. J Cell Sci *123*, 4195-4200.

Goetz, J.A., Singh, S., Suber, L.M., Kull, F.J., and Robbins, D.J. (2006). A highly conserved amino-terminal region of sonic hedgehog is required for the formation of its freely diffusible multimeric form. J Biol Chem *281*, 4087-4093.

Goetz, S.C., and Anderson, K.V. (2010). The primary cilium: a signalling centre during vertebrate development. Nat Rev Genet *11*, 331-344.

Gradilla, A.C., Gonzalez, E., Seijo, I., Andres, G., Bischoff, M., Gonzalez-Mendez, L., Sanchez, V., Callejo, A., Ibanez, C., Guerra, M.*, et al.* (2014). Exosomes as Hedgehog carriers in cytoneme-mediated transport and secretion. Nat Commun *5*, 5649.

Graham, F.L., Abrahams, P.J., Mulder, C., Heijneker, H.L., Warnaar, S.O., De Vries, F.A., Fiers, W., and Van Der Eb, A.J. (1975). Studies on in vitro transformation by DNA and DNA fragments of human adenoviruses and simian virus 40. Cold Spring Harb Symp Quant Biol *39 Pt 1*, 637-650.

Grobe, K., Inatani, M., Pallerla, S.R., Castagnola, J., Yamaguchi, Y., and Esko, J.D. (2005). Cerebral hypoplasia and craniofacial defects in mice lacking heparan sulfate Ndst1 gene function. Development *132*, 3777-3786.

Gualeni, B., de Vernejoul, M.C., Marty-Morieux, C., De Leonardis, F., Franchi, M., Monti, L., Forlino, A., Houillier, P., Rossi, A., and Geoffroy, V. (2013). Alteration of proteoglycan sulfation affects bone growth and remodeling. Bone *54*, 83-91.

Gualeni, B., Facchini, M., De Leonardis, F., Tenni, R., Cetta, G., Viola, M., Passi, A., Superti-Furga, A., Forlino, A., and Rossi, A. (2010). Defective proteoglycan sulfation of the growth plate zones causes reduced chondrocyte proliferation via an altered Indian hedgehog signalling. Matrix Biol *29*, 453-460.

Gulberti, S., Jacquinet, J.C., Chabel, M., Ramalanjaona, N., Magdalou, J., Netter, P., Coughtrie, M.W., Ouzzine, M., and Fournel-Gigleux, S. (2012). Chondroitin sulfate N-acetylgalactosaminyltransferase-1 (CSGalNAcT-1) involved in chondroitin sulfate initiation: Impact of sulfation on activity and specificity. Glycobiology *22*, 561-571.

Gulberti, S., Lattard, V., Fondeur, M., Jacquinet, J.C., Mulliert, G., Netter, P., Magdalou, J., Ouzzine, M., and Fournel-Gigleux, S. (2005). Modifications of the glycosaminoglycan-linkage region of proteoglycans: phosphorylation and sulfation determine the activity of the human beta1,4-galactosyltransferase 7 and beta1,3-glucuronosyltransferase I. ScientificWorldJournal *5*, 510-514.

Han, C., Belenkaya, T.Y., Khodoun, M., Tauchi, M., Lin, X., and Lin, X. (2004a). Distinct and collaborative roles of Drosophila EXT family proteins in morphogen signalling and gradient formation. Development *131*, 1563-1575.

Han, C., Belenkaya, T.Y., Wang, B., and Lin, X. (2004b). Drosophila glypicans control the cell-to-cell movement of Hedgehog by a dynamin-independent process. Development *131*, 601-611.

Hayes, A.J., Hughes, C.E., and Caterson, B. (2008). Antibodies and immunohistochemistry in extracellular matrix research. Methods *45*, 10-21.

Holmborn, K., Habicher, J., Kasza, Z., Eriksson, A.S., Filipek-Gorniok, B., Gopal, S., Couchman, J.R., Ahlberg, P.E., Wiweger, M., Spillmann, D.*, et al.* (2012). On the roles and regulation of chondroitin sulfate and heparan sulfate in zebrafish pharyngeal cartilage morphogenesis. J Biol Chem *287*, 33905-33916.

Huang, H., and Kornberg, T.B. (2016). Cells must express components of the planar cell polarity system and extracellular matrix to support cytonemes. Elife *5*.

Huegel, J., Mundy, C., Sgariglia, F., Nygren, P., Billings, P.C., Yamaguchi, Y., Koyama, E., and Pacifici, M. (2013). Perichondrium phenotype and border function are regulated by Ext1 and heparan sulfate in developing long bones: a mechanism likely deranged in Hereditary Multiple Exostoses. Dev Biol *377*, 100-112.

Humke, E.W., Dorn, K.V., Milenkovic, L., Scott, M.P., and Rohatgi, R. (2010). The output of Hedgehog signaling is controlled by the dynamic association between Suppressor of Fused and the Gli proteins. Genes Dev *24*, 670-682.

Ingham, P.W., and McMahon, A.P. (2001). Hedgehog signaling in animal development: paradigms and principles. Genes Dev *15*, 3059-3087.

Jakobs, P., Exner, S., Schurmann, S., Pickhinke, U., Bandari, S., Ortmann, C., Kupich, S., Schulz, P., Hansen, U., Seidler, D.G.*, et al.* (2014). Scube2 enhances proteolytic Shh processing from the surface of Shh-producing cells. J Cell Sci *127*, 1726-1737.

Jakobs, P., Schulz, P., Ortmann, C., Schurmann, S., Exner, S., Rebollido-Rios, R., Dreier, R., Seidler, D.G., and Grobe, K. (2016). Bridging the gap: heparan sulfate and Scube2 assemble Sonic hedgehog release complexes at the surface of producing cells. Sci Rep *6*, 26435.

Jao, T.M., Li, Y.L., Lin, S.W., Tzeng, S.T., Yu, I.S., Yen, S.J., Tsai, M.H., and Yang, Y.C. (2016). Alteration of colonic epithelial cell differentiation in mice deficient for glucosaminyl N-deacetylase/N-sulfotransferase 4. Oncotarget *7*, 84938-84950.

Jessell, T.M. (2000). Neuronal specification in the spinal cord: inductive signals and transcriptional codes. Nat Rev Genet *1*, 20-29.

Jochmann, K., Bachvarova, V., and Vortkamp, A. (2014). Reprint of: Heparan sulfate as a regulator of endochondral ossification and osteochondroma development. Matrix Biol *35*, 239-247.

Karp, S.J., Schipani, E., St-Jacques, B., Hunzelman, J., Kronenberg, H., and McMahon, A.P. (2000). Indian hedgehog coordinates endochondral bone growth and morphogenesis via parathyroid hormone related-protein-dependent and -independent pathways. Development *127*, 543-548.

Kelly, M.A., and Hirschi, K.K. (2009). Signaling hierarchy regulating human endothelial cell development. Arterioscler Thromb Vasc Biol *29*, 718-724.

Kitagawa, H., Izumikawa, T., Uyama, T., and Sugahara, K. (2003). Molecular cloning of a chondroitin polymerizing factor that cooperates with chondroitin synthase for chondroitin polymerization. J Biol Chem *278*, 23666-23671.

Kitagawa, H., Uyama, T., and Sugahara, K. (2001). Molecular cloning and expression of a human chondroitin synthase. J Biol Chem *276*, 38721-38726.

Kluppel, M., Wight, T.N., Chan, C., Hinek, A., and Wrana, J.L. (2005). Maintenance of chondroitin sulfation balance by chondroitin-4-sulfotransferase 1 is required for chondrocyte development and growth factor signaling during cartilage morphogenesis. Development *132*, 3989-4003.

Koleva, M.V., Rothery, S., Spitaler, M., Neil, M.A., and Magee, A.I. (2015). Sonic hedgehog multimerization: a self-organizing event driven by post-translational modifications? Mol Membr Biol *32*, 65-74.

Koziel, L., Kunath, M., Kelly, O.G., and Vortkamp, A. (2004). Ext1-dependent heparan sulfate regulates the range of Ihh signaling during endochondral ossification. Dev Cell *6*, 801-813.

Kreuger, J., and Kjellen, L. (2012). Heparan sulfate biosynthesis: regulation and variability. J Histochem Cytochem *60*, 898-907.

Kronenberg, H.M. (2003). Developmental regulation of the growth plate. Nature *423*, 332-336.

Kusche-Gullberg, M., Nybakken, K., Perrimon, N., and Lindahl, U. (2012). Drosophila heparan sulfate, a novel design. J Biol Chem *287*, 21950-21956.

Laemmli, U.K. (1970). Cleavage of structural proteins during the assembly of the head of bacteriophage T4. Nature *227*, 680-685.

Lamanna, W.C., Frese, M.A., Balleininger, M., and Dierks, T. (2008). Sulf loss influences N-, 2-O-, and 6-O-sulfation of multiple heparan sulfate proteoglycans and modulates fibroblast growth factor signaling. J Biol Chem *283*, 27724-27735.

Lanske, B., Karaplis, A.C., Lee, K., Luz, A., Vortkamp, A., Pirro, A., Karperien, M., Defize, L.H., Ho, C., Mulligan, R.C.*, et al.* (1996). PTH/PTHrP receptor in early development and Indian hedgehog-regulated bone growth. Science *273*, 663-666.

Le Jan, S., Hayashi, M., Kasza, Z., Eriksson, I., Bishop, J.R., Weibrecht, I., Heldin, J., Holmborn, K., Jakobsson, L., Soderberg, O.*, et al.* (2012). Functional overlap between chondroitin and heparan sulfate proteoglycans during VEGF-induced sprouting angiogenesis. Arterioscler Thromb Vasc Biol *32*, 1255-1263.

Lee, R.T., Zhao, Z., and Ingham, P.W. (2016). Hedgehog signalling. Development *143*, 367-372.

Li, J.P., Gong, F., Hagner-McWhirter, A., Forsberg, E., Abrink, M., Kisilevsky, R., Zhang, X., and Lindahl, U. (2003). Targeted disruption of a murine glucuronyl C5-epimerase gene

results in heparan sulfate lacking L-iduronic acid and in neonatal lethality. J Biol Chem *278*, 28363-28366.

Li, Y., Zhang, H., Litingtung, Y., and Chiang, C. (2006). Cholesterol modification restricts the spread of Shh gradient in the limb bud. Proc Natl Acad Sci U S A *103*, 6548-6553.

Lind, T., Tufaro, F., McCormick, C., Lindahl, U., and Lidholt, K. (1998). The putative tumor suppressors EXT1 and EXT2 are glycosyltransferases required for the biosynthesis of heparan sulfate. J Biol Chem *273*, 26265-26268.

Long, F., Chung, U.I., Ohba, S., McMahon, J., Kronenberg, H.M., and McMahon, A.P. (2004). Ihh signaling is directly required for the osteoblast lineage in the endochondral skeleton. Development *131*, 1309-1318.

Long, F., and Ornitz, D.M. (2013). Development of the endochondral skeleton. Cold Spring Harb Perspect Biol *5*, a008334.

Long, F., Zhang, X.M., Karp, S., Yang, Y., and McMahon, A.P. (2001). Genetic manipulation of hedgehog signaling in the endochondral skeleton reveals a direct role in the regulation of chondrocyte proliferation. Development *128*, 5099-5108.

Luo, Y., Lu, W., Mohamedali, K.A., Jang, J.H., Jones, R.B., Gabriel, J.L., Kan, M., and McKeehan, W.L. (1998). The glycine box: a determinant of specificity for fibroblast growth factor. Biochemistry *37*, 16506-16515.

Maes, C., Kobayashi, T., Selig, M.K., Torrekens, S., Roth, S.I., Mackem, S., Carmeliet, G., and Kronenberg, H.M. (2010). Osteoblast precursors, but not mature osteoblasts, move into developing and fractured bones along with invading blood vessels. Dev Cell *19*, 329-344.

Malfait, F., Syx, D., Vlummens, P., Symoens, S., Nampoothiri, S., Hermanns-Le, T., Van Laer, L., and De Paepe, A. (2010). Musculocontractural Ehlers-Danlos Syndrome (former EDS type VIB) and adducted thumb clubfoot syndrome (ATCS) represent a single clinical entity caused by mutations in the dermatan-4-sulfotransferase 1 encoding CHST14 gene. Hum Mutat *31*, 1233-1239.

Mariani, F.V., and Martin, G.R. (2003). Deciphering skeletal patterning: clues from the limb. Nature *423*, 319-325.

Matsumoto, Y., Matsumoto, K., Irie, F., Fukushi, J., Stallcup, W.B., and Yamaguchi, Y. (2010). Conditional ablation of the heparan sulfate-synthesizing enzyme Ext1 leads to dysregulation of bone morphogenic protein signaling and severe skeletal defects. J Biol Chem *285*, 19227-19234.

Matusek, T., Wendler, F., Poles, S., Pizette, S., D'Angelo, G., Furthauer, M., and Therond, P.P. (2014). The ESCRT machinery regulates the secretion and long-range activity of Hedgehog. Nature *516*, 99-103.

Maun, H.R., Wen, X., Lingel, A., de Sauvage, F.J., Lazarus, R.A., Scales, S.J., and Hymowitz, S.G. (2010). Hedgehog pathway antagonist 5E1 binds hedgehog at the pseudo-active site. J Biol Chem *285*, 26570-26580.

McCloy, R.A., Rogers, S., Caldon, C.E., Lorca, T., Castro, A., and Burgess, A. (2014). Partial inhibition of Cdk1 in G 2 phase overrides the SAC and decouples mitotic events. Cell Cycle *13*, 1400-1412.

Mikami, T., and Kitagawa, H. (2013). Biosynthesis and function of chondroitin sulfate. Biochim Biophys Acta *1830*, 4719-4733.

Minina, E., Wenzel, H.M., Kreschel, C., Karp, S., Gaffield, W., McMahon, A.P., and Vortkamp, A. (2001). BMP and Ihh/PTHrP signaling interact to coordinate chondrocyte proliferation and differentiation. Development *128*, 4523-4534.

Mitchell, K.J., Pinson, K.I., Kelly, O.G., Brennan, J., Zupicich, J., Scherz, P., Leighton, P.A., Goodrich, L.V., Lu, X., Avery, B.J.*, et al.* (2001). Functional analysis of secreted and transmembrane proteins critical to mouse development. Nat Genet *28*, 241-249.

Miyake, N., Kosho, T., Mizumoto, S., Furuichi, T., Hatamochi, A., Nagashima, Y., Arai, E., Takahashi, K., Kawamura, R., Wakui, K.*, et al.* (2010). Loss-of-function mutations of CHST14 in a new type of Ehlers-Danlos syndrome. Hum Mutat *31*, 966-974.

Motoyama, J., Takabatake, T., Takeshima, K., and Hui, C. (1998). Ptch2, a second mouse Patched gene is co-expressed with Sonic hedgehog. Nat Genet *18*, 104-106.

Mouw, J.K., Ou, G., and Weaver, V.M. (2014). Extracellular matrix assembly: a multiscale deconstruction. Nat Rev Mol Cell Biol *15*, 771-785.

Mundy, C., Yasuda, T., Kinumatsu, T., Yamaguchi, Y., Iwamoto, M., Enomoto-Iwamoto, M., Koyama, E., and Pacifici, M. (2011). Synovial joint formation requires local Ext1 expression and heparan sulfate production in developing mouse embryo limbs and spine. Dev Biol *351*, 70-81.

Murone, M., Rosenthal, A., and de Sauvage, F.J. (1999). Sonic hedgehog signaling by the patched-smoothened receptor complex. Curr Biol *9*, 76-84.

Nakamura, T., Aikawa, T., Iwamoto-Enomoto, M., Iwamoto, M., Higuchi, Y., Pacifici, M., Kinto, N., Yamaguchi, A., Noji, S., Kurisu, K.*, et al.* (1997). Induction of osteogenic differentiation by hedgehog proteins. Biochem Biophys Res Commun *237*, 465-469.

Nusslein-Volhard, C., and Wieschaus, E. (1980). Mutations affecting segment number and polarity in Drosophila. Nature *287*, 795-801.

Ohlig, S., Farshi, P., Pickhinke, U., van den Boom, J., Hoing, S., Jakuschev, S., Hoffmann, D., Dreier, R., Scholer, H.R., Dierker, T.*, et al.* (2011). Sonic hedgehog shedding results in functional activation of the solubilized protein. Dev Cell *20*, 764-774.

Ohlig, S., Pickhinke, U., Sirko, S., Bandari, S., Hoffmann, D., Dreier, R., Farshi, P., Gotz, M., and Grobe, K. (2012). An emerging role of Sonic hedgehog shedding as a modulator of heparan sulfate interactions. J Biol Chem *287*, 43708-43719.

Ortega, N., Behonick, D.J., and Werb, Z. (2004). Matrix remodeling during endochondral ossification. Trends Cell Biol *14*, 86-93.

Ortmann, C., Pickhinke, U., Exner, S., Ohlig, S., Lawrence, R., Jboor, H., Dreier, R., and Grobe, K. (2015). Sonic hedgehog processing and release are regulated by glypican heparan sulfate proteoglycans. J Cell Sci *128*, 2374-2385.

Pak, E., and Segal, R.A. (2016). Hedgehog Signal Transduction: Key Players, Oncogenic Drivers, and Cancer Therapy. Dev Cell *38*, 333-344.

Pallerla, S.R., Lawrence, R., Lewejohann, L., Pan, Y., Fischer, T., Schlomann, U., Zhang, X., Esko, J.D., and Grobe, K. (2008). Altered heparan sulfate structure in mice with deleted NDST3 gene function. J Biol Chem *283*, 16885-16894.

Pallerla, S.R., Pan, Y., Zhang, X., Esko, J.D., and Grobe, K. (2007). Heparan sulfate Ndst1 gene function variably regulates multiple signaling pathways during mouse development. Dev Dyn *236*, 556-563.

Palm, W., Swierczynska, M.M., Kumari, V., Ehrhart-Bornstein, M., Bornstein, S.R., and Eaton, S. (2013). Secretion and signaling activities of lipoprotein-associated hedgehog and non-sterol-modified hedgehog in flies and mammals. PLoS Biol *11*, e1001505.

Panakova, D., Sprong, H., Marois, E., Thiele, C., and Eaton, S. (2005). Lipoprotein particles are required for Hedgehog and Wingless signalling. Nature *435*, 58-65.

Parmantier, E., Lynn, B., Lawson, D., Turmaine, M., Namini, S.S., Chakrabarti, L., McMahon, A.P., Jessen, K.R., and Mirsky, R. (1999). Schwann cell-derived Desert hedgehog controls the development of peripheral nerve sheaths. Neuron *23*, 713-724.

Pepinsky, R.B., Zeng, C., Wen, D., Rayhorn, P., Baker, D.P., Williams, K.P., Bixler, S.A., Ambrose, C.M., Garber, E.A., Miatkowski, K.*, et al.* (1998). Identification of a palmitic acid-modified form of human Sonic hedgehog. J Biol Chem *273*, 14037-14045.

Percival, C.J., and Richtsmeier, J.T. (2013). Angiogenesis and intramembranous osteogenesis. Dev Dyn *242*, 909-922.

Pereira, J., Johnson, W.E., O'Brien, S.J., Jarvis, E.D., Zhang, G., Gilbert, M.T., Vasconcelos, V., and Antunes, A. (2014). Evolutionary genomics and adaptive evolution of the Hedgehog gene family (Shh, Ihh and Dhh) in vertebrates. PLoS One *9*, e74132.

Porter, J.A., Ekker, S.C., Park, W.J., von Kessler, D.P., Young, K.E., Chen, C.H., Ma, Y., Woods, A.S., Cotter, R.J., Koonin, E.V.*, et al.* (1996). Hedgehog patterning activity: role of a

lipophilic modification mediated by the carboxy-terminal autoprocessing domain. Cell *86*, 21-34.

Porter, J.A., von Kessler, D.P., Ekker, S.C., Young, K.E., Lee, J.J., Moses, K., and Beachy, P.A. (1995). The product of hedgehog autoproteolytic cleavage active in local and long-range signalling. Nature *374*, 363-366.

Ratzka, A., Kalus, I., Moser, M., Dierks, T., Mundlos, S., and Vortkamp, A. (2008). Redundant function of the heparan sulfate 6-O-endosulfatases Sulf1 and Sulf2 during skeletal development. Dev Dyn *237*, 339-353.

Ratzka, A., Mundlos, S., and Vortkamp, A. (2010). Expression patterns of sulfatase genes in the developing mouse embryo. Dev Dyn *239*, 1779-1788.

Reznikoff, C.A., Bertram, J.S., Brankow, D.W., and Heidelberger, C. (1973). Quantitative and qualitative studies of chemical transformation of cloned C3H mouse embryo cells sensitive to postconfluence inhibition of cell division. Cancer Res *33*, 3239-3249.

Riddle, R.D., Johnson, R.L., Laufer, E., and Tabin, C. (1993). Sonic hedgehog mediates the polarizing activity of the ZPA. Cell *75*, 1401-1416.

Riesenfeld, J., Hook, M., and Lindahl, U. (1982). Biosynthesis of heparin. Concerted action of early polymer-modification reactions. J Biol Chem *257*, 421-425.

Rubin, J.B., Choi, Y., and Segal, R.A. (2002). Cerebellar proteoglycans regulate sonic hedgehog responses during development. Development *129*, 2223-2232.

Sanders, T.A., Llagostera, E., and Barna, M. (2013). Specialized filopodia direct long-range transport of SHH during vertebrate tissue patterning. Nature *497*, 628-632.

Sarrazin, S., Lamanna, W.C., and Esko, J.D. (2011). Heparan sulfate proteoglycans. Cold Spring Harb Perspect Biol *3*.

Sato, T., Kudo, T., Ikehara, Y., Ogawa, H., Hirano, T., Kiyohara, K., Hagiwara, K., Togayachi, A., Ema, M., Takahashi, S.*, et al.* (2011). Chondroitin sulfate N-acetylgalactosaminyltransferase 1 is necessary for normal endochondral ossification and aggrecan metabolism. J Biol Chem *286*, 5803-5812.

Senay, C., Lind, T., Muguruma, K., Tone, Y., Kitagawa, H., Sugahara, K., Lidholt, K., Lindahl, U., and Kusche-Gullberg, M. (2000). The EXT1/EXT2 tumor suppressors: catalytic activities and role in heparan sulfate biosynthesis. EMBO Rep *1*, 282-286.

Shi, Q., Li, S., Li, S., Jiang, A., Chen, Y., and Jiang, J. (2014). Hedgehog-induced phosphorylation by CK1 sustains the activity of Ci/Gli activator. Proc Natl Acad Sci U S A *111*, E5651-5660.

Silbert, J.E., and Sugumaran, G. (2002). Biosynthesis of chondroitin/dermatan sulfate. IUBMB Life *54*, 177-186.

St-Jacques, B., Hammerschmidt, M., and McMahon, A.P. (1999). Indian hedgehog signaling regulates proliferation and differentiation of chondrocytes and is essential for bone formation. Genes Dev *13*, 2072-2086.

Sugahara, K., and Schwartz, N.B. (1979). Defect in 3'-phosphoadenosine 5'-phosphosulfate formation in brachymorphic mice. Proc Natl Acad Sci U S A *76*, 6615-6618.

Takei, Y., Ozawa, Y., Sato, M., Watanabe, A., and Tabata, T. (2004). Three Drosophila EXT genes shape morphogen gradients through synthesis of heparan sulfate proteoglycans. Development *131*, 73-82.

Takeo, S., Akiyama, T., Firkus, C., Aigaki, T., and Nakato, H. (2005). Expression of a secreted form of Dally, a Drosophila glypican, induces overgrowth phenotype by affecting action range of Hedgehog. Dev Biol *284*, 204-218.

The, I., Bellaiche, Y., and Perrimon, N. (1999). Hedgehog movement is regulated through tout velu-dependent synthesis of a heparan sulfate proteoglycan. Mol Cell *4*, 633-639.

Theocharis, A.D., Skandalis, S.S., Gialeli, C., and Karamanos, N.K. (2016). Extracellular matrix structure. Adv Drug Deliv Rev *97*, 4-27.

Tukachinsky, H., Kuzmickas, R.P., Jao, C.Y., Liu, J., and Salic, A. (2012). Dispatched and scube mediate the efficient secretion of the cholesterol-modified hedgehog ligand. Cell Rep *2*, 308-320.

Varjosalo, M., and Taipale, J. (2008). Hedgehog: functions and mechanisms. Genes Dev *22*, 2454-2472.

Volpi, N., Galeotti, F., Yang, B., and Linhardt, R.J. (2014). Analysis of glycosaminoglycan-derived, precolumn, 2-aminoacridone-labeled disaccharides with LC-fluorescence and LC-MS detection. Nat Protoc *9*, 541-558.

Vortkamp, A., Gessler, M., and Grzeschik, K.H. (1991). GLI3 zinc-finger gene interrupted by translocations in Greig syndrome families. Nature *352*, 539-540.

Vortkamp, A., Lee, K., Lanske, B., Segre, G.V., Kronenberg, H.M., and Tabin, C.J. (1996). Regulation of rate of cartilage differentiation by Indian hedgehog and PTH-related protein. Science *273*, 613-622.

Vyas, N., Goswami, D., Manonmani, A., Sharma, P., Ranganath, H.A., VijayRaghavan, K., Shashidhara, L.S., Sowdhamini, R., and Mayor, S. (2008). Nanoscale organization of hedgehog is essential for long-range signaling. Cell *133*, 1214-1227.

Vyas, N., Walvekar, A., Tate, D., Lakshmanan, V., Bansal, D., Lo Cicero, A., Raposo, G., Palakodeti, D., and Dhawan, J. (2014). Vertebrate Hedgehog is secreted on two types of extracellular vesicles with different signaling properties. Sci Rep *4*, 7357.

Wang, B., Fallon, J.F., and Beachy, P.A. (2000). Hedgehog-regulated processing of Gli3 produces an anterior/posterior repressor gradient in the developing vertebrate limb. Cell *100*, 423-434.

Watanabe, Y., Takeuchi, K., Higa Onaga, S., Sato, M., Tsujita, M., Abe, M., Natsume, R., Li, M., Furuichi, T., Saeki, M.*, et al.* (2010). Chondroitin sulfate N-acetylgalactosaminyltransferase-1 is required for normal cartilage development. Biochem J *432*, 47-55.

Whalen, D.M., Malinauskas, T., Gilbert, R.J., and Siebold, C. (2013). Structural insights into proteoglycan-shaped Hedgehog signaling. Proc Natl Acad Sci U S A *110*, 16420-16425.

Williams, E.H., Pappano, W.N., Saunders, A.M., Kim, M.S., Leahy, D.J., and Beachy, P.A. (2010). Dally-like core protein and its mammalian homologues mediate stimulatory and inhibitory effects on Hedgehog signal response. Proc Natl Acad Sci U S A *107*, 5869-5874.

Wilson, D.G., Phamluong, K., Lin, W.Y., Barck, K., Carano, R.A., Diehl, L., Peterson, A.S., Martin, F., and Solloway, M.J. (2012). Chondroitin sulfate synthase 1 (Chsy1) is required for bone development and digit patterning. Dev Biol *363*, 413-425.

Witt, R.M., Hecht, M.L., Pazyra-Murphy, M.F., Cohen, S.M., Noti, C., van Kuppevelt, T.H., Fuller, M., Chan, J.A., Hopwood, J.J., Seeberger, P.H.*, et al.* (2013). Heparan sulfate proteoglycans containing a glypican 5 core and 2-O-sulfo-iduronic acid function as Sonic Hedgehog co-receptors to promote proliferation. J Biol Chem *288*, 26275-26288.

Wojcinski, A., Nakato, H., Soula, C., and Glise, B. (2011). DSulfatase-1 fine-tunes Hedgehog patterning activity through a novel regulatory feedback loop. Dev Biol *358*, 168-180.

Wuelling, M., and Vortkamp, A. (2010). Transcriptional networks controlling chondrocyte proliferation and differentiation during endochondral ossification. Pediatr Nephrol *25*, 625-631.

Wuelling, M., and Vortkamp, A. (2011). Chondrocyte proliferation and differentiation. Endocr Dev *21*, 1-11.

Yang, B., Solakyildirim, K., Chang, Y., and Linhardt, R.J. (2011). Hyphenated techniques for the analysis of heparin and heparan sulfate. Anal Bioanal Chem *399*, 541-557.

Yasuda, T., Mundy, C., Kinumatsu, T., Shibukawa, Y., Shibutani, T., Grobe, K., Minugh-Purvis, N., Pacifici, M., and Koyama, E. (2010). Sulfotransferase Ndst1 is needed for mandibular and TMJ development. J Dent Res *89*, 1111-1116.

Zeng, X., Goetz, J.A., Suber, L.M., Scott, W.J., Jr., Schreiner, C.M., and Robbins, D.J. (2001). A freely diffusible form of Sonic hedgehog mediates long-range signalling. Nature *411*, 716-720.

Zhang, L., and Esko, J.D. (1994). Amino acid determinants that drive heparan sulfate assembly in a proteoglycan. J Biol Chem *269*, 19295-19299.

Zhao, L., Li, G., Chan, K.M., Wang, Y., and Tang, P.F. (2009). Comparison of multipotent differentiation potentials of murine primary bone marrow stromal cells and mesenchymal stem cell line C3H10T1/2. Calcif Tissue Int *84*, 56-64.

9 Supplementary figures

9.1 Relative amount of multimers of IhhNp, ShhNp and CW1-exchange mutants, separated by size.

Table 9. 1 Quantification of the relative levels of IhhNp, ShhNp and CW1-exchange mutant multimers.
Hh proteins were expressed in HEK-293Ebna cells and analyzed by size-exclusion chromatography, immunoblotted and quantified using ImageJ software. Protein amounts for each data point were normalized to the total recovered protein and are mean values ± s.e.m., n≥3. The protein amount at each data point was compared to these of wild-type IhhNp protein. Statistical analysis was carried out using two-tailed, unpaired Student's *t*-test. *p<0.05. (see Fig. 4. 6).

Relative protein (%) recovered in size-exclusion chromatography					
molecular weight (kDa)	IhhNp	ShhNp	$IhhNp^{R75K/P78H/R80K}$	$IhhNp^{V72G/V73F/S74\Delta/R75K/P78H/R80K}$	$ShhNp^{K33/RH36P/K38R}$
> 660	41.67 ± 4.2	8.7 ± 4 *	33 ± 10	49.1 ± 22	30 ± 11
	22.35 ± 4.6	8.5 ± 3.3	15.7 ± 4.6	18.9 ± 8	10.3 ± 4.6
	4.59 ± 1.3	12.2 ± 4.3	12.6 ± 7.8	13.7 ± 9.7	21 ± 13
550	7.87 ± 2.6	9.3 ± 2.4	14.1 ± 3.7	4 ± 3.4	8.8 ± 0.7
340	10.6 ± 3	12.9 ± 4.7	9.4 ± 3.6	7.2 ± 2.2	7.6 ± 3.1
250	1.84 ± 0.4	5.1 ± 1.7	3.7 ± 1.6	1.9 ± 1.1	1.5 ± 0.6
120	1 ± 0.4	4.1 ± 2.1	1.9 ± 0.6	0.3 ± 0.1	0.5 ± 0.1
75	0.98 ± 0.4	3.8 ± 2.6	1.4 ± 0.5	0.3 ± 0.2	0.4 ± 0.1
45	0.97 ± 0.4	2.4 ± 1	1.3 ± 0.6	0.3 ± 0.2	1 ± 0.4
27	0.97 ± 0.4	3.5 ± 0.7	1.1 ± 0.7	0.3 ± 0.2	10 ± 4
17	1.8 ± 1	4.5 ± 1.6	1.1 ± 0.7	0.4 ± 0.3	6 ± 2
	0.97 ± 0.4	7.4 ± 1.7	1.1 ± 0.7	0.3 ± 0.2	1 ± 0.3
	0.97 ± 0.4	5.9 ± 3.3	0.9 ± 0.5	0.1 ± 0.2	0.6 ± 0.1

9.2 Disaccharide analysis of GAGs purified from *Ext1* and *Hs2st* mutants and wild-type skeletons

Table 9. 2 HS disaccharides obtained from *Hs2st*$^{-/-}$, *Ext1*$^{gt/gt}$ and control mouse skeletons by exhaustive heparin lyase cleavage.
Disaccharides were generated by cleavage with heparin lyases mixture and analyzed by RPIP-HPLC. Values are given in mol (%) of total disaccharides and are the mean ± s.e.m. of six (*Ext1*) and three samples (*Hs2st*). The degree and type of sulfation are calculated from disaccharides species. Total amounts are given as pmol/µg/ml DNA starting material as calculated from peak areas relative to known amounts of standard disaccharides. Statistical significance was calculated by two-way ANOVA with Bonferroni post-test, * $p < 0.05$, ** $p < 0.01$, *** $p < 0.001$ (see section 4.2.1.2 and 4.2.2.2).

	HS disaccharide composition (%)								Sulfates per 100 disaccharides					
	ΔUA-GlcNAc	ΔUA-GlcNS	ΔUA-GlcNAc6S	ΔUA2S-GlcNAc	ΔUA-GlcNS6S	ΔUA2S-GlcNS	ΔUA2S-GlcNAc6S	ΔUA2S-GlcNS6S	0S	NS	6S	2S	total S	HS amount (pmol/µg/ml DNA)
Hs2st$^{+/+}$	42.9 ± 0.8	19.4 ± 0.4	3.8 ± 1.6	2.8 ± 0.12	2.9 ± 0.17	5.5 ± 1.6	3.3 ± 2.1	19.4 ± 1	42.9 ± 0.8	47.2 ± 1	29.4 ± 0.6	31.1 ± 2.4	107.7 ± 2.5	28.8 ± 4.8
Hs2st$^{-/-}$	45.3 ± 2	34.7 ± 2.3***	2.8 ± 1.2	2.4 ± 0.2	12.9 ± 2.1***	0.73 ± 0.2	1.1 ± 1.1	0***	45.4 ± 2	48.3 ± 0.3	16.9 ± 4.1 **	4.3 ± 1.1***	69.5 ± 5***	30.4 ± 4.4
Ext1$^{+/+}$	44.33 ± 2.4	21.57 ± 1.3	3.4 ± 0.7	2.4 ± 0.3	3.5 ± 0.7	5.1 ± 1.2	2 ± 1.6	17.6 ± 2.4	44.3 ± 2.4	47.9 ± 2.8	26.6 ± 3.2	27.2 ± 3.6	101.7 ± 8	18 ± 5
Ext1$^{gt/gt}$	45.7 ± 4	12.5 ± 1.2*	5 ± 0.9	0	9.8 ± 1.3	2.4 ± 1.1	3.1 ± 3.1	21.4 ± 3.7	45.7 ± 4	46.1 ± 3.5	39.4 ± 3.7 *	26.9 ± 4	112.3 ± 10.3	3.6 ± 1.3*

Table 9. 3 CS disaccharides obtained from *Hs2st*$^{-/-}$, *Ext1*$^{gt/gt}$ and control mouse skeletons by exhaustive chondroitinase ABC cleavage.
Disaccharides were generated by cleavage with chondroitinase ABC and analyzed by RPIP-HPLC. Values are given in mol (%) of total disaccharides and are the mean ± s.e.m. of six (*Ext1*) and three samples (*Hs2st*). The degree and type of sulfation are calculated from the disaccharide species. Total amounts are given as pmol/µg/ml DNA starting material as calculated from peak areas relative to known amounts of standard disaccharides. Statistical significance was calculated by two-way ANOVA with Bonferroni post-test * $p < 0.05$, ** $p < 0.01$, *** $p < 0.001$ (see section 4.2.1.2 and 4.2.2.2).

	CS disaccharide composition (%)					Sulfates per 100 disaccharides					
	ΔUA-GalNAc	ΔUA-GalNAc4S	ΔUA-GalNAc6S	ΔUA-GalNAc4S6S	ΔUA2S-GalNAc6S	0S	2S	6S	4S	total S	CS amount (pmol/µg/ml DNA)
Hs2st$^{+/+}$	22.33 ± 0.433	68.57 ± 0.367	0.83 ± 0.03	0.67 ± 0.167	7.6 ± 0.36	22.33 ± 0.43	7.63 ± 0.34	9.23 ± 0.54	69.3 ± 0.3	86.1 ± 0.9	3485.9 ± 194
Hs2st$^{-/-}$	21.67 ± 0.57	68.7 ± 0.3	0.7 ± 0.06	0.8 ± 0.06	8 ± 0.43	21.67 ± 0.6	8.13 ± 0.4	9.6 ± 0.44	69.63 ± 0.24	87.4 ± 0.9	4570.8 ± 150 *
Ext1$^{+/+}$	23.42 ± 0.34	71.92 ± 1.43	0.92 ± 0.09	0.267 ± 0.13	3.5 ± 1.44	23.4 ± 0.34	3.5 ± 1.5	4.7 ± 1.5	72.2 ± 1.3	80.34 ± 1.7	2011.4 ± 208
Ext1$^{gt/gt}$	23.52 ± 2.07	71.6 ± 1.3	0.8 ± 0.06	0.35 ± 0.2	3.72 ± 1.6	23.5 ± 2.1	3.8 ± 1.6	4.9 ± 1.8	72 ± 1.3	80.6 ±3.6	3423 ± 773

Table 9. 4 CS disaccharide composition of *Hs2st*$^{-/-}$ and *Ext1*$^{gt/gt}$ and control cartilage analyzed by RPIP-HPLC.
CS disaccharide composition was analyzed by RPIP-HPLC. Values are given as pmol/µg/ml DNA starting material and are mean ± s.e.m. of six (*Ext1*) and three (*Hs2st*) samples. Statistical significance was calculated by two-way ANOVA . * $p < 0.05$, ** $p < 0.01$, *** $p < 0.001$ (see section 4.2.1.2 and 4.2.2.2).

	CS disaccharide composition (pmol/µg/ml DNA)					
	ΔUA-GalNAc	ΔUA-GalNAc4S	ΔUA-GalNAc6S	ΔUA-GalNAc4S6S	ΔUA2S-GalNAc6S	ΔUA2S-GalNAc4S6S
Hs2st+/+	778.5 ± 54	2389.3 ± 123	28.6 ± 1.2	22.9 ± 5.5	264.3 ± 19	2.27 ± 0.13
Hs2st-/-	992.9 ± 60	3138.8 ± 95***	31.8 ± 2	37.2 ± 3	364.1 ±10.2	6.1 ± 2.13
Ext1+/+	469 ± 45	1433 ± 124	17.9 ± 1.7	5.8 ± 3.3	84.6 ± 36.8	0.72 ± 0.4
Ext1gt/gt	832.5 ± 206 *	2423.4 ± 526 *	25.6 ± 4.2	8.9 ± 4.6	131 ± 62.6	1.6 ± 1.4

9.3 Analysis of the chain length of total GAGs, HS and CS, purified from E13.5 *Ext1*$^{gt/gt}$, *Hs2st*$^{-/-}$ and control chondrocytes

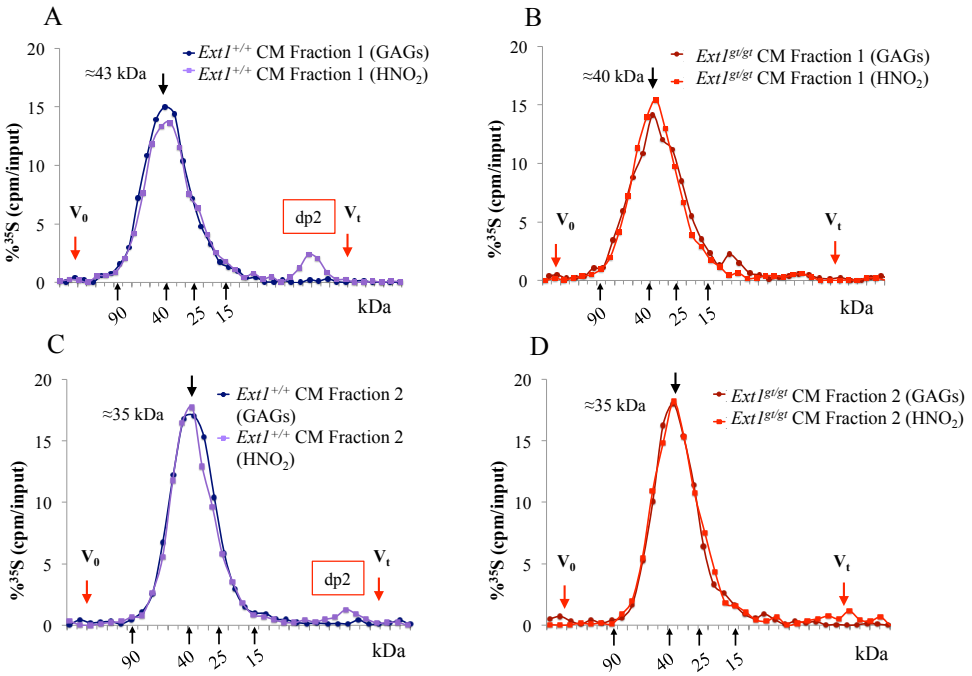

Fig. 9. 1 CS predominates the ECM of chondrocytes.
^{35}S labeled total GAGs and CS secrted by *Ext1*$^{gt/gt}$ and control chondrocytes were analyzed by size-exclusion chromatography. Both fractions of secreted GAGs were predominated by CS. Minor difference was observed between the sizes of the wild-type chains in fraction 1 and 2 of secreted PGs (A, C). In fraction 1, the mutant GAGs were slightly shorter than the wild-type chains (A, B). No difference was observed in their size in fraction 2 of secreted GAGs (C, D). Data are given as (%) cpm relative to the input. dp2–disaccharide peak, V_0–void volume, V_t–total column volume. The sizes of molecular weight standards are indicated. n=3, one representative experiment is shown. (see section 4.2.3.1)

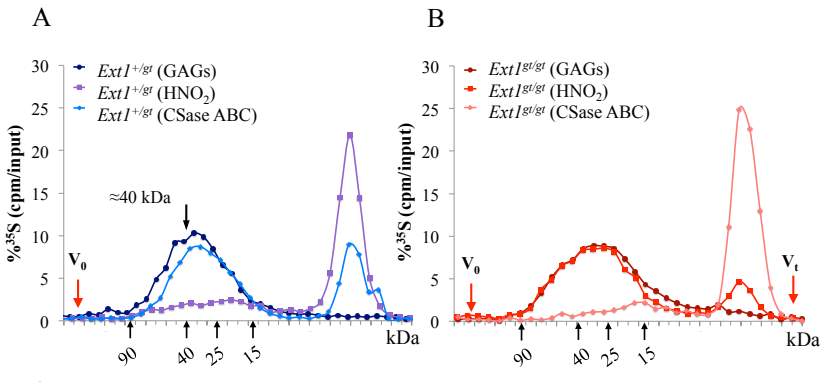

Fig. 9. 2 Primary undifferentiated *Ext1*$^{gt/gt}$ chondrocytes upregalate CS.
The chain length of ^{35}S labeled primary undifferentiated *Ext1*$^{gt/gt}$ (B) and control chondrocytes (A) was compared by size. Wild-type cells contained limited CS amount (A), while in mutant cells CS was strongly enriched (B). Values are given as (%) cpm relative to the input. n=2. One representative experiment is shown. V_0–void volume, V_t–total column volume. The sizes of molecular weight standards are indicated. (see section 4.2.3.2)

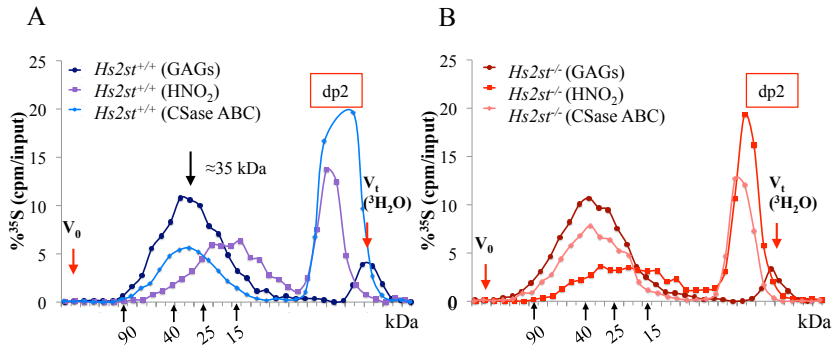

Fig. 9. 3 Hs2st deficient chondrocytes are characterized by elevated HS levels in their cell surface GAG fraction.
Chain length of ^{35}S labeled total GAGs, CS (HNO_2) and HS (CSase ABC) of primary *Hs2st*$^{-/-}$ (B) and control (A) chondrocytes were compared by size. In the wild-type, the cell-surface GAG population contain equal levels of CS and HS (A), while more HS was detected in the mutant cells (B). No alterations in GAG chain length were observed. Values are given as (%) cpm relative to the input. dp2–disaccharide peak, V_0–void volume, V_t–total column volume. The sizes of molecular weight standards are indicated. n=3, one representative experiment is shown. (see section 4.2.3.3)

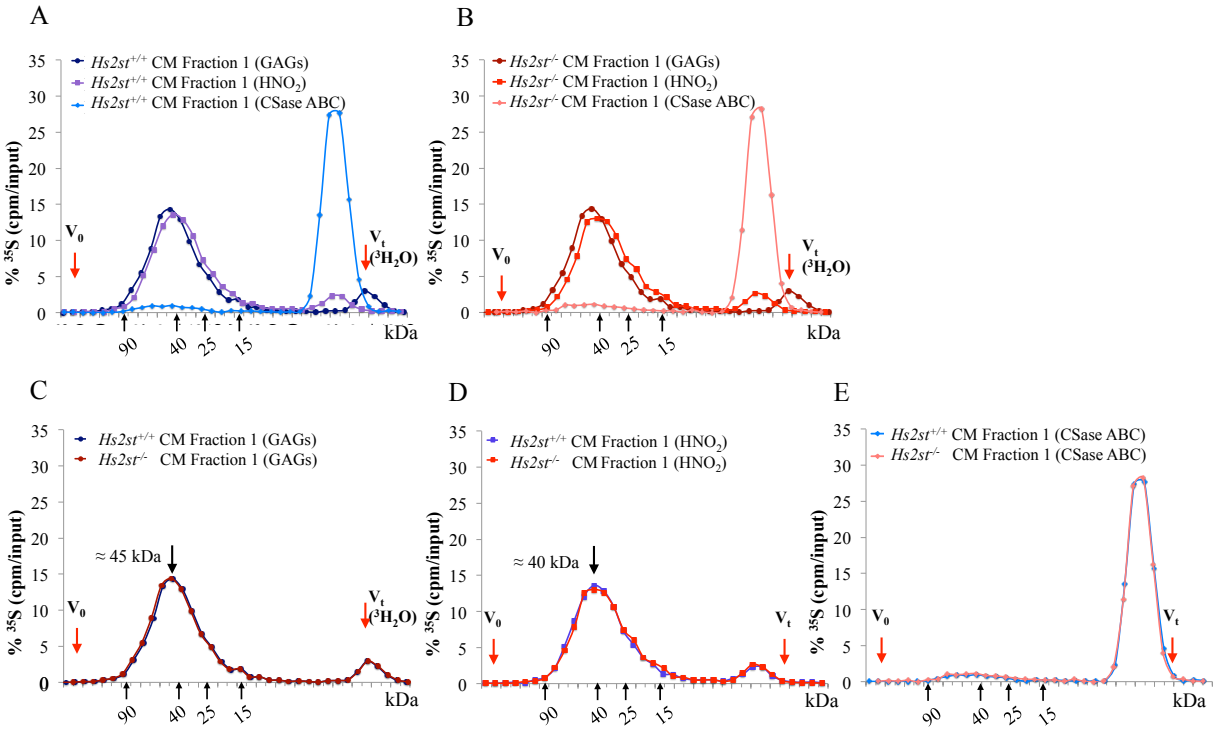

Fig. 9. 4 GAGs of the secreted Fraction 1 of *Hs2st*$^{-/-}$ chondrocytes retain wild-type chain length.

The chain length of the secreted total GAGs (C), CS (D) and HS (E) recovered in Fraction 1 of *Hs2st*$^{-/-}$ and control chondrocytes was analyzed by size-exclusion chromatography. No alterations were observed between the levels or length of the wild-type and mutant secreted GAGs. Data are given as (%) cpm, relative to the input. dp2–disaccharide peak, V_0–void volume, V_t–total column volume. The sizes of molecular weight standards are indicated. n=3, one representative experiment is shown (see section 4.2.3.3).

Table 9. 5 Relative amount of HS and CS of *Ext1*$^{gt/gt}$ and control chondrocytes, recovered in size-exclusion chromatography.
The relative CS and HS amount of *Ext1*$^{gt/gt}$ and wild-type chondrocytes recovered from the cell surface and secreted GAG fractions were estimated following size-exclusion chromatography. Values are given as (%) cpms detected in CS or HS polymer and dp2 peaks, normalized to the total PGs, recovered in a preparative separation. The data are presented as mean velues ± s.e.m. n=3. (see section 4.2.3.1)

	HS levels (%)		CS levels (%)	
	Ext1$^{+/+}$	Ext1$^{gt/gt}$	Ext1$^{+/+}$	Ext1$^{gt/gt}$
Cell Lysates	47.1 ± 4.1	29 ± 5	43 ± 8.3	61 ± 10
Conditioned medium, Fraction 1	9 ± 2	4 ± 1.5	88 ± 2.4	93 ± 1.7
Conditioned medium, Fraction 2	9 ± 5.3	4 ± 1.5	89 ± 5.4	92 ± 1.7

Table 9. 6 Relative amount of HS and CS of *Hs2st*$^{-/-}$ and control chondrocytes, recovered in size-exclusion chromatography.
The relative CS and HS amount of *Hs2st*$^{-/-}$ and wild-type chondrocytes recovered from the cell surface and secreted GAG fractions were estimated following size-exclusion chromatography. Values are given as (%) cpms detected in GAGs polymer and dp2 peaks, normalized to the total PGs level, recovered in a preparative separation. The data are presented as mean velues ± s.e.m. n=3. Statistical significance was calculated by two-tailed, unpaired Student's *t*-test, * $p < 0.05$. (see section 4.2.3.3)

	HS levels (%)		CS levels (%)	
	Hs2st$^{+/+}$	Hs2st$^{-/-}$	Hs2st$^{+/+}$	Hs2st$^{-/-}$
Cell Lysates	44 ± 2	59 ± 3 *	47 ± 6	34 ± 5
Conditioned medium, Fraction 1	9 ± 1.6	8.3 ± 0.1	83 ± 7.8	86 ± 4
Conditioned medium, Fraction 2	7 ± 0.8	8 ± 1.76	88 ± 0.8	88 ± 1.75

9.4 Low levels of *N*-sulfated HS domains in prehypertrophic chondrocytes

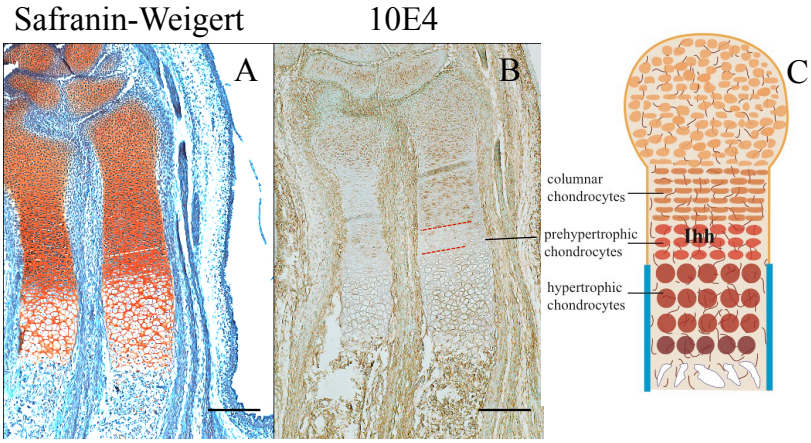

Fig. 9. 5 Prehypertrophic chondrocytes express low levels of *N*-sulfated HS domains.
E16.5 wild-type limb sections were stained with Safranin-Weigert (A) and 10E4 antibody (B), recognizing mixed (GlcA-GlcNS)/(GlcA-GlcNAc) epitopes in HS. The antibody stained strong in the zone columnar chondrocytes, while lower levels of the mixed epitope were observed in prehypertrophic Ihh producing cells. The chondrocyte populations are indicated on the schematic representation of the bone (C). Scale bar = 200 µm. (see section 5.1.3).

List of publications

Publications related to the PhD work:

Altered heparin sulfate structure in Glce$^{-/-}$ mice leads to increased hedgehog signaling in endochondral bones. Tabea Dierker, **Velina Bachvarova**, Yvonne Krause, Jin-Ping Li, Lena Kjellen, Daniela Seidler, Andrea Vortkamp. *Matrix biology: journal of the International Society for Matrix Biology 06/2015;* DOI:10.1016/j.matbio.2015.06.004

Sweet on Hedgehogs: Regulatory Roles of Heparan Sulfate Proteoglycans in Hedgehog-Dependent Cell Proliferation and Differentiation. Shyam Bandari, Sebastian Exnerm, Corinna Ortmann, **Velina Bachvarova**, Andrea Vortkamp, Kay Grobe. review, *Current Protein and Peptide Science 02/2015; 16(1):66-76.* DOI:10.2174/1389203716666150213162649

Heparan sulfate as a regulator of endochondral ossification and osteochondroma development. Katja Jochmann*, **Velina Bachvarova*** and Andrea Vortkamp, review, *Matrix biology: journal of the International Society for Matrix Biology 12/2013; 35.* DOI:10.1016/j.matbio.2013.11.003
*** shared first authorship**

Other publications:

Interactions of the Mont Terri Opalinus Clay isolate Sporomusa sp. MT-2.99 with curium(III) and europium(III). Henry Moll, Laura Lütke, **Velina Bachvarova**, Andrea Cherkouk, Sonja Selenska-Pobell, Gert Bernhard, *Geomicrobiology 03/2014;* DOI:10.1080/01490451.2014.889975

Phylogenetic Diversity of Archaea and the Archaeal Ammonia Monooxygenase Gene in Uranium Mining-Impacted Locations in Bulgaria. Galina Radeva, Anelia Kenarova, **Velina Bachvarova**, Katrin Flemming, Ivann Popov, Dimitar Vassilev, Sonja Selelnska-Pobell, *Archaea 03/2014; 2014:196140.* DOI:10.1155/2014/196140

Bacterial Diversity at Abandoned Uranium Mining and Milling Sites in Bulgaria as Revealed by 16S rRNA Genetic Diversity Study. Galina Radeva, Anelia Kenarova, **Velina Bachvarova**, Katrin Fleming, Ivan Popov, Dimitar Vassilev, Sonja Selenska-Pobell, (2013), *Water, Air and Soil Pollution, 244:1748*

The U(vi) speciation influenced by a novel Paenibacillus isolate from Mont Terri Opalinus clay. Laura Lütke, Henry Moll, **Velina Bachvarova**, Sonja Selenska-Pobell, Gert Bernhard, (2013), *Dalton Transactions, **4**, 6979-6988*

High Archaeal diversity in Varvara hot spring, Bulgaria. Ivanova, I., Atanassov, I. Lyutskanova, D., Stoilova-Disheva, M., Tomova, I., Derekova, A., Radeva, G., **Bachvarova, V.**, Kambourova, M., (2010), *J. Basic Microbiol. 2, 163-72*

Posters:

Heparan sulfate as regulator of Ihh signaling
Velina Bachvarova, Tabea Dierker, Bruce Caterson, Lena Kjellen and Andrea Vortkamp
Gorden Research Seminar and Gorden Research Conference on Proteoglycans, 9-15.07.2016, Andover, NH, USA

Cardin-Weintraub-Motif dependent interaction of Indian Hedgehog with Heparan sulfate
Velina Bachvarova, Tabea Dierker, Andrea Vortkamp
8th International Conference on Proteoglycans, 25-29. 08.2013, Frankfurt/Main, Germany

Oral presentations:

Heparan sulfate as regulator of Indian hedgehog signaling. **Bachvarova, V.**, 28.01.2015, *Institute seminar, Center of medical biotechnology, University of Duisburg-Essen*

Interactions of Heparan sulfate with growth factors. **Bachvarova, V.**, 19.09.12, *Institute seminar, Center of medical biotechnology, University of Duisburg-Essen*

Curriculum vitae

Not available online

Acknowledgments

First, I would like to express my gratitude to Prof. Andrea Vortkamp for giving me the opportunity to work under her supervision and for introducing me to the amazing world of developmental biology. I would like to honor you for your guidance and advice, the fruitful discussions and your patience during the last years.

An important part of my thesis was conducted at BMC, University of Uppsala under the mentorship of Prof. Lena Kjellen and Dr. Tabea Dierker. Dear Lena and Tabea, please accept my deepest gratitude for taking me into your lab and supporting my work, and well being during my stay in Uppsala.

I would like to thank to Prof. Daniel Hoffmann and Prof. Kay Grobe for sharing their knowledge and experience during our "Hedgehog" meetings.

Special thanks go to Dr. Rocio Rebollido-Rios, who always had time to discuss Hedgehog-dependent and independent stories with me.

I would like to express my gratefulness to my colleagues Tina Severmann, Melanie Zuk, Yvonne Krause, Elena Rastew, Virginia Piombo, Verena Schneider and Andrea Thiesen … for their friendship and support.

Dr. Manuela Wuelling, thank you for being ready to answer any question and being there for me and all other students in the group.

Herzlichen Dank to Heike Becker, Sabine Schneider and Nadine Schröder for everything they are and all they have done for me.

It would be inappropriate not to mention Dr. Katja Jochmann. Thank you for your friendship and great deal of help, especially during the first months of my work in Essen and the recent weeks.

I must mention Tanja Wilke, Elke Neisse, Marianne Gillner, Guiseppe Gulino and Mandy Sandmann for being so kind and taking great care of our dear mice. Thank you!

During my stay in Germany I got to know many amazing people. Sasha Lougovski, Boyka Markova, Anna Ferrari, Carina Moll, Pegah Seddigh, Sebastian Exner, Shyam Bandari … Thank you from all my heart.

And while I was in DE, I still had my lovely ladies in Bulgaria to support me–Galina Radeva, Viky Kircheva, Stanislava Shiboykova, Marina Marinova, Zori Petrova.

Next, I would like to express my gratitude to my family for everything they have done for me. I am sorry for putting you through so much, complaining about things you couldn't fully understand and thank you for the full support. Обичам Ви! Благодаря Ви от цялото си сърце.

Finally, I would like to thank to my boyfriend Andrija Matic. Thank you for everything you are!

This work is dedicated to my beloved late grandfather Valko Godumov–the biggest inspiration of my life. / Посвещавам тази дисертация на моя любим дядо Вълко Годумов – най-голямото вдъхновение в живота ми.

Erklärungen

Erklärung

Hiermit erkläre ich, gem. § 6 Abs. (2) f) der Promotionsordnung der Fakultäten für Biologie, Chemie, und Mathematik zur Erlangung des Dr. rer. nat., dass ich das Arbeitsgebiet, dem das Thema „Role of Heparan sulfate in Indian hedgehog signaling and Glycosaminoglycan composition“ zuzuordnen ist, in Forschung und Lehre vertrete und den Antrag von Frau Velina Dimitrova Bachvarova befürworte und die Betreuung auch im Falle eines Weggangs, wenn nicht wichtige Gründe dem entgegenstehen, weiterführen werde.

Essen, den _____ _____

(Prof. Dr. Andrea Vortkamp)

Erklärung:

Hiermit erkläre ich, gem. § 7 Abs. (2) d) + f) der Promotionsordnung der Fakultät für Biologie zur Erlangung des Dr. rer. nat., dass ich die vorliegende Dissertation selbständig verfasst und mich keiner anderen als der angegebenen Hilfsmittel bedient, bei der Abfassung der Dissertation nur die angegeben Hilfsmittel benutzt und alle wörtlich oder inhaltlich übernommenen Stellen als solche gekennzeichnet habe.

Essen, den _____ _____

(Velina Dimitrova Bachvarova)

Erklärung:

Hiermit erkläre ich, gem. § 7 Abs. (2) e) + g) der Promotionsordnung der Fakultät für Biologie zur Erlangung des Dr. rer. nat., dass ich keine anderen Promotionen bzw. Promotionsversuche in der Vergangenheit durchgeführt habe und dass diese Arbeit von keiner anderen Fakultät/Fachbereich abgelehnt worden ist.

Essen, den _____ _____

(Velina Dimitrova Bachvarova)